UNDERSTANDING THE EARTH STRUCTURE UNDERNEATH BOTSWANA: THE TECTONIC MODEL AND ITS RELATIONSHIP TO THE BASEMENT AND CRUSTAL THICKNESS

CHIKONDI CHISENGA
March, 2015

SUPERVISORS:
Dr. M. (Mark) van der Meijde
Mr. Islam Fadel (MSc)

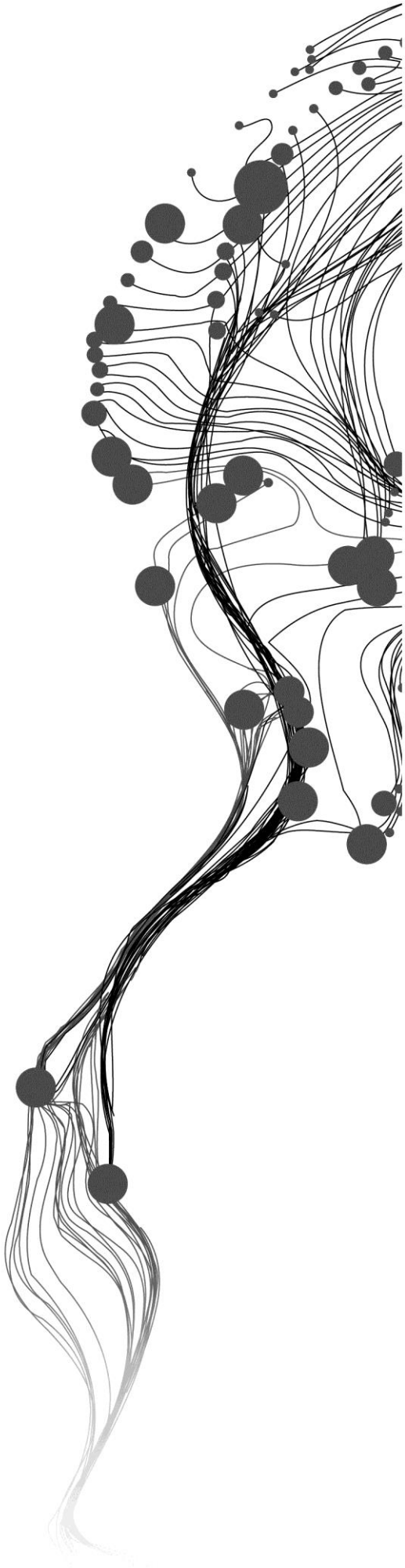

UNDERSTANDING THE EARTH STRUCTURE UNDERNEATH BOTSWANA: THE TECTONIC MODEL AND ITS RELATIONSHIP TO THE BASEMENT AND CRUSTAL THICKNESS

CHIKONDI CHISENGA

Enschede, The Netherlands, March, 2015

Thesis submitted to the Faculty of Geo-Information Science and Earth Observation of the University of Twente in partial fulfilment of the requirements for the degree of Master of Science in Geo-information Science and Earth Observation,
Specialization: Applied Earth Sciences - Earth Resource Exploration

SUPERVISORS:
Dr. M. (Mark) van der Meijde
Mr. Islam Fadel (MSc)

THESIS ASSESSMENT BOARD:
Prof. Dr. F.D. (Freek) van der Meer (Chair)
Dr. M.W.N. (Mike) Buxton (External Examiner, University Delft)

ABSTRACT

The geophysical studies in southern Africa in general and Botswana in particular have focuses on the selected areas within Botswana especially in the south and south-eastern part of the country. Such studies have contributed to the science world but have not tried to understand the tectonic evolution and the geodynamic processes that resulted in the formation and evolution of Botswana crust. The relationship of the crust thickness and the tectonic terranes to the geodynamic activities are still unclear. Furthermore, Botswana does not have a high resolution resolved discontinuity between the earth crust and upper mantle. These limitations can cause problems in the upper mantle tectonic studies. Upper mantle studies, including seismic tomography and 3D subsurface structure of crust and upper mantle cannot be effectively done if the tectonic boundaries and major discontinuities are not well resolved.

In this research, the tectonic boundaries and terranes were delineated and improved using automatic lineaments extraction method. The method, which is mostly used on Digital elevation models (DEM) and satellite images (e.g. ASTER and LANDSAT), was applied in the extraction of tectonic lineaments on geophysical data (gravity and magnetic). The major mafic complexes in Botswana were mapped from magnetic data and added to the tectonic terranes to produce the Precambrian basement geology of Botswana. Furthermore, using the geology of the basement of Botswana, new method of mapping the geology in a covered environment was introduced. The method, called apparent physical mapping, combines the magnetic susceptibility and density distribution calculated from the magnetic and gravity data to predict the geology of the covered environment using colour scheme. The apparent physical mapping was used to improve the tectonic terrane boundaries based on the physical parameters of different tectonic terrane. Finally, high resolution Moho discontinuity topography was resolved using the iterative inversion method. The variations of crustal thickness in relation to the tectonic terrane were also discussed in Botswana.

Finally, the geodynamic evolution of Botswana based on the evidence from geophysical data (gravity and magnetic data) was presented. The geodynamic evidence and crust movement were produced by combining information obtained from the tectonic terranes, the mafic complexes, geology, earthquake epicentre distribution map and the crustal thickness of Botswana. The combined information from these products have proved that the axis of suturing between the Kalahari and Congo craton in the Damara belt is not a straight line running through the centre of Botswana from north east to southwest as shown by Begg et al., (2009); Hutchins & Reeves, (1980); and Reeves & Canada, (1982). No evidence from the new geophysical data supports such a theory. This study has found that the extension within Botswana is due to the sinking microcontinent in the western part, the recent reactivation of deep fault in the eastern part and the continuing rifting movement in the north western and north eastern part of Botswana.

Keywords: Iterative Inversion, Tectonic Model, Basement Geology, Crustal Thickness Map, Lineament Extraction, Derivatives, Apparent Physical Mapping, Geodynamic Processes, Southern Africa Tectonic Region

ACKNOWLEDGEMENTS

First of all, I give thanks to the almighty God for the precious gift of life; wisdom and understanding that made me sail through academic turbulence. I also thank the Malawi government for offering me the scholarship to study for this Master's degree.

Secondly, I give my heartfelt gratitude to my two supervisors, Dr Mark van Meijde and Mr Islam Fadel for the untiring work and their fruitful discussions that helped me to finish this work. With no background in geophysics, they trusted in my ability to do a research in geophysics and guide me in areas where I was lacking until I finished this work. He who walks alone goes fast but he who walk with people go farther. You made me to go farther. BRAVO.

Deepest gratitude to the members of stuff in the earth systems analysis department especially the earth resource exploration domain for the lectures and academic nurturing you provided me for the entire duration of my study. To my classmates, you guys ROCK, you made my stay at ITC, university of Twente an academic heaven.

I cannot forget to mention the work and encouragement of Mr. Nkhoma and Mrs Susan Mtuwa Phiri, my Mathematics and Geography secondary school teachers respectively, who saw the potential in me and encouraged me and set aside personal time for me. I am here, academically, because of you two. If I ever forget the work and invaluable insight and academic prowess you installed in me and what you did in my academic life let my hands wither and the tongue sticks to the roof of my mouth. It had been 10 years but the academic standards you set for me exist to this day.

To my two workmates, Hendrix kaonga and Harrison mtumbuka: you guys made sure my work is always good by discussing ideas and proof reading my work for any mistakes and scientific soundness of the work and I thank you for that.

To my brothers, Chisi and Levi, my sister Ntchowa and my Dearest Anaphiri, I thank you for the time you have been there for me.

This research work is dedicated to the two sweetest people in my life: Levison Chisenga Sr. and Rosemary Narrat Chisenga.

TABLE OF CONTENTS

LIST OF FIGURES

Chapter 5

Chapter 6

LIST OF TABLES

1. INTRODUCTION

1.1. Background

Solid earth geophysics is the main field for understanding the subsurface and the interior of the earth. It is a main source of information about the lithosphere i.e. crust and the upper mantle. The lithospheric activities include geodynamics and tectonic activities of the earth. This research will use geophysics to study the tectonic activity in Botswana, which is part of the southern African tectonic region.

Regional and continental geophysical studies in Africa have not been extensively done due to incomplete and inadequate geophysical data in some areas. Relatively little was known about the African crust in comparison to other continents (Tedla et al., 2011). As a result, the large part of African crustal thickness is still unstudied (van der Meijde et al., 2014). This affected the global estimates of earth structure including Moho depth which did not reflect the crust thickness in some parts of African. It also prevented the geo-scientific community from doing a detailed crustal and upper mantle modelling using seismology or any geophysical data since the crustal thickness is a crucial parameter for such modelling approach.

The African continent is a very interesting continent in terms of earth's structure. The lithospheric architecture of Africa contains some of the interesting cratons and small fragmented cratons in the world which is sutured by younger mobile belts, cratonic margins and the intra cratonic domain boundaries (Begg et al., 2009). These boundaries and mobile belts along the cratons have been a source of localized successive cycles of extensions, rifting and accretion (Begg et al., 2009). The cratonic movement and its relationship to the mobile belt provide an understanding in the tectonic evolution of African continent (Begg et al., 2009) and the geodynamics of the southern Africa tectonic activities.

The geodynamic evolution of Africa, especially the southern part of Africa, is influenced by the African superswell. The African superswell is the anomalous topographic feature that affected the southern African uplift (Brandt et al., 2011). The African superswell is responsible for the rifting in the east African rift system and the cratonic movement in southern Africa. These cratonic movement, which encompass continental assemblage and cratonic movement between 2.6 billion years and 600 million years ago, resulted in the formation of southern African tectonic region with the major axis in Botswana, Zimbabwe and Namibia (Begg et al., 2009). Of major interest is the converging movement of Kalahari and Congo craton in southern Africa. The axis of suturing of the Kalahari craton in the south and the Congo craton in the north happened along the Damara and Rehoboth belts in Botswana. This zone was called seismicity axis (Hutchins & Reeves, 1980; Reeves, 2000).

Despite being along the interesting tectonic region in southern Africa, Botswana remains one of the least studied countries despite having mineral resources especially diamond within its crust (Schlüter, 2006). Despite this fact, few tectonic studies have been done in Botswana mostly focusing on the tectonic activities in the incipient rift region e.g. Bufford et al., (2012;), the Kalahari Craton in the south to south-eastern part of Botswana e.g. Khoza et al., (2013); and Ranganai et al., (2002) and some isolated tectonic terranes in Botswana e.g. Bordy et al, (2010); and Modie, (2000). The incipient rift region, termed the Okavango rift zone, is an incipient continental rift basin found at the terminal of the south-western branch of the East African Rift System north of Botswana which did not develop into a rift system

(Bufford et al., 2012). These partial studies of isolated region render the tectonic evolution of Botswana not to be fully understood.

Previously, some works has been done in the region to understand the tectonic evolution and the basement geology of Botswana. Two different tectonic models of Botswana have been developed, a regional model and a local model. The regional tectonic model is part of the southern African's tectonic model used in different geophysical studies after Begg et al., (2009). The tomography study by Begg et al., (2009) did not produce good results to resolve the tectonic evolution in the study area and the mantle dynamics. On the other hand, local tectonic model has been developed over the years that include the basement geology of Botswana. Hutchins & Reeves, (1980) studied the tectonic provinces of Botswana based on the magnetic data. In their study, they delineate major mafic complexes, the dyke swarms and tectonic boundaries of these mafic complexes. Their work was improved by Carney et al., (1994); Key & Mothibi, (1999) and Key & Ayres, (2000) who included geological information and log data to improve the basement geology, tectonic model and their boundaries in Botswana. Moreover, Singletary et al., (2003) improved the tectonic model and the basement geology of Key & Ayres, (2000) using geochronology data. They used geochronological results of the isolated basement exposures and drill core samples in Botswana to determine the distribution and temporal evolution of Proterozoic crustal provinces.

Furthermore, Botswana does not have a high resolution crustal thickness model covering the whole country. Crustal thickness provides details and information on the crustal evolution, lithological variation and subsurface tectonic processes (Assumpção et al., 2013). In addition, continental crustal thickness mapping studies like Tugume et al., (2013) have helped to identify areas within the continent for further studies. As such, local studies have been done to further understand the earth crust in high resolution. The crustal thickness models that exist in Botswana are either low resolution from gravity data or cover just part of the country in high resolution. The low resolution crustal thickness models of Botswana are extracts from crustal thickness models of Africa. These include model from receiver function and 1D seismic data (Begg et al., 2009; Tugume et al., 2013), EIGEN-6C gravity model (Tugume et al., 2013) and GRACE level 1B EIGEN-GLO04 gravity model (Tedla et al., 2011). On the other hand, the high resolution crustal thickness models only cover southern and south-eastern part of Botswana. These were produced from seismic data e.g. (Kgaswane et al., 2009; Youssof et al., 2013). These different crustal thickness models have different Moho depths which are not even in agreement in the same tectonic terranes in Botswana. For instance, Youssof et al., (2013) estimated the crustal thickness of Kheis belt to be 48 km. However, Tugume et al., (2013) estimated the thickness to be 39 km with a standard deviation of 3km and Begg et al., (2009) found it to be 41km. These variations in crustal thickness of the tectonic terranes in Botswana are also noticed in some terranes especially the central and northern part of the country. This is probably because the southern and south-eastern part of the country, Kalahari Craton, has been extensively studied.

The availability of high resolution geophysical data of Botswana would improve the understanding of the tectonic and geodynamic evolution of Botswana. The new geophysical data is of high resolution and cover all parts of Botswana unlike previous data that only covered some parts of the country (Hutchins & Reeves, 1980).

1.2. Problem statement

The research aims at improving the tectonic model of Botswana. The geodynamic processes that resulted into the formation of the earth crust underneath Botswana will be explained based on the information obtained from crustal thickness, the tectonic boundaries, tectonic terranes and the major mafic intrusion

in Botswana. Despite all the previous work, no attempt has been done to improve the tectonic model using the high resolution gravity and magnetic data to understand the temporal movement of the African crust in Botswana. The tectonic boundaries, internal architecture and temporal evolution of the buried Proterozoic belts in many cases are still unclear in Botswana (Singletary et al., 2003). Furthermore, the area does not have a high resolution crustal thickness map and the relationship between tectonic terranes and crustal thickness has not been done.

1.3. Research objectives

The main objective of this research is to derive the geodynamic evolution of Botswana based on the tectonic model, crustal thickness and basement geology. The research has the following specific objectives:

1. To improve the tectonic provinces and tectonic boundaries in Botswana.
2. To improve the major mafic subsurface geological structures of basement complex of Botswana.
3. To improve the understanding of the geodynamic evolution of Botswana based on the crustal thickness model
4. To construct the geodynamic processes in Botswana by combining information from crustal thickness, tectonic terranes and mafic intrusions.

1.4. Research questions

1. What improvement does the new geophysical data have on the tectonic terranes and boundaries in Botswana?
2. What relationships have the mafic intrusions of the basement complex of Botswana to the geodynamics processes?
3. What is the relationship of the tectonic terrane boundaries to the geodynamic processes in Botswana?
4. How good can the crustal thickness map explain the geodynamic processes and tectonic evolution in Botswana?
5. What is the variation of the crustal thickness in relation to the tectonic regions of Botswana?

1.5. Methodology

In this section, the methodology used in the research is summarised below and its implementation shown in the flowchart (Figure 1-1). The research used geophysical data (gravity, magnetic and seismic), topographic data, existing basement geology and crustal thickness model (Chapter 3).

1. **Derivatives calculation:** the derivatives in the vertical and horizontal direction are calculated from magnetic and gravity data. The calculated derivatives are used as input in lineament extraction.
2. **Automatic lineament extraction:** the calculated derivatives are used to extract lineaments. The lineaments extracted are used to define the tectonic boundary and tectonic terranes of the study area.
3. **Basement mapping:** the magnetic data is used to delineate mafic complexes of Botswana. The mafic complex is combined with tectonic terrane and compared to geology to produce the basement geology of Botswana.
4. **Apparent physical mapping:** the apparent magnetic susceptibility and apparent density is calculated from magnetic and gravity data respectively. The two are combined to give the apparent physical map which is used to improve the tectonic terranes boundary and basement geology of Botswana.
5. **Inversion:** the gravity data is inverted to produce the crustal thickness of Botswana. The crustal thickness model is validated using the depth estimate produced from seismic data.
6. **Interpretation:** The information from crustal thickness, mafic intrusions and tectonic terranes are combined and interpreted to understand the geodynamic and tectonic evolution of Botswana.

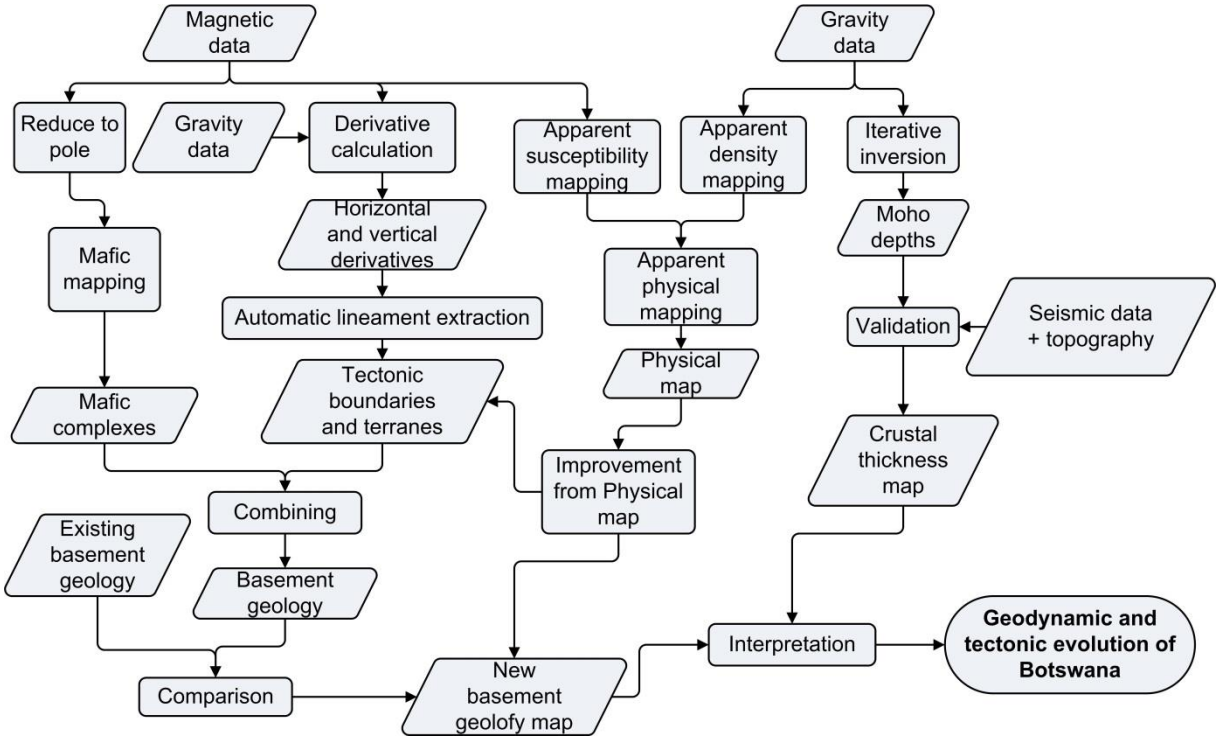

Figure 1-1: flowchart describing the methodology of the research

1.6. Thesis structure

Chapter 1: Introduction

Explains the background to the research, the problem statement, objectives of the research and the questions used to answer the objectives and the summary of the methodology.

Chapter 2: Study area

Description of the study area including the tectonic evolution and the basement geology based on previous studies.

Chapter 3: Dataset

The description of the dataset used in the research

Chapter 4: Tectonic boundary mapping

The description of how geophysical data is used to delineated tectonic boundaries and terranes

Chapter 5: Basement geology mapping

Gives the description of the mafic complex delineation and its combination to the tectonic terrane and the relationship to geology

Chapter 6: Crust thickness and geodynamic modeling

This chapter gives the description of the crustal thickness mapping and its relationship to the geology and tectonic terranes. Finally, the description of the geodynamic processes based on the information from crustal thickness, geology and tectonic terranes

Chapter 7: Conclusion and recommendation

2. STUDY AREA

2.1. Location of Study area

The study area lies within the southern African tectonic region between latitude -18° to -27° N and longitude 18° and 29° E within the boundaries of Botswana. The southern Africa crust comprise of granites and greenstone terrane belonging to early-late Archaean period and subsequent mobile belts in between belonging to the Proterozoic period with the Phanerozoic cover in most areas (Kgaswane et al., 2009; Youssof et al., 2013).

The major tectonic regions of the study area after Youssof et al, (2013), include the Limpopo belt, Kaapvaal craton, Zimbabwe craton, Magondi belt, Kheis belt, Okwa block, Angola-Congo craton, Rehoboth belt and Damara mobile belt (Figure 2-1).

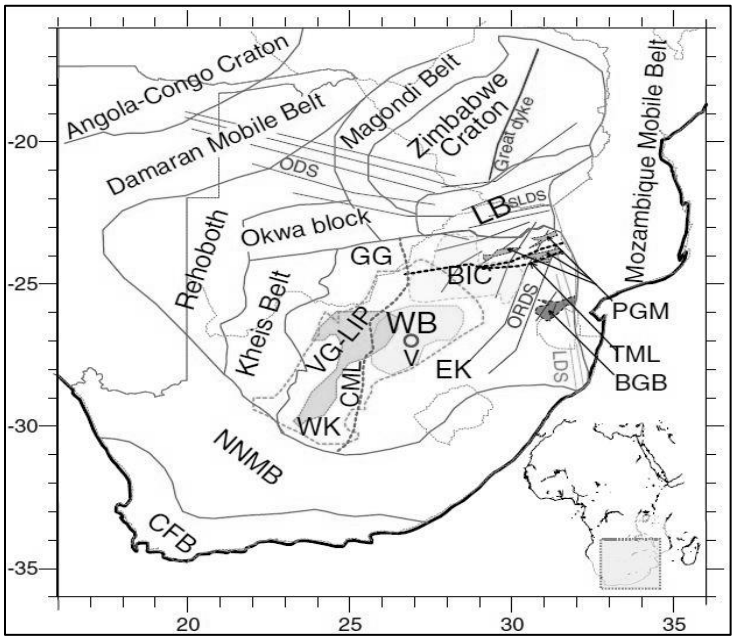

Figure 2-1: Tectonic map of southern Africa showing major tectonic terranes after Youssof et al., (2013): LB = Limpopo belt, GG = Gaborone granite, BIC = Bushveld intrusion complex, VG-LIP = Ventersdop group, WK = Western Kaapvaal craton, CML = Colesberg magnetic lineament, WB = Witwatersrand basin , V = Vredefold impact structure, PGM = Pietsberg-Giyani-Murchison belt, TML = Thambazimbi-Murchison lineament, BGB = Barbeton greenstone belt , NNMB = Namaque-Natal mobile belt , CFB = Cape fold belt, LDS = Lebombo, ODS = Okavango dyke swarms and ORDS =Orifernt river .

2.2. Geology of Study area

The geology of Botswana comprises Precambrian and Phanerozoic geology. The Precambrian geology is comprised of Archaean cratons, Archaean to Proterozoic mobile belts and Proterozoic belts. The Precambrian geology forms the basement complex geology and major tectonic terranes of Botswana. The major rocks of the basement of Botswana are indicated in table 2-1 below. On the other hand, the Phanerozoic geology is comprised of the Mesozoic dyke swarms, the kimberlitic pipes and the Karoo supergroup (Key, & Ayres, 2000). However, most of the study area is covered by Kalahari sands which make it difficult to map the basement and tectonic terranes. The basement is mostly exposed in the eastern part of the country where the Archaean and Proterozoic terranes are exposed (Key, & Ayres, 2000). Beneath the Kalahari sands, in the central and western part of Botswana, exist a Karoo super group called Kalahari basin (Catuneanu et al., 2005; Johnson et al., 1996) which sediments were estimated from drill holes to be up to 2000 meters thick (Key & Ayres, 2000) and about 12000 meters thick from the seismically derived data (Laske & Masters, 1997).

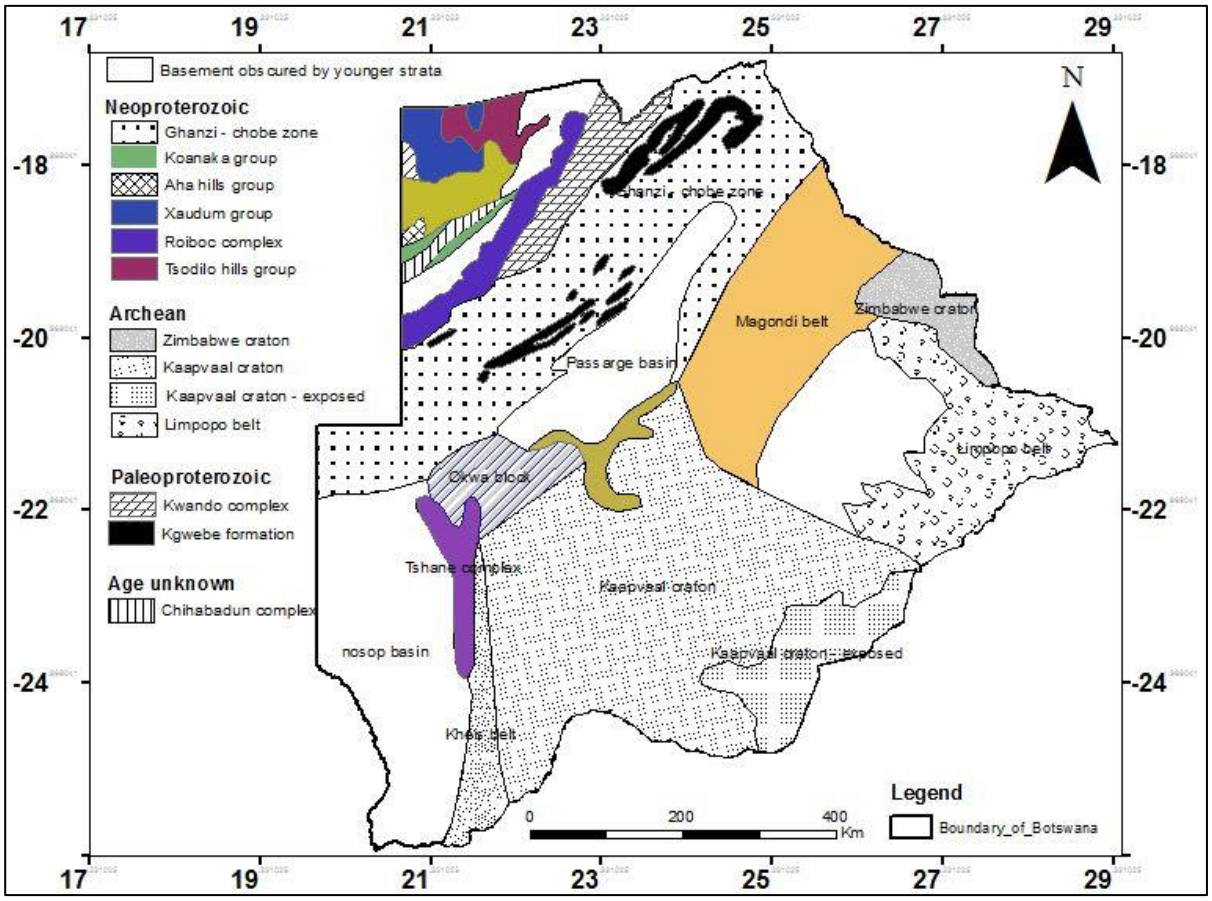

Figure 2-2: The basement geology of Botswana after (Singletary et al., 2003)

Key & Ayres, (2000) produced a Precambrian tectonic terranes and mafic complexes map of Botswana which was improved by Singletary et al., (2003) (Figure 2-2), which include parts of the unexposed geology of Botswana. The basement and tectonic terranes that are unexposed in the Botswana were determined based on the following studies:

1) Routine geological mapping by the geological survey department with the associated drilling of cored boreholes e.g. Carney et al., (1994); Key & Mothibi, (1999); and Key & Ayres, 2000).
2) Groundwater exploration e.g. Zeil & Volk, (1991).
3) Regional airborne geophysical survey e.g. Hutchins & Reeves, (1980).
4) Geochronology data e.g. Singletary et al., (2003).

Rocks	**Av. Density (g/cm3)**	**Av mag Sus (SI)**
Gneissetic granitoid	2.67	0.025
Gabbro	3.03	0.09
Granites	2.64	0.05
Migmitite	2.8	0.025
Basic rocks	2.79	0.12
Ultra-basic rocks	3.15	0.2
Amphibolite	2.96	0.00075
Granite gneiss	2.67	0.025
Dolerite	2.89	0.062
Syenite	2.5	0.051
Sedimentary rocks	2.3 – 2.7	0.018

Table 2-1: rocks of the basement of Botswana after Key & Ayres, (2000) their Average densities after Hunt et al., (1995) and magnetic susceptibility after Clark & Emerson, (1991)

2.3. Tectonic evolution of study area

The southern African crust sits on top of the African superswell which is the anomalous topographic feature that affected the southern African uplift (Brandt et al, 2011). The main tectonic feature in the region is the Kalahari craton which, consist of Zimbabwe craton, Kaapvaal craton and the Limpopo belt, mobile belts and sedimentary basins belonging to Archaean and Proterozoic period (Figure 2-3). The major tectonic evolution of Botswana happened between 2.9-1.2 billion years ago.

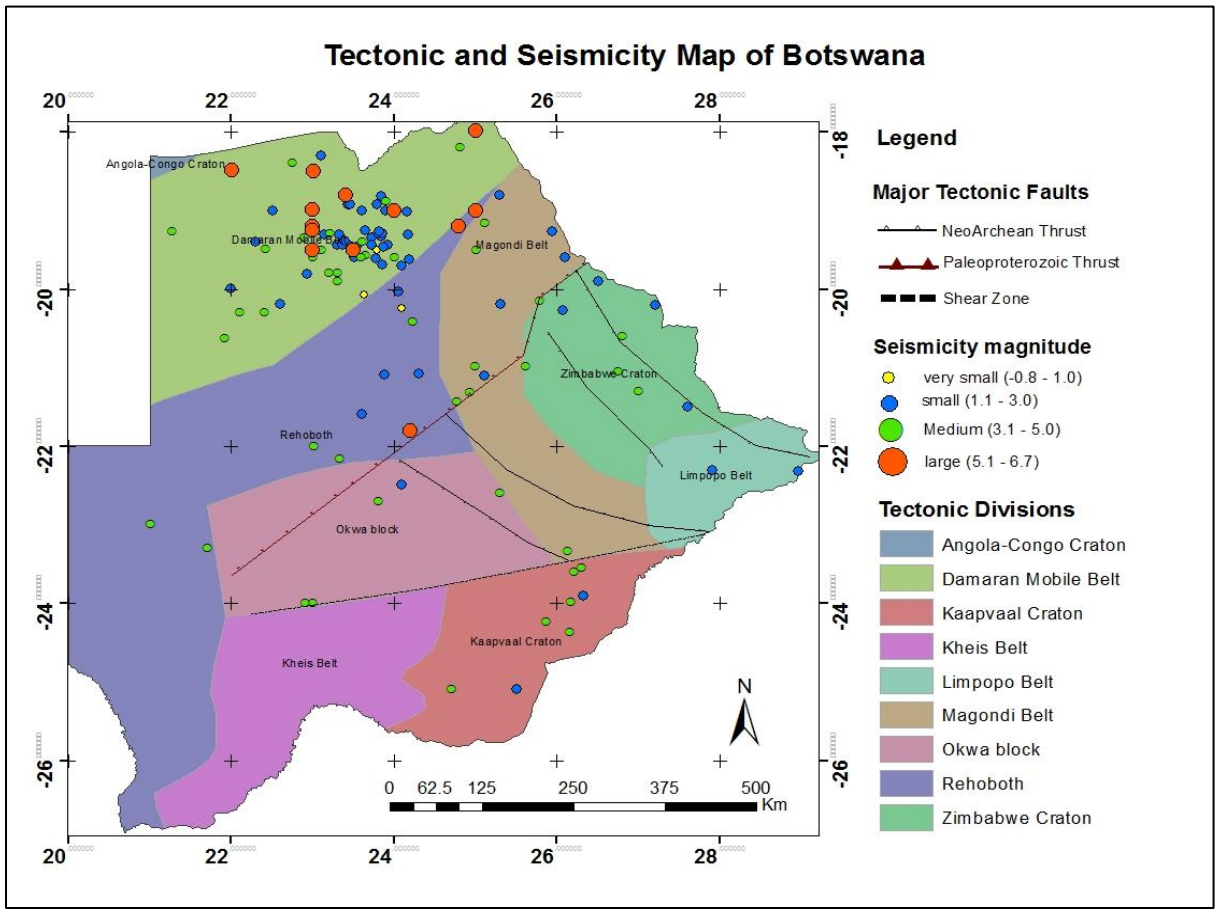

Figure 2-3: The seismic and tectonic map of Botswana (adapted from the tectonic map of southern Africa after Youssof et al., (2013) and structural map of southern Africa after Ranganai et al., (2002)

2.3.1. Archaean terrane

The major Archaean crusts in Botswana consist of Zimbabwe craton and Kaapvaal craton (Figure 2-3). These cratons were formed between 2.9 and 2.6 billion years ago. The Kaapvaal craton consists of granitoid with gneisses and narrow greenstone belt. The craton is covered by the upper Archaean basin (Begg et al., 2009). It was formed earlier than the Zimbabwe craton around 2.9-2.8 billion years ago and was intruded by granitoid around 2.7-2.6 billion years ago (Begg et al., 2009). The Zimbabwe craton on the other hand, was formed around 2.68 billion years ago by amalgamation of east-direction collision (Begg et al., 2009). The Archean crust forms some of the thickest part of Botswana which goes up to 50 km in crustal thickness (Table 2-2).

2.3.2. Archaean with Proterozoic reworked terrane

The Limpopo belt is Archaean crust that was reworked in the Proterozoic era. It is the Archaean mobile belt between the Zimbabwe and the Kaapvaal cratons. It is estimated that it was formed during the 2.7-2.6 billion years collision (Begg et al., 2009) and was affected by granulite-facies metamorphism and granitoid

magmatism at 2.7-2.57 billion years ago. The Archaean crust that was reworked in Proterozoic shows a relatively thicker crust that the other Proterozoic belt (Table 2-2).

2.3.3. Proterozoic terrane

The major Proterozoic crusts in Botswana consist of Kheis belt, Rehoboth province, Magondi belt, Damara belt and Okwa block. These Proterozoic terranes were formed between 2.1 and 1.2 billion years ago. The first to be formed among the Proterozoic terranes was the Magondi belt. The Magondi belt was formed around 2.1-1.19 billion years ago. It consists of thick sequences of sediments and volcanic rocks which were deformed and metamorphosed. To the west of the Kaapvaal craton, basalts and clastic sediments were deposited and formed a tectonic terrane around 1.98 billion years ago. This belt corresponds to Kheis belt. The belt was folded and metamorphosed around 1.9 billion years ago and intruded by granitic rocks around 1.27 billion years and by mafic dikes and sills around 1.12 billion years ago (Begg et al., 2009). The Kheis belt, sutures the Kaapvaal craton to the east and the Rehoboth belt to the west. Around 1.79 – 1.73 billion years ago, a metamorphic event of gneisses and migmatite formed the Rehoboth belt which was underlain by bimodal volcanic around 1.25-1.1 billion years ago and intruded by mafic-ultramafic rocks and granites around 1.4 and 1.2 billion years respectively. The crustal thickness of mobile belts in Botswana is inhomogeneous (Table 2-2). This signifies the working and reworking of these mobile belts which makes them to have very large variation in crustal thickness.

Crust type	Tectonic terrane	Y-study	B-study	T-study	G-study
Archaean crust	Kaapvaal craton, Pietersburg block	34-39km	40km	39km +/-5km	36km
	Zimbabwe craton, Tati block and Okavango dyke swarms	47-51km		36km +/- 1km	34km
Archaean with Proterozoic reworking	Limpopo belt, Central zone	43-45km		44km+/- 3km	
Proterozoic crust	Damara belt		39km +/- 1km		
	Kheis belt	48km	41km	39km +/- 3km	
	Rehoboth		40km		
	Magondi belt		38km +/- 2km		
	Okwa block	34-35km		43km	

Table 2-2: crustal thickness of different terranes from different studies: Y-study = Youssof et al., (2013), B-study = (Begg et al., 2009), T-study = Tugume et al., (2013) and G-study = Gwavava et al., (1992).

In this chapter, the study area was discussed based on the areas that are directly linked to geodynamics processes. Two areas of interest were discussed based on literature, geology and tectonic evolution. Next chapter explains about the datasets obtained from the study area that were used in the research.

3. DATASET

The datasets used in the research are crustal thickness model, magnetic data, gravity data, topography data and seismic depth estimates of Botswana.

3.1. Crust thickness model

A crustal thickness model from satellite gravity was used to compare the improvements that airborne and ground gravity derived crustal thickness has.

The crustal thickness model used in this research was extracted from the crustal thickness map produced by Tugume et al., (2013). The model was produced from EIGEN-6C gravity model. EIGEN-6C is the global gravity model based on data from GOCE (Gravity field and Ocean Circulation Explorer) and other previous satellite data (van der Meijde et al., 2013). This model was chosen over Crust 2.0 (Bassin et al,. 2000) model because Crust 2.0 used few point constraints on crustal thickness for Africa such that difference is substantial in some parts of Africa (Tugume et al., 2013). However, a new global thickness map, Crust 1.0. was produced in 2013 (Laske et al, 2013) (Figure 3-1 (A)). Crust1.0 is better than Crust2.0 and has a higher spatial resolution of "1 degree", which is approximately 110km. However, it has the same problem as Crust2.0 since it cannot be used in areas where there is no seismic information. This is the reason why we cannot rely on it in Botswana (van der Meijde et al., 2014).

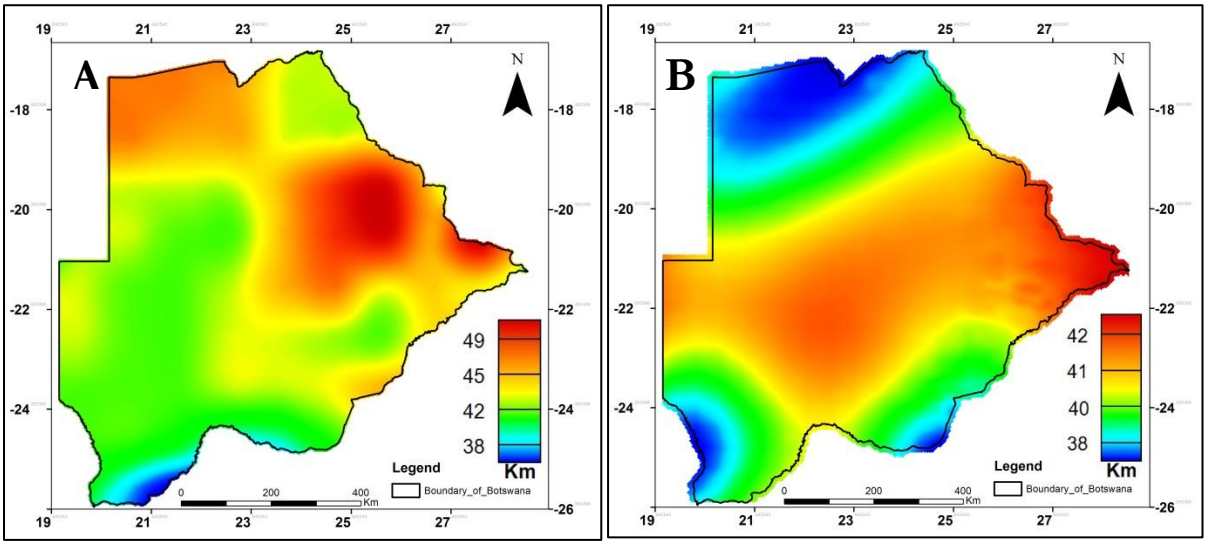

Figure 3-1: crustal thickness models extracts of Botswana (A) crust 1.0 model after Laske et al, (2013) and (B) Tedla et al., (2011) model

Another crustal thickness map of Africa is Tedla et al., (2011) model (Figure 3-1 (B)). The model was produced from Euler deconvolution, which is an automatic inversion method. Euler deconvolution methods as used in the study, used gravity derivatives to locate horizontal surface within the derivatives. Reid et al, (2012) discussed the limitation of Tedla et al., (2011) model in crustal thickness modelling. In their discussion, they compared the crustal thickness of southern Africa from previous seismic studies with the Tedla et al., (2011)model. They concluded that the Tedla et al., (2011) model marked differently on the crustal thickness map of southern Africa. However, Meijde & Nyblade, (2014) replied to the issues raised by Reid et al, (2012). Despite that, their explanation did not solve the problem of difference in crustal thickness between the model and seismic models in southern Africa. Furthermore, the model by Tedla et al., (2011) used a minimum cut-off of 33.25 Km for Euler solutions (Tugume et al., 2013), hence

using the model for comparison might produce unrealistic results if part of Botswana has a crustal thickness thinner than 33.25Km and since it already show considerable difference from the seismic derived crustal thickness model. Therefore, Tugume et al., (2013) model (Figure 3-2 (C)) was adopted as the model to be used in the research.

3.2. Magnetic data

The magnetic data (Figure 3-2 (A)) was used for delineating the tectonic terranes and boundaries, apparent physical mapping and mafic complex mapping.

The magnetic survey of Botswana was conducted between 1976 and 1987 ("ACP Data by country," 2014). The first aeromagnetic survey of Botswana started in October 1975. A total of 150 000 km lines survey was flown and interpreted in 1977 (Hutchins & Reeves, 1980). However, new magnetic data were obtained between 1977 and 1987 which covered the entire Botswana. The magnetic data has a spatial resolution of 250 meters. The coordinate system used was the World Geodetic system of 1984 (WGS1984) datum and Universal transverse Mercator zone 34 and 35 south projections.

3.3. Gravity data

The gravity was used for delineating the tectonic terranes and boundaries, apparent physical mapping and crustal thickness modelling,

The gravity data of Botswana was obtained in two surveys. The national wide gravity survey of Botswana was conducted in 1972-1973 gravity survey and the 1998-1999 gravity survey.

The first national gravity survey of Botswana started in 1972 with funding from the British oversees development ministry (Hutchins & Reeves, 1980). The survey was done in two phases; the first phase was thrown by aircraft with a gravitational reading accuracy of 0.02 mGal and a total of 23 gravitational base stations. The second phase involved the establishment of 1854 gravity stations, tying of 277 gravity stations from Ngami land survey. The survey was ground survey with a sampling distance of 10 km. furthermore, 300 station in inaccessible areas were done using helicopter (Hutchins & Reeves, 1980). The gravity survey of 1972-1973 had an average density of 37 gravity stations per 100 km2 (Yawsangratt, 2002). The 1998-1999 gravity survey was conducted to fill in the gap not covered by the first gravity survey of 1972-1973.

The gravity data provided for the research was Bouguer anomaly map data (Figure 3-2 (B)). Bouguer anomaly is the gravity anomaly in which correction has been done for height at which it was measured and the attraction due to terrain. The coordinate system for the Bouguer anomaly map was World Geodetic system of 1984 (WGS1984) datum and Universal transverse Mercator zone 34 and 35 south projections.

3.4. Seismic data

In this research, seismic data was used to validate the crustal thickness model derived from gravity data. The seismic data used in this research was the Moho depth estimates for receiver function at 13 locations in eastern and south-eastern Botswana.

The seismic data was collected from work by Youssof et al.,(2013) and Kgaswane et al., (2009) (Table 3-1 and their spatial location shown on Figures 3-2 (A)-(D)). The depth estimates from these two datasets ranges from 39km to 50 km which is higher than the ranges from regional gravity model by Tugume et al., (2013). However, Kgaswane et al., (2009) used joint inversion of surface waves and receiver function

method in their research while Youssof et al.,(2013) used HK-stacking technique in the determination of earth structure in their research. The method by Kgaswane et al., (2009), joint inversion of surface waves and receiver function method, has a weaker vertical and lateral resolution which can introduce non-uniqueness in the results. The Youssof et al.,(2013) overcame these limitation by using the full HK-stacking interpretation of the available data. HK-stacking is the method which uses the average Moho depth (K) and the ratio of velocity of primary wave to velocity of secondary wave (K) of several predicted amplitude and wave arrival times to estimate the crustal thickness. Their approach distinguished the small variation in the crustal structure in the Kalahari Craton. With this back ground, the Youssof et al.,(2013) seismic data points were used to validate the gravity derived Moho depth of Botswana produced from this research.

Point ID	Lat	Long	Kgaswane et al., (2009)	Youssof et al. ,(2013)
Kaapvaal - SA59	-24.84	24.4	40.5	41.5
Kaapvaal - SA60	-23.85	24.9	40.5	41.5
Kheis-Okwa belt - SA61	-23.95	24.0	43.0	43.5
Kaapvaal - SA62	-24.85	25.1	40.5	40.5
Kaapvaal - SA63	-23.66	26.0		43
Kheis-Okwa belt - SA64	-22.97	26.2	40.5	41
Limpopo belt - SA65	-22.82	27.2	40.5	43
W Zimbabwe - SA66	-21.9	26.3	48	46.5
W Zimbabwe - SA67	-21.89	27.2	45.5	39.5
Limpopo belt - SA68	-21.95	28.1	45.5	41
W Zimbabwe - SA70	-21.09	26.3	50.5	50.5
W Zimbabwe - SA71	-20.93	27.1	43.0	40.5
LBTB	-26.93	23.04	43.0	41.5

Table 3-1: Seismic points data from different sources for depth estimates.

3.5. Topographic data

Topography data was used for crustal thickness modelling. The data was added to the Moho depth to produce crustal thickness of Botswana. The Moho depth is the distance between sea level, the reference geoid, and the Moho discontinuity which is the boundary between the earth crust and the upper mantle. The elevation is the distance between the sea level and the surface. Therefore, the crustal thickness is the distance from the surface to the Moho discontinuity.

The topographic data used in the research was ETOPO1 data. The data was downloaded from the National Geophysical data centre's National Oceanic and Atmospheric Administration (NOAA) website (http://www.ngdc.noaa.gov/mgg/global/global.html). The ETOPO1 was used as it is high resolution, about 1.8 km, compared with previous ETOPO data, ETOPO 2 and ETOPO5. ETOPO1 is a 1 arc-minute global relief model of Earth's surface that integrates land topography and ocean bathymetry. It was built from numerous global and regional data sets (National Geophysical Data Center, 2014).

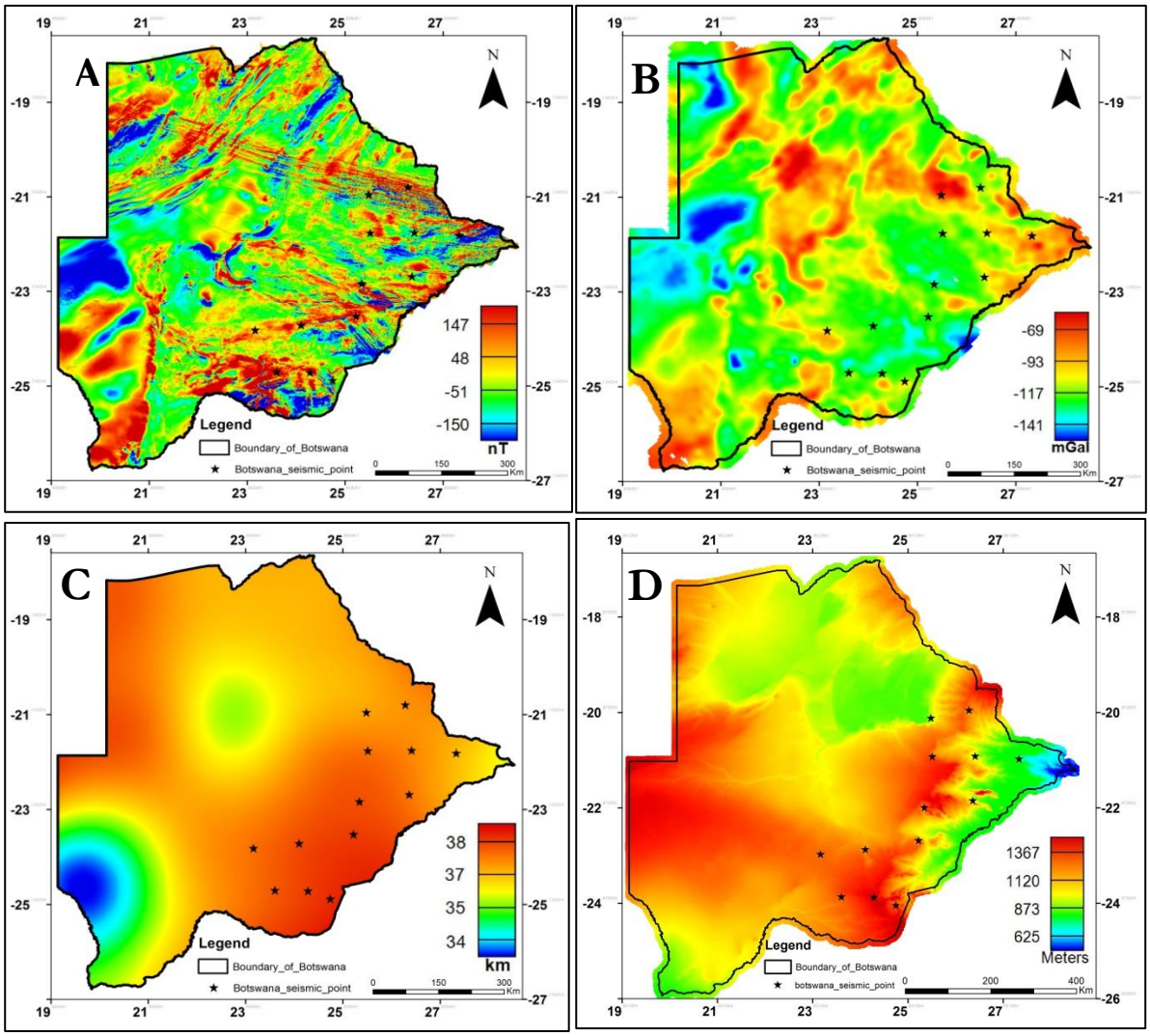

Figure 3-2: Map of datasets used in the research, boundary of the study area is shown in black and the seismic point stations shown as black stars (A) Total Magnetic Intensity Map (B) Bouguer Anomaly Map (C) crustal thickness map of Botswana from Tugume et al., (2013) and (D) Elevation Map of Botswana from ETOPO1 data

The datasets used in the research was discussed in this chapter. The previous chapters have discussed the study area and the problem statement which act as a basis for this research. The information from these previous chapters together with dataset chapter will be used in the subsequent 3 chapters which are: chapter 4: Tectonic boundary mapping, Chapter 5: Basement mapping and Chapter 6: Crustal thickness and geodynamic modelling.

4. TECTONIC BOUNDARY MAPPING

4.1. Introduction

This chapter explains how to delineate the tectonic boundary and the tectonic terranes using automatic lineament extraction from first vertical (VD) and horizontal derivatives (HD) of gravity and magnetic data. The output of this chapter is the delineated tectonic terranes and boundaries which will be used as input in the basement mapping.

In this research, a tectonic province, sometimes referred to as tectonic terrane, is defined as fault-bounded area or region with a distinctive faults and structure orientation, shape and pattern, and lithology from the surrounding. On the other hand, tectonic boundary is defined as a fault, or connection of faults, that separates different tectonic provinces.

4.2. Methodology

Figure 4-1 below summaries the implementation of tectonic boundary mapping.

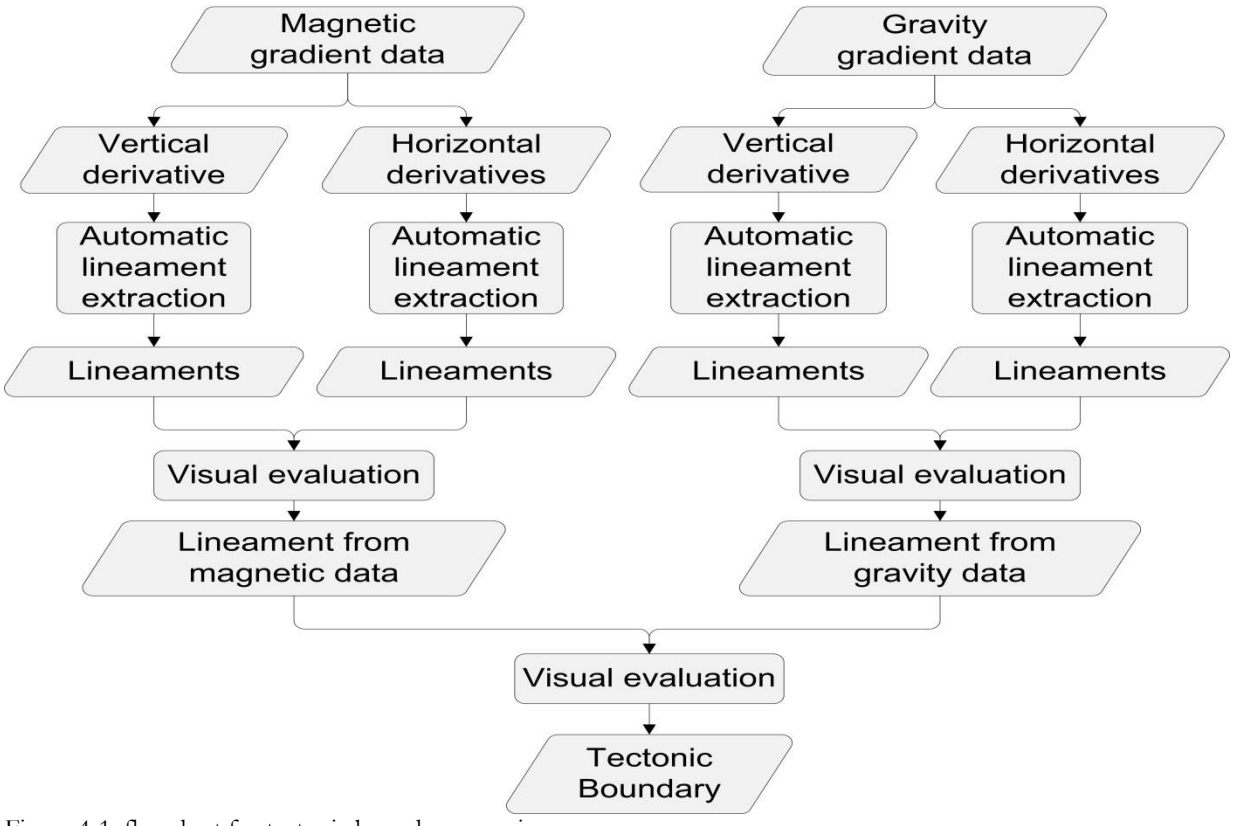

Figure 4-1: flowchart for tectonic boundary mapping

The automatic lineament extraction was used to extract tectonic lineaments from the input data. Then, visual image classification was used to classify the extracted lineaments and derivative images into tectonic terranes and boundaries. The implementation steps for this chapter are:

1. Calculating vertical and horizontal derivatives from magnetic and gravity data
2. Extracting lineaments from the calculated derivatives

3. Interpret boundaries and terranes from gravity extracted lineaments
4. Interpret boundaries and terranes from magnetic extracted lineaments
5. Combining boundaries and terranes interpreted from gravity and magnetic derived lineaments
6. Comparing the delineated terranes with existing terranes from literature

4.2.1. Derivatives

The derivatives enhance the lateral and horizontal variation of geophysical signal and other data e.g. gravity and magnetic data. The derivative calculation sharpens anomalies caused by abrupt changes in near-surface bodies at the expense of broader anomalies caused by deeper or more gradual signal changes (Jachens & Blakely, 1986). Derivatives also enhance short wavelength anomalies while suppressing long wavelength components caused by deep-seated features, allowing more accurate geological/tectonic contact and edge detection (Ranganai & Ebinger, 2008). Short wavelength anomaly are associated with surface to near surface bodies while long wavelength anomaly are associated with bodies that are not close to the surface.

The derivatives have been used before in structural interpretation, geological mapping and basin modelling e.g. Boyce & Morris, (2002); and Oruç et al, (2013). However, the derivatives act as a high pass filter which enhances short wavelengths while suppressing long wavelength signals which can be hard to identify deep seated faults and boundaries (Mantlík & Matias, 2010). Vaish & Pal, (2014) have tried to enhance the tectonic boundaries for geological mapping using derivatives and correlate it with the tectonic setting and subsurface geological structures of the region. In their study, they delineated the major lineaments using derivatives and compare them with the deep earth structures to establish the relationships. They concluded that lithological boundaries and structural boundaries are well correlated with the existing geological map of the area they were working in. Furthermore, the structural mapping could be used to improve the understanding of gravitational imprints of the geological units, faults, lineaments and seismo-tectonic set up of a region. Most studies use the first order derivative to delineate faults and lineaments, for instance Feumoe & Ndougsa-mbarga, (2012). However, the second order derivative is more effective than first order derivative in delineating the boundaries as well as structural faults (Vaish & Pal, 2014). However, it is difficult to delineate major faults especially the faults with no or little vertical displacement. Zeng et al., (1997) suggested a method of identifying such faults using second vertical derivatives of potential filed data. This background establishes the capability of derivative data to delineate the tectonic faults despite working with the short wavelength signal of the potential filed data.

4.2.1.1. Derivatives calculation

The first step in the tectonic boundary mapping was to calculate the input data used for lineaments extraction. The vertical derivatives (Figure 4-2 (A) and (B)) and horizontal derivatives were calculated in space domain using a vertical derivative convolution utility and horizontal gradient calculation utility respectively in Oasis Montaj.

The horizontal derivatives were calculated to enhance boundaries in four major directions to enhance trending pattern in the N-S, W-E, NE-SW and NW-SE trends (Table 4-1). The angle of enhancement of horizontal derivative was from the x-direction in the counter clock wise (CCW) direction.

The four directional derivatives showed different enhancement based on the enhanced directional. Individually, each of the directional horizontal derivatives contributes information. However, the combination of the four gradient derivatives gave the 4 directional horizontal derivatives on one image. The first order horizontal derivatives for gravity data were combined (Figure 4-3 (A)). Likewise, the first order horizontal derivatives for magnetic data were also combined (Figure 4-3 (B)).

Derivative direction		uses
Horizontal Derivative	CCW, x + 45 o	To enhance boundaries trending in the Northeast – Southwest direction
	CCW, x + 90 o	To enhance boundaries trending in the North – South direction
	CCW, x + 135o	To enhance boundaries trending in the Northwest – Southeast direction
	CCW, x + 180o	To enhance boundaries trending in the East – west direction

Table 4-1: parameter for calculation of boundary of the horizontal derivative.

The derivatives were exported from Oasis Montaj as geotiff using 256 grey scale colour depth of 8 bit which is the image format acceptable in the automatic lineaments extraction software used in this research.

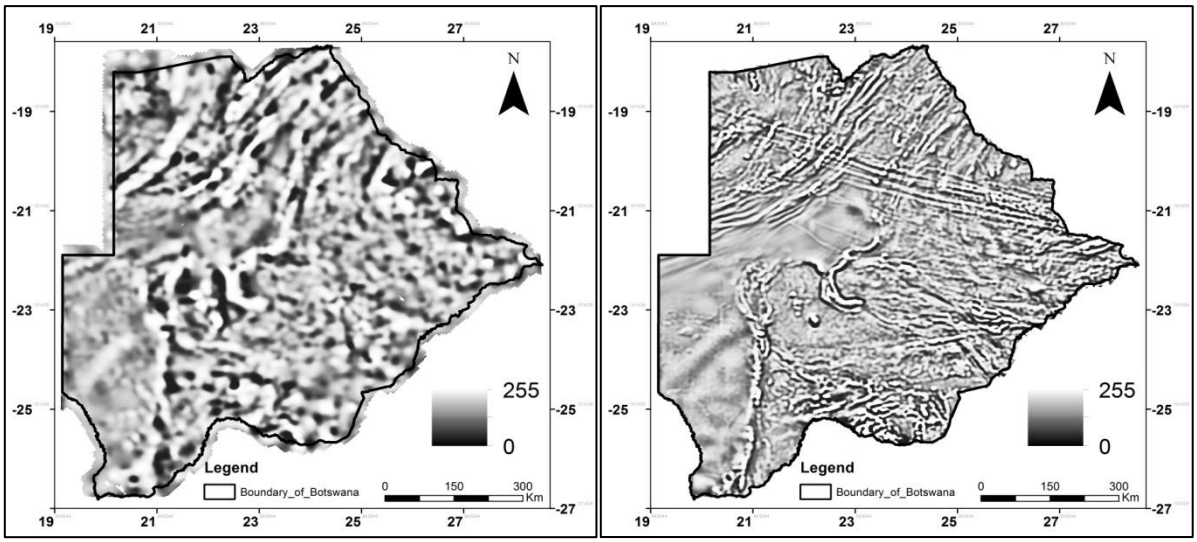

Figure 4-2: (A) 1st vertical derivative of gravity data and (B) 1st vertical derivative of magnetic data

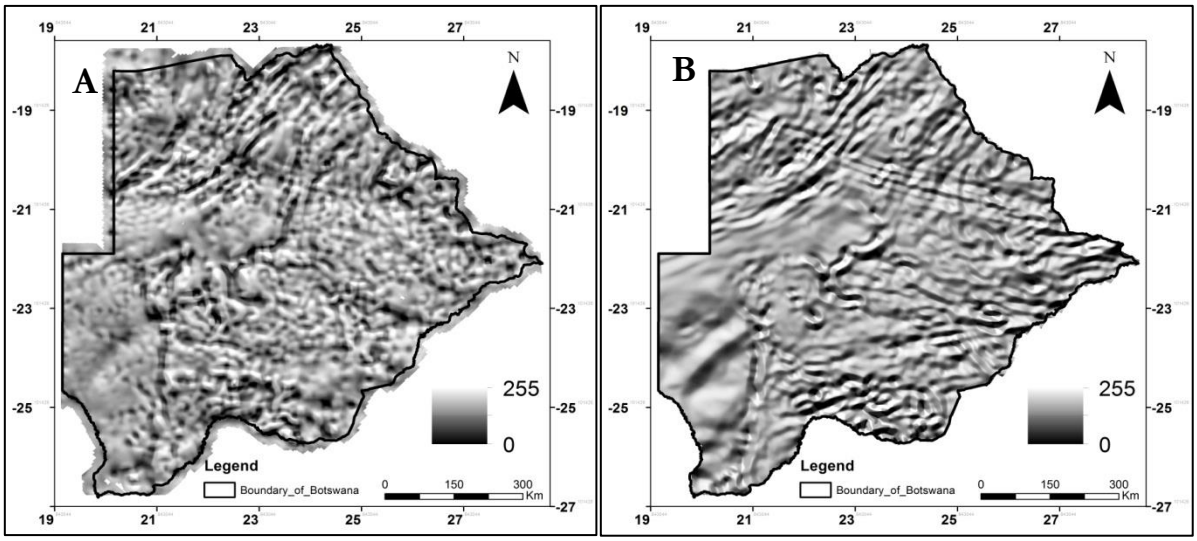

Figure 4-3: (A) Combined first horizontal derivative for gravity data and (B) Combined first horizontal derivative for magnetic data

4.2.2. Lineament extraction

Lineaments are any linear features e.g. tectonic fault, roads, and lithological boundaries. In this research, lineaments are all linear features that are geological in nature i.e. faults, joints and boundaries.

The lineaments extraction process is divided into two category, 1) the visual extraction and 2) automatic or (semi) – automatic extraction (Sukumar & Nelson Kennedy Babu, 2014). Both categories are useful depending on the circumstances (Table 4-2). The visual lineaments extraction methods involve visually digitising the lineaments on an image. However, enhancement on the image is done before digitising. These enhancements are done using directional and non-directional filters like vertical and horizontal derivatives, principal component analysis, and contrast stretching among others. The automatic lineaments extraction, on the other hand, uses the computer aided techniques based on edge filtering techniques (Hung et al., 2005). The algorithms that are used in edge detection extracts lineaments from either the first derivative or second derivative of the input image. The algorithms that extract lineaments from the first derivative of an input image include Canny algorithm (Canny, 1986), Sobel algorithm (Sobel, 2014) and Prewitt algorithm (Prewitt, 1970) while those that extract lineaments from the second derivatives of an input image includes laplacian algorithm.

Visual extraction	**Automatic lineament extraction**
- Depend on the quality of the performance of the image (on paper and/or screen)	- Depend on only the quality of the image
- Partly depend on the complexity of the research area	- Totally depend on the complexity of the research area
- Strongly depended on human experience and ability	- Totally depend on the mathematical function of software
- Takes a lot of time	- Very quick
- Strong effect of human subjectiveness	- Little effect of human subjectiveness
- Easy to distinguish the kind of lineament (tectonic setting, manmade, etc.)	- Cannot recognize the kind of lineament, so the result may be confused.
- Simple but subjective method	- Complex but objective method

Table 4-2: difference between visual and automatic lineament extraction after Hung, (2001)

In this research, canny edge detection method was used in extracting linear features. Canny edge detection method was developed by Canny, (1986). The algorithm was chosen because it is a well-defined and mostly used algorithm because of being a good detector, good localized algorithm and has an ability to a single response to an edge compared to other edge detection algorithms (Ding & Goshtasby, 2001) The lineament extraction is implemented in three steps;

1) The production of the edge strength image which involves the filtering of the image with a Gaussian filter (Kiran R.S & Ahmed, 2014), Gaussian filter smoothen the image to remove noise pixel. Then the calculation of the first derivative from an image both in the vertical and horizontal direction (Marghany & Hashim, 2010) and finally the suppression of pixels that do not represent local maxima of the edge strength map to zero..
2) The edge strength image is then thresholded to produce a binary image based on the input threshold parameter**.** All the pixels that represent local maxima edge on the binary image are returned on the binary map.
3) Lastly, the linear features are extracted from the binary image. In their paper, Kiran et al., (2014) described two steps of extracting lineaments from the binary image; the first was the application of a thinning algorithm described by Lam et al., (1992) where the line is iteratively eroding the boundary cells until its one cell size thick. The remaining layers represent the linear boundary in binary skeleton linear features. Then, it is followed by a sequence of pixels for each feature which are extracted from the image to form a linear feature.

The canny edge detection algorithm is implemented in the Line module within PCI Geomatica software. Previously, Line module in PCI Geomatica has also been used in geological work to extract faults and lineaments for structure and geological interpretation (Bishta, 2009; Hubbard et al,. 2012; Kocal et al., 2003; Saud, 2008; Thannoun, 2013).

4.3. Automatic lineament extraction

This section explains the process of extracting lineaments from the derivative data.

4.3.1. Edge detection

The first derivatives of the magnetic and gravity data were used as input in the algorithm. As such, the resulting lineaments are from the second derivatives since the algorithm calculates a first derivative on the input image.

4.3.2. Parameters

Two approaches are used in making the choices of optimal parameters for lineaments extraction. The first one is the knowledge based approach. In knowledge based approach, known lineaments are used as references for the extraction process. The parameters are adjusted until the extracted matches the reference lineaments. The rest of the extracted lineaments are considered to be the true lineaments based on those parameters defined using reference lineaments. The second approach is the data driven approach. In this approach, the parameters are adjusted and the sensitivity of each parameter in extracting process is considered. The data driven approach is not done blindly but based on the type of data and the area of interest as well as the spatial resolution of the extracted lineaments.

This study used the data driven approach in the lineament extraction process. Previous studies in the region, as described in chapter 1, did not delineate tectonic lineaments using geophysical data. The existing lineaments are estimated based on drill core data, geochronology data, geological data and finally the mafic complexes delineated from magnetic gravity (Carney et al., 1994; Hutchins & Reeves, 1980; Key & Ayres, 2000; Reeves & Canada, 1982; Singletary et al., 2003). As such, to avoid using estimated lineaments, the data driven approach was used.

To produce optimal parameters in the data driven approach, parameters are adjusted until suitable lineaments are produced (Hung et al,. 2005). However, In their study, Kocal et al., (2003) produced suitable parameters for rock discontinuity from satellite imagery and Thannoun, (2013) produced optimum parameters for extracting lineaments in tectonic environment. Kocal et al., (2003) advocated that you cannot define the scale but rather changing the parameters, until reaching acceptable value, the lineament of interest are delineated. Their approach was also used by other authors (Hubbard et al,. 2012; Thannoun, 2013). In the current study the following parameters: Edge gradient threshold, Curve length threshold, Line fitting cross threshold, Angular difference, Linking distance threshold parameters were defined as indicated in table 4-3 below.

	Gravity gradient data		Magnetic gradient data	
Parameter/image	VD	HD	VD	HD
Filter radius (pixels)	20	20	20	20
Edge gradient threshold	75	75	75	75
Curve length threshold	10	10	10	10
Line fitting cross threshold	2	2	2	2
Angular difference	90	90	90	90
Linking distance threshold	0	0	0	0

Table 4-3: optimal parameters for automatic lineament extraction of derivative data

- **Filter Radius:** This defines the radius of edge detection and Gaussian filter, in pixels. A pixel, cell size, in this research is equivalent to 1 km cell size for gravity data and 0.25 km for magnetic data. The Gaussian filter determines the spatial resolution and filtering of noise and high frequency data based on the size of the kernel defined. This parameter roughly determines the smallest-detail level in the input image to be detected. A 40 km kernel for gravity and 10 km kernel for magnetic had been chosen representing a 20 pixel sized kernel radius. This value had been chosen to include lineaments of 10 km (Thannoun, 2013) long and above.
- **Edge Gradient Threshold:** the parameter defines the minimum change in brightness which is used for defining edges. Derivative images have a positive and a negative part of a lineament indicated by a white and black color on the gray scale image. The black represented by 0 or near zero values while white represented by 255 or near 255 values. The parameter's threshold takes every abrupt change between 0 and 255 as a lineament above the defined parameter values. Thannoun, (2013) defined the values of 75 on a 0-255 grey scale image as an appropriate value to extract lineaments associated with tectonic environment.
- **Curve Length Threshold:** This parameter specifies the minimum length of curve in pixel distance, it maps linear curve features as valid lineaments. This research extracted all lineaments above 10km in length for gravity data and 2.5km in length for magnetic data. These length correspond to the value of 10 pixels in a tectonic setting (Thannoun, 2013).
- **Line Fitting Threshold:** This specifies the maximum error in pixel distance allowed in fitting a polyline to pixels defining a curve. In this research, 2 pixels error margin was chosen representing 2 km for gravity data and 0.5 km for magnetic data. Previous studies had used the value of 2 pixels (Thannoun, 2013) and 3 pixels (Hung et al,. 2005; S & Ahmed, 2014) for the line fitting threshold.
- **Angular Distance Threshold:** This specifies the maximum angle in degrees between segments of a polyline below which they can be linked as a single line or vector. The algorithm accepts values between 0-90 degrees. To extract all the lineaments in for all angles, 90 degrees angular distance threshold was used for both magnetic and gravity data.
- **Linking Distance Threshold:** This specifies the minimum distance in pixels between end points or two polylines for them to be linked. Lineaments cannot be connected when the data values indicate no such lineament. As such, the value of 0 was used in the research.

4.4. Tectonic boundary mapping methodology

In this section, visual classification of lineaments is explained which was used for tectonic boundary mapping. The criteria used for the mapping of boundaries are shown in table 4-4 below.

criteria	Element	Reason
Visual interpretation	Continuity	-The lineament pattern has to indicate a boundary like feature in the continuity form despite having gap in between.
	Pattern	-The arrangement of lineaments and the form of occurrence was an indication of tectonic pattern. Similar pattern was indicative of same tectonic province.
	Texture	-the lineament texture, e.g. density of lineaments, regions of no lineaments, was used as indication of tectonic terrane
	Association	-The lineaments association in relation to their surroundings. Dense lineaments surrounded by no or few lineaments were indicators of a tectonic province.
	Size	-Since the lineament and edges delineated can either be faults, boundary of lithologies or tectonic boundaries, long lineaments may indicate tectonic boundary in some cases. However, this criteria was not used in isolation as other criteria were considered as well
Image combination	The extracted lineament cannot give the best tectonic province on its own but rather combined it with derivative images. This criteria was introduced by Hung, (2001) as indicated in visual vs automatic interpretation in table 4-2 above.	

Table 4-4: interpretation criteria based on the extracted lineament

The criteria defined above were used to delineate boundaries from the lineaments extracted from first vertical and horizontal derivatives of the magnetic and gravity data. The boundaries from vertical and horizontal derivatives of magnetic data were combined to produce one boundary from magnetic data. Likewise, the same was applied to gravity derivatives derived lineaments to produce the boundary from gravity data. Finally, the two boundaries were combined to produce one single tectonic boundary from these two dataset.

4.5. Tectonic boundary mapping from gravity data

This section explains how lineaments extracted from gravity data, both from first vertical and horizontal derivate, were interpreted for tectonic boundaries. In the interpretation, the visual classification criteria as described in table 4-4 above were used.

4.5.1. Boundary from vertical derivative

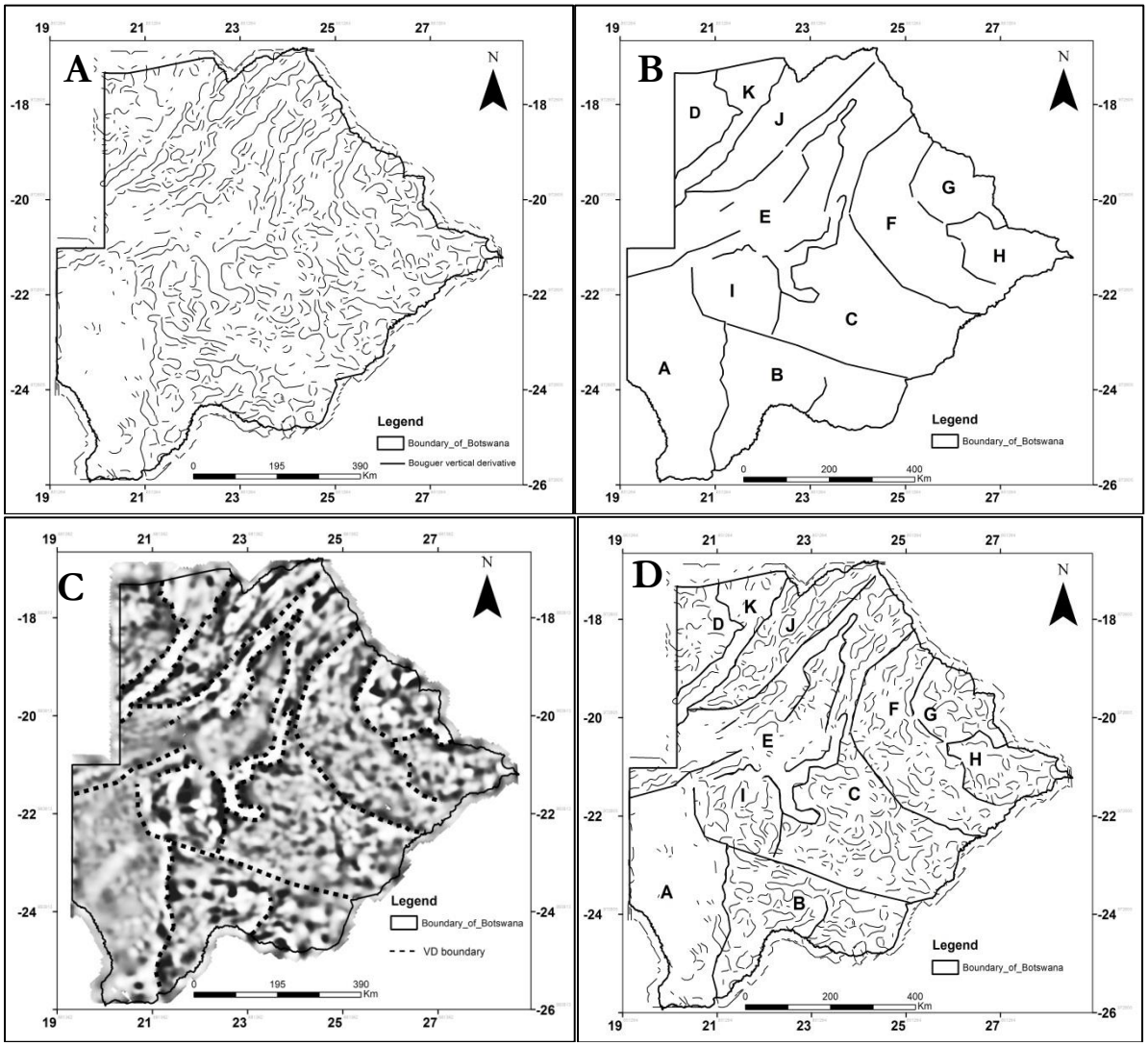

Figure 4-4: (A) lineaments extracted from VD gravity; (B) tectonic boundary from VD gravity, (C) tectonic boundary overlaid on VD gravity and (D) tectonic boundary overlaid on extracted lineaments

The main interpretation was the continuity and pattern of the extracted lineaments. For instance, boundaries between regions D, K and J on the north-western part of the study area had a clear continuity boundary (Figure 4-4 (A), (C) and (D)). Region G had continuous long lineament boundary on the north eastern part (Figure 4-4 (A), (C) and (D)). However, shape and pattern of the lineaments differentiate it from region F to its west and H to its south (Figure 4-4 (A), (C) and (D)). These two regions have a north-south trending almost straight pattern and rounded uneven distributed patterns, respectively. Some regions, for instance regions A and E, were classified as tectonic province based on the lack of or very few lineaments (Figure 4-4 (A) and (D)). From these areas, especially A had very few lineaments associated with it. However, region E was different. It had a slightly higher lineaments density than region A. As such, tectonic boundaries were delineated but the extent of different tectonic provinces not defined. The areas B, C, F and I were delineated based on the texture and shape of lineaments. The region encompassing these 4 has almost similar trending of lineaments. However, F has longer lineaments with mostly North-south trending as boundaries (Figure 4-4 (A), (C) and (D)), region B had mostly almost west-east trending lineaments and a region to its north of few lineaments which indicate probably a different province (Figure 4-4 (A)) and finally region C has uneven shaped, size and trending lineaments.

4.5.2. Boundary from Horizontal derivative

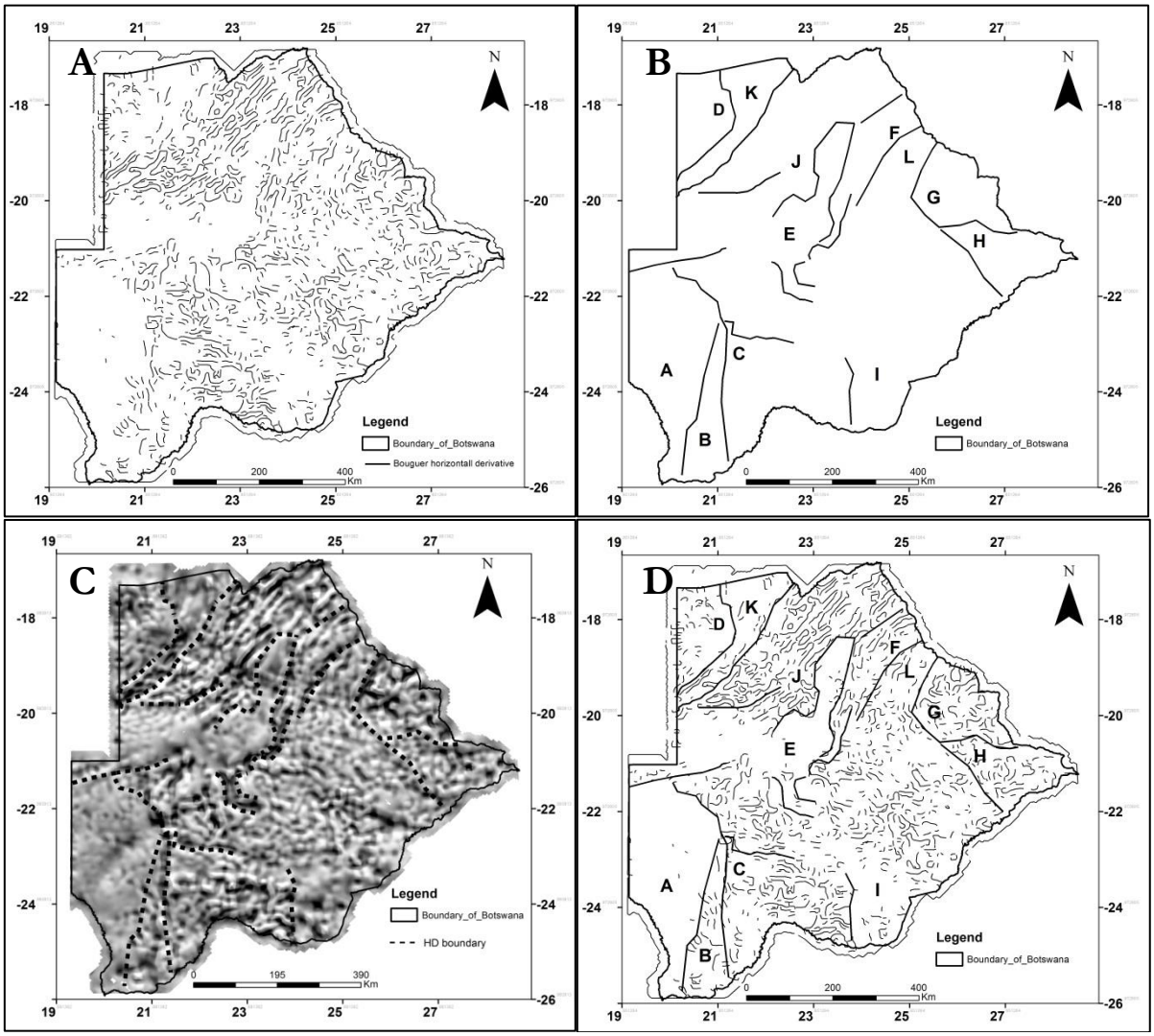

Figure 4-5: (A) lineaments extracted from HD gravity; (B) tectonic boundary from HD gravity, (C) tectonic boundary overlaid on HD gravity and (D) Tectonic boundary overlaid on extracted

The tectonic provinces interpreted from lineaments extracted from the horizontal derivatives (Figure 4-5 (A), (C) and (D)) are more difficult to interpret than those delineated from the vertical derivatives (Figure 4-4 (A), (C) and (D)). A similar interpretation of lineaments as from vertical derivative was used for the horizontal derivative. However, some differences were visible from the interpreted boundaries. Some new region exist from the horizontal derivative derived boundaries that were not there on the vertical derivative derived boundaries, for instance regions B and F. The eastern boundary of region B (Figure 4-5 (D)) coincides with the boundary of region A on the vertical derived boundary (Figure 4-4 (D)). To the west of the boundary of B some lineaments exists which were not visible on the vertical derivative derived lineaments, this region corresponds to a new tectonic region. This new boundary between region A and B was based on the different texture of lineament (Figure 4-5 (A), (C) and (D)) and not so clear boundary, which may be a representation of a fault, on it. Another region was F which was not on the vertical derived boundaries, (Figure 4-4 (D) in section 4.6.1). The boundary was delineated from continuous lineaments that separate F from J regions. Unlike vertical derived boundaries, section 4.6.1, most of the horizontal derived boundaries are based on the association and density of lineaments rather than a clear boundary between them especially for region G, H and B on figure 4-5 (A), (C) and (D).

4.5.3. Combining VD and HD boundaries from gravity

The boundaries extracted from the vertical and horizontal derived lineaments were combined to give tectonic boundaries from gravity data. The combination of these two boundaries indicates a good spatial correlation between them. However, in some cases, one derivative produced a boundary which is not delineated on the other. The following criteria was used to combine the boundaries

- **Missing boundary** – if a region had a boundary from one data and missing in the other, that boundary was included in the final model.
- **Correlated boundary** – if the two boundary from the data sets were in the same position, the boundary was maintained
- **Slightly different boundary** – if the two boundaries were slightly on different position but that represent the same boundary, a choice between the two will be taken based on how well the boundary delineation was as described.

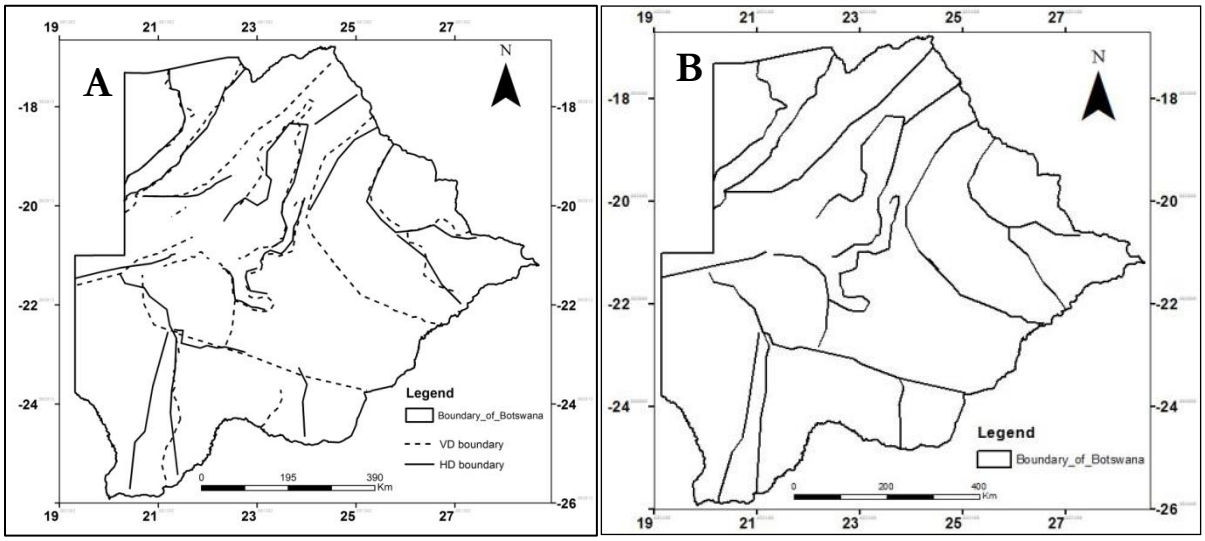

Figure 4-6: (A) overlay of two boundaries from gravity and (B) combined boundary from gravity

The criteria defined above produced the tectonic boundary (Figure 4-6 (B)) based on the combination of vertical and horizontal derived boundaries (Figure 4-6 (A)).

4.6. Tectonic boundary mapping from magnetic data

The interpretation of the tectonic boundary from magnetic data used the same approach taken in interpreting the gravity lineaments, section 6.5. The vertical and horizontal derived lineaments of the magnetic data were used in the interpretation.

4.6.1. Boundary from vertical derivative

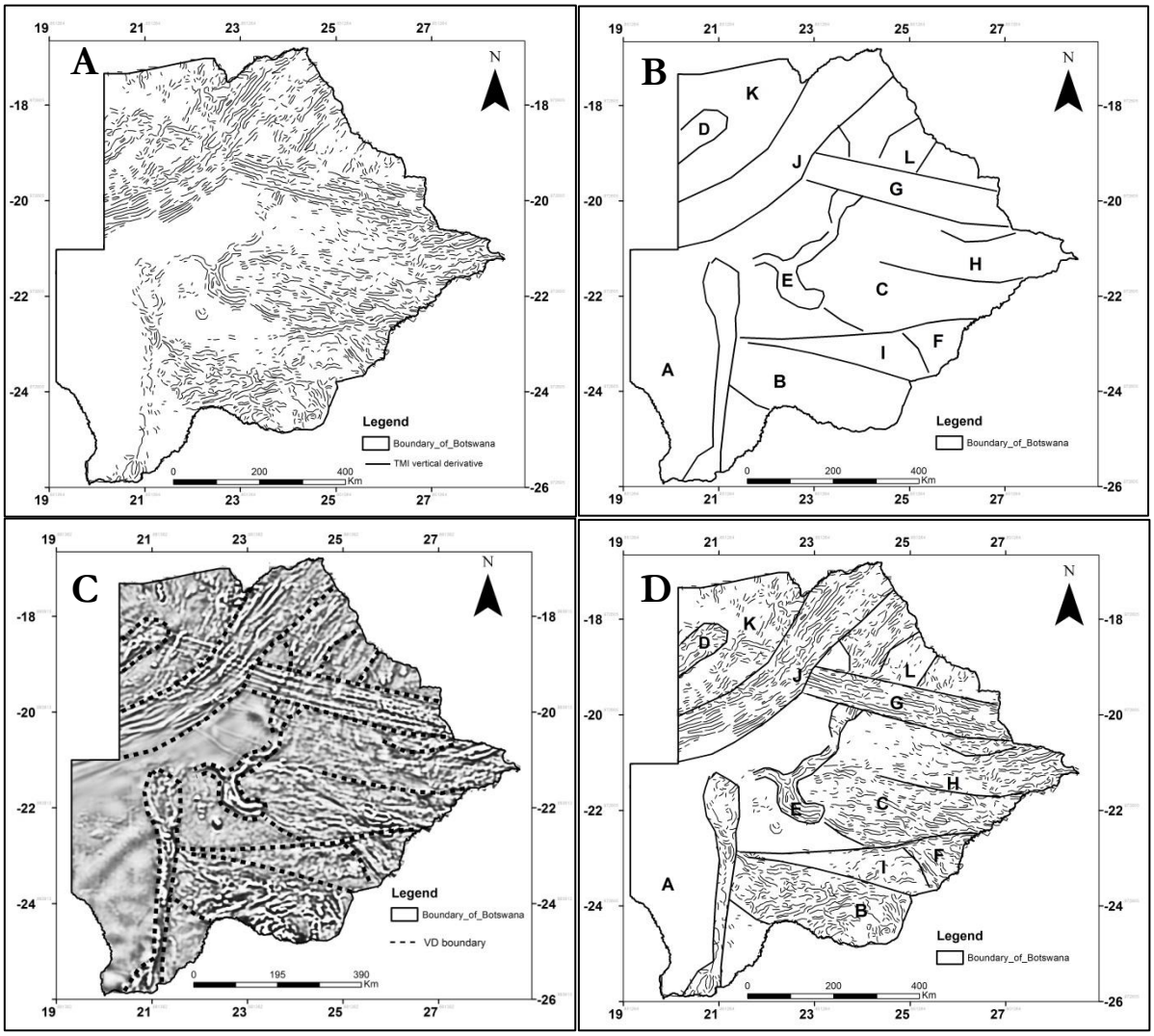

Figure 4-7: (A) lineaments extracted from VD magnetic; (B) tectonic boundary from VD magnetic, (C) tectonic boundary overlaid on VD magnetic and (D) Tectonic boundary overlaid on extracted lineaments

The interpretation and delineation of boundaries from the vertical derivative derived lineaments of magnetic data used the same classification method defined above, section 5.4.

The region A is characterized by no lineaments, (Figure 4-7 (A) and (D)) and a smooth texture on the derivative image (Figure 4-7 (C)). However, continuity and length of the lineament for boundaries were also used. The region J is characterized by long lineaments oriented in the northeast southwest direction (Figure 4-7 (A) and (D)) and long near surface structures oriented in the same direction (Figure 4-7 (C)). North-west of region J, 2 regions existed; D and K. Region D had short very dense lineaments surrounded by a region of uneven texture of lineaments corresponding to region K (Figure 4-7 (A) and (D)). The difference is also visible on the derivative image (Figure 4-7 (C)) based on the texture and structure of these two regions.

Unlike gravity derived boundaries, most of the lineaments in the magnetic derived lineaments have a high density of lineaments. As such, other interpretation criteria were used in addition. The main used criteria were the pattern, shape and texture of the lineaments which differentiated regions B, I, F C H and L. Additionally, the region G corresponds to the dyke swarms running across the study area.

4.6.2. Boundary from Horizontal derivative

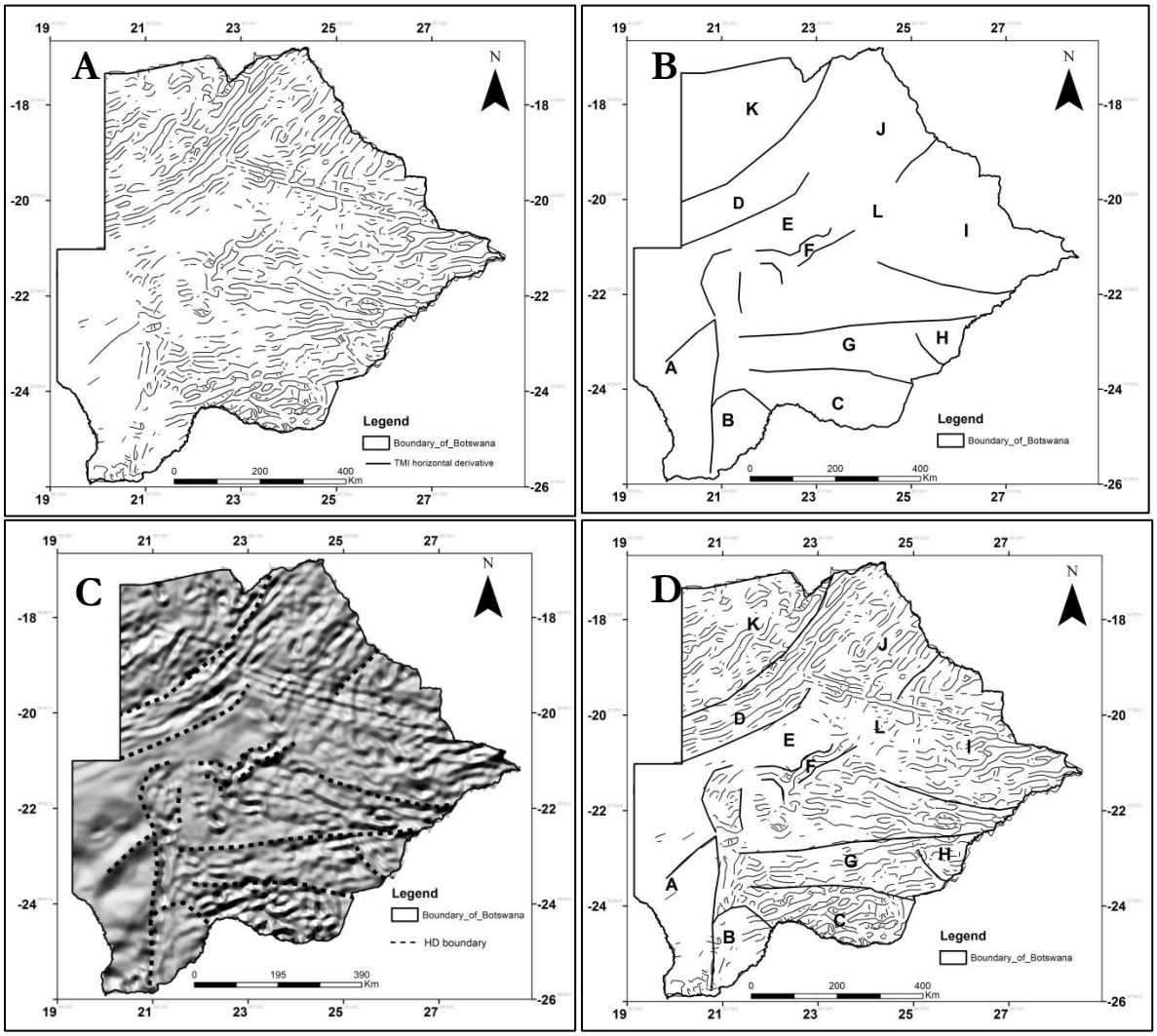

Figure 4-8: (A) lineaments extracted from HD magnetic; (B) tectonic boundary from HD magnetic, (C) tectonic boundary overlaid on HD magnetic and (D) Tectonic boundary overlaid on extracted lineaments

The interpretation of boundary from horizontal derivative derived lineaments of magnetic data produced long, uneven lineaments which are difficult to interpret. However, some regions had a pattern.

The regions A and E in the study area were associated with very few or no lineaments (Figure 4-8 (A) and (D)) and a smooth texture on the derivative image (Figure 4-8 (C)). However, for region E, no clear boundary was visible that made it a tectonic province. The same also applies to region D which has a clear pattern, long lineaments and trending in the same direction, northeast southwest direction, but with not so clear boundary with region J (on both maps on Figure 4-8 (A), (C) and (D)). Region C was defined by dense shaped lineaments (Figure 4-8 (A) and (D)) and protruding structure (Figure 4-8 (C)) while G to the north had north east trending lineaments which makes them different tectonic region. Some regions were hard to define the provinces but only the boundaries. These boundaries were not closed to produce a tectonic province. These are I, K and F (Figure 4-8 (D)).

4.6.3. Combining VD and HD boundaries from magnetic

The boundaries delineated from lineaments derived from vertical and horizontal derivatives were combined (figure 4-9 (A)), to produce the boundary from magnetic data (figure 4-10 (B)). The same criteria used in section 4.6.3 were used in the combination.

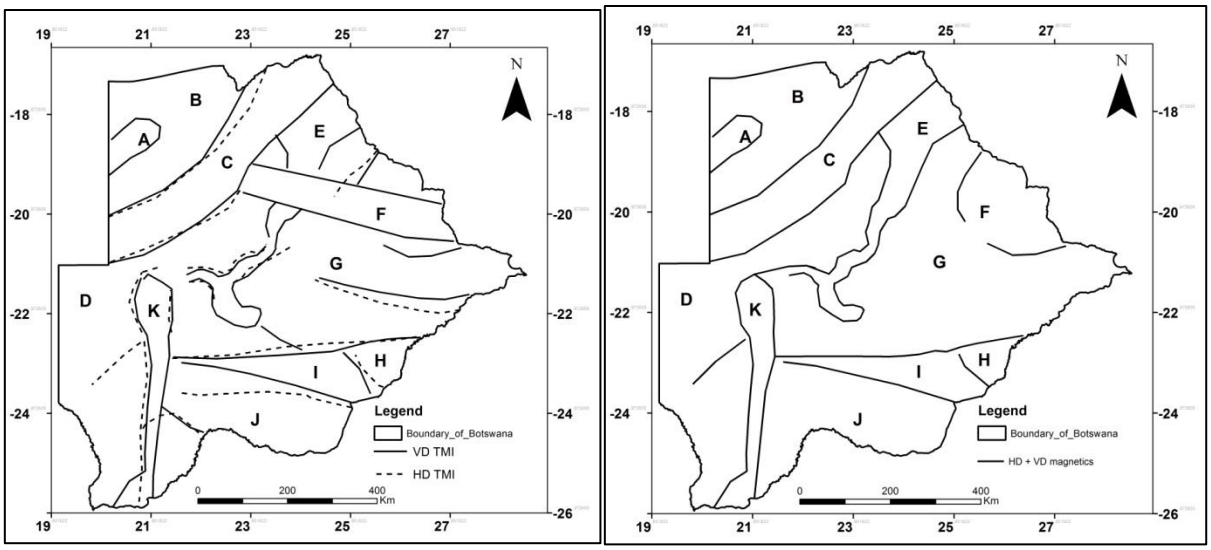

Figure 4-9: (A) overlay of vertical and horizontal derived boundaries from magnetic data and (B) combined boundary from magnetic data

The delineated regions from the vertical and horizontal derived lineaments of magnetic data are almost similar. However slight differences are visible especially on the location of boundaries (Figure 4-9 (A)). Between region J and I , a vertical derivative derived boundary was used because the classification based on the derivative images indicate a bigger region J as delineated by vertical derived lineaments and not horizontal derived lineaments. Furthermore, more evidence supported VD boundary (Figure 6-2 (C), Figure 4-9 (A) and (C) and Figure 4-9 (A) and (C)). The two boundaries between regions G and F were not included in the final tectonic model. Both of them indicate a general trending pattern of lineaments. However, addition data, gravity derived boundary (figure 4-6 (B)), was used to complement the boundary as it showed a clearer boundary than the magnetic derived boundary.

4.7. Combining mapped boundaries from gravity and magnetic

To produce the final tectonic boundary, the magnetic and gravity delineated boundaries were combined. The combination criteria used in the choice of final boundary between the two boundaries were:

- **Continuity** – in cases where the magnetic delineated boundary shows some gaps between two lines and in between the gravity delineated boundary exist or vice versa, the boundaries from those data sets was assumed to be one and were connected.
- **Clear boundary** – in cases where the boundary was clear, where only boundary from one dataset exist, the boundary was adopted to represent the tectonic boundary.
- **Association** – in cases where the two boundaries exists and one boundary is inclusive of the other, i.e. the tectonic boundary within a tectonic boundary, the outer boundary was used after considering the visual classification criteria on both the extracted lineaments and derivative of magnetic and gravity data and other information from literature.

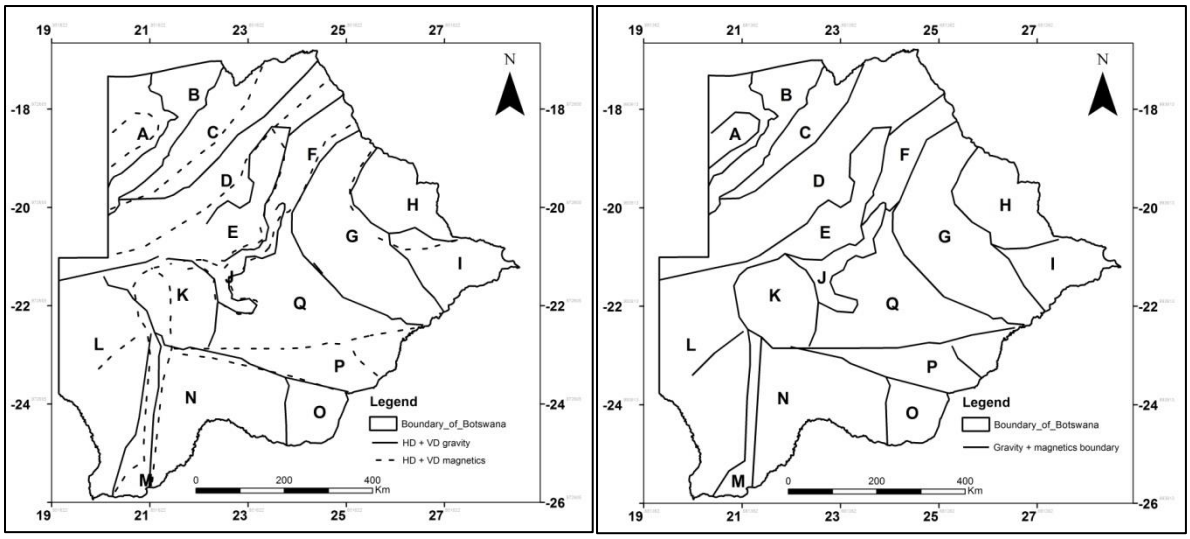

Figure 4-10: (A) overlay of gravity and magnetic boundaries and (B) delineated tectonic model

4.8. Discussion on the combined boundaries

This section discusses the combining of the boundaries and partially relates them to the geology and tectonic terranes of Botswana based on literature. Figures 4-10 (A)-(B) are used in the discussion.

The region A and B were maintained from the magnetic and gravity derived lineaments respectively. However, region C and D had overlapping of boundaries and regions existed between the magnetic and gravity derived boundaries (Figures 4-10 (A)). The region D on the magnetic derived regions correspond to region with intruded magma forming structures running northeast southwest in the study area (Singletary et al., 2003). This structures correspond to Kgwebe formation (Singletary et al., 2003) which correspond to all volcanic rocks in the northwest Botswana rift. These structures were not part of the other side of region C (Figures 4-10 (A)) which indicates different tectonic regions. As such, region C as delineated from gravity data may be smaller than originally delineated. Thus being the case, the boundary of C was on the magnetic delineated boundary. Likewise, the southern part boundary of D took the gravity derived boundary which is in very close proximity with the magnetic derived boundary. This implies that the structures intruded in this tectonic province lies within a broader tectonic province bigger than the boundary of these structures (Modie, 2000). This region corresponds to the Ghazi-Chobe belt of northern Botswana.

Region J and F had a clear boundaries from both dataset. The boundary of F on the south side was taken from magnetic derived lineaments (Figures 4-10 (B)) while on the northern side it was taken from gravity derived lineaments (Figures 4-10 (B)). The region J and F was delineated as one region from magnetic data while the gravity data had a boundary between the two which was used to separate the two regions. The region J had been previously demarcated (Carney et al., 1994; Hutchins & Reeves, 1980; Key & Mothibi, 1999; Key & Ayres, 2000; Singletary et al., 2003) which makes it different region from F. Region J correspond to Xade complex and region F may correspond to Botswana northeast rift (Singletary et al., 2003). The region M took the boundary from the magnetic derived lineaments. However, on gravity derived lineaments the western boundary of region M was just estimated based on the distribution of lineaments in the region as such the magnetic derived lineaments was adopted. Hutchins & Reeves, (1980) and Key & Ayres, (2000) discussed this region as part of the Kheis belt and gabbroic Tshane terrane. Their boundary, based on magnetic data, is applied in the delineation of this region.

The region K is characterized by long lineaments on the gravity derived lineaments. The boundary of the region from the west took the boundary of a magnetic derived boundary, Hutchins & Reeves, (1980)

delineated this boundary using magnetic data as the eastern part of Okwa block and on the eastern part of the region took the gravity derived boundary. The magnetic delineated boundary within the region K correspond not to a tectonic boundary as evidence from the gravity data but rather to one of the major structures within the region (Figures 4-10 (A)). The region Q and G had their separating boundary taken from the gravity data. The region's magnetic boundary was not conclusive as several lineaments indicated possible boundaries. Other regions where single boundary from single data set exist, for instance boundaries between G and I, P and Q, N and O, the boundaries were adopted. The work by Key & Ayres, (2000) and Singletary et al., (2003) descrided the area that regions N, O, P and Q falls in the Kaapvaal craton. The boundary between P and Q does not show much on derivatives data. However, Ranganai et al., (2002) and Schaller et al., (1999) describe this boundary as a tectonic lineament that breaks the northern part of Kaapvaal Craton. It is called the Palala shear zone.

4.9. The mapped tectonic terranes of Botswana

This section shows the delineated tectonic boundary of Botswana based on the automatically extracted lineaments from gravity and magnetic data. These delineated tectonic provinces were compared with already existing model for few provinces to correlate with the geological information (Figure 4-11).

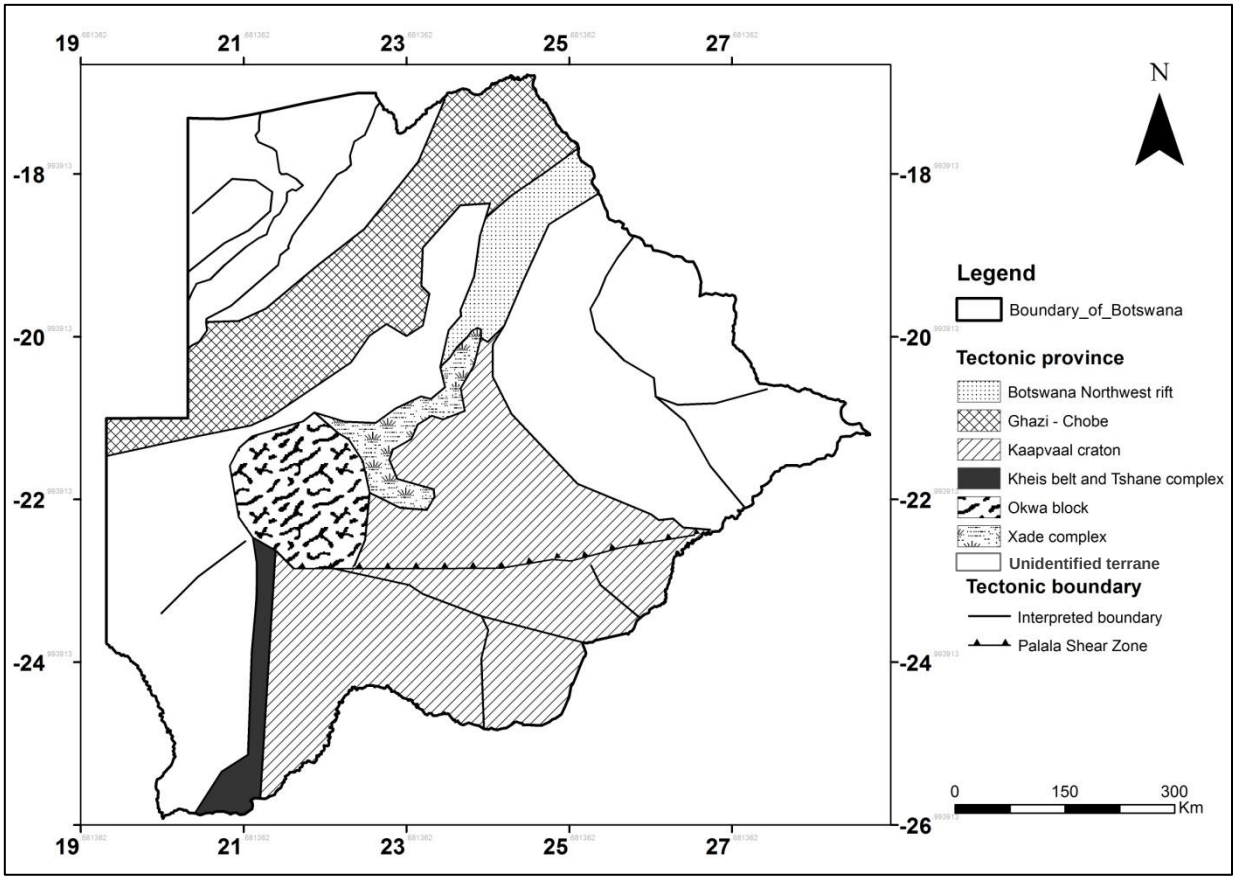

Figure 4-11: The delineated tectonic boundaries and terranes of Botswana

In this chapter, a delineated tectonic terranes and boundaries have been presented based on the magnetic and gravity derivatives derived lineaments. The lineaments were extracted using automatic lineament extraction method. However, the output was improved in chapter 5 using physical map and combined with mafic complex to produce the basement of Botswana.

5. BASEMENT MAPPING

5.1. Introduction

This chapter explains how to update the already existing basement geology of Botswana using gravity and magnetic data. The basement of Botswana comprise of tectonic terranes and the major mafic to ultra-mafic complexes. Furthermore, the basement mapping was done to compare the spatial location of mafic intrusion with the tectonic terranes which can be used for tectonic and geodynamic modelling. The reworking of earth crust causes extension and rifting. These processes may cause magma to come to the surface and form mafic complexes.

In this research, the basement geology is defined as the Precambrian tectonic terranes of Botswana which include the basins, the mafic complexes, the mobile belts, cratons and the boundaries between them with its related geology.

5.2. Methodology

This section shows the steps of the methodology for basement mapping as explained (Figure 5-1). The main method used was apparent physical mapping.

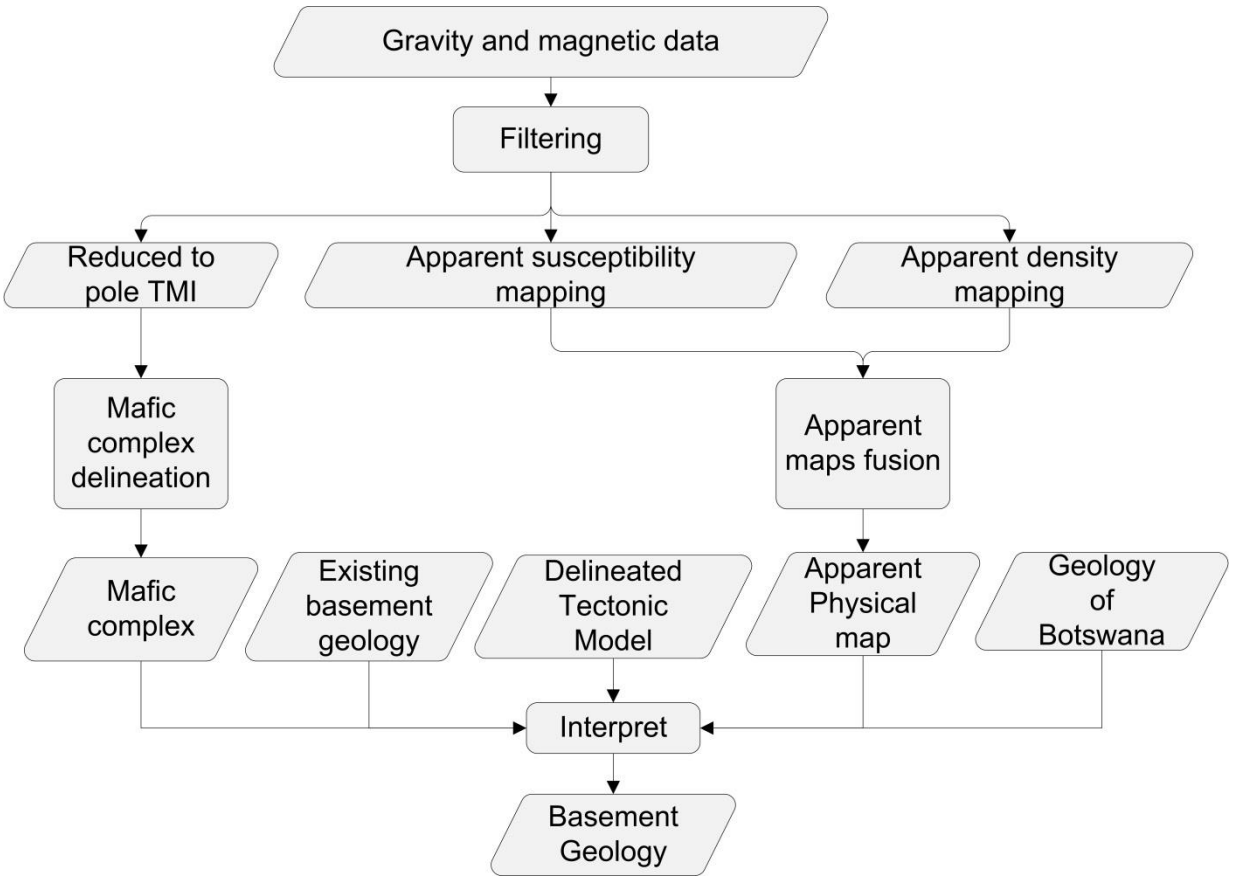

Figure 5-1: flowchart for basement mapping

The steps used in the basement mapping are shown below:

1. Magnetic and gravity data filtering
2. Calculation of apparent susceptibility and apparent density

3. Combining the apparent susceptibility and density map to produce the apparent physical map
4. Improving the delineated tectonic terranes and boundaries using the apparent physical map
5. Mapping the mafic complex using reduced to pole magnetic data
6. Combining improved delineated tectonic terranes and boundaries and mafic complex to produce a delineated basement of Botswana.
7. Comparing and combining the delineated basement of Botswana with the existing basement geology of Botswana. Geology was assigned to each terrane and mafic complex based on the existing geology of the basement. Furthermore, geochronological data is added based on literature
8. The new basement geology is improved using the physical map

5.3. Gravity and magnetic filtering

Magnetic and gravity data was filtered using MAGMAP extension in Oasis Montaj (Table 5-1). The filtering was done for 3 reasons: 1) the magnetic data was filtered to remove the effect due to near surface bodies for mafic intrusions mapping and make its signal comparable with gravity data for apparent physical mapping, 2) the gravity data was filtered to remove the effect of upper mantle such that we remain with signal due to the crust for apparent density mapping and 3) the reduce to the pole was done to move the dipole effect of magnetic signal such that the signal is directly above the anomaly making it correlates with geology (Jachens & Blakely, 1986).

On the reduce to pole parameters, a single declination and inclination was used for the whole study area. The differential reduce to pole which calculates declination and inclination for every magnetic data point was presented by Cooper & Cowan, (2005). However, its implementation for large dataset cannot be possible at present cause of implementation limitations. As such, a single declination and inclination was calculated in Oasis Montaj. The calculation estimates the suitable single declination and inclination based on the given longitude and latitudes in a magnetic database.

Filtering	Parameters	Purpose
Butterworth low pass filter of magnetic data	10km, 50 Km (in ground units)	-10 km low pass filtered data (Figure 5-1 (A)) was used in mafic delineation -50 km low pass filtered data (Figure 5-1 (B)) was used for apparent susceptibility calculation
Upward continuation of gravity data	36 km	-The 36 km upward continuation of gravity data produce regional anomaly (Figure 5-1 (C)) - The regional anomaly was subtracted from the Bouguer anomaly to create the residual anomaly (Figure 5-1 (D)) -Residual anomaly is used in apparent density calculation
Reduce to pole of magnetic data	Declination, -12.74 Inclination, -66.82	-Delineation of high magnetic anomaly regions which could represent basement mafic complex - The same parameters were used for apparent susceptibility calculation

Table 5-1: magnetic and gravity filtering, parameters used and purpose

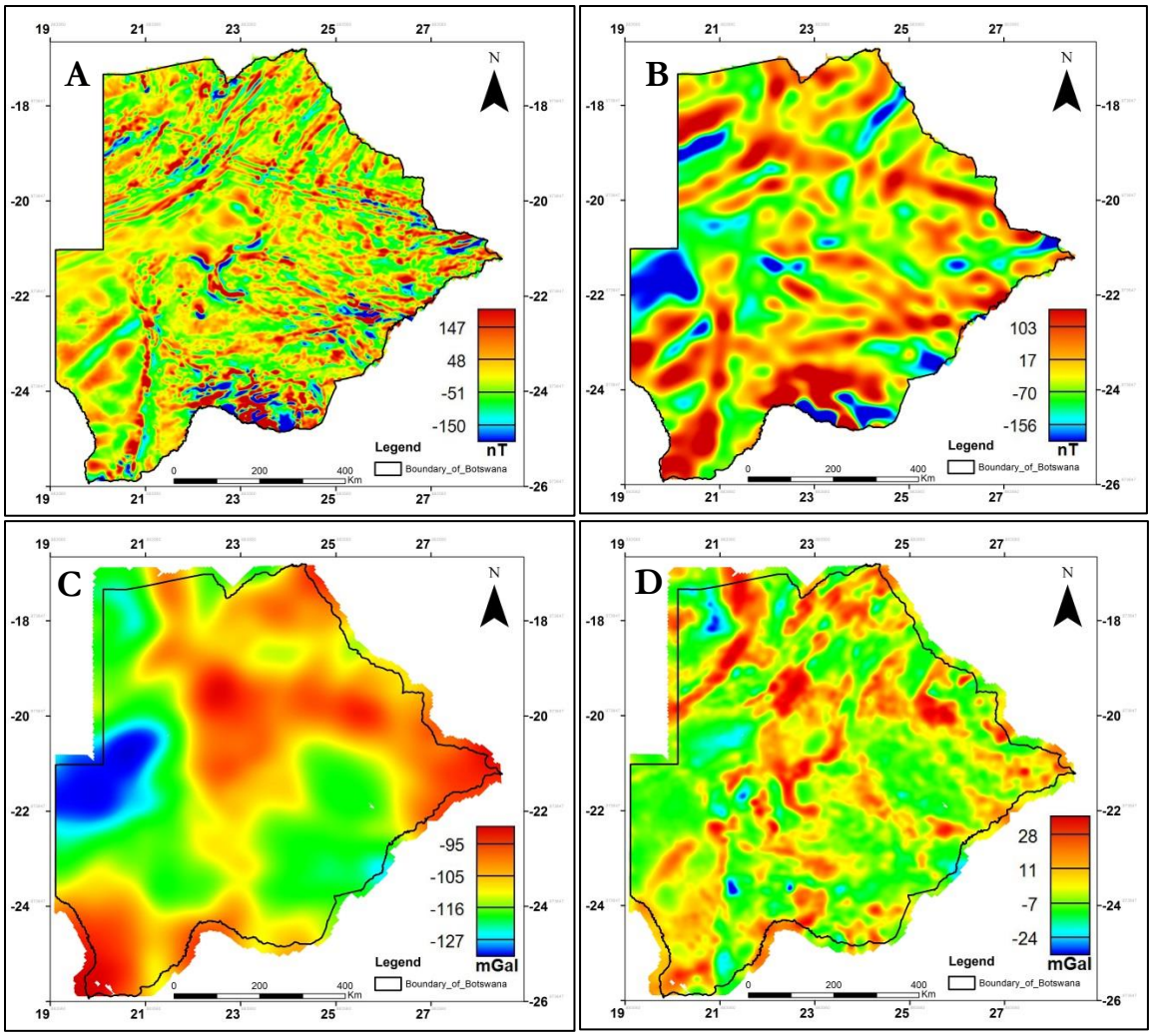

Figure 5-2: (A) 10km low pass filtered magnetic data, (B) 50km low pass filtered magnetic data, (C) Regional anomaly of gravity data and (D) Residual anomaly of gravity data

5.4. Apparent Physical Mapping

This section explains the calculation of apparent density and apparent susceptibility from gravity and magnetic data respectively. It also explains how apparent density and apparent susceptibility are combined using a colour scheme to produce apparent physical map as introduced by Everaerts, (1990). The apparent density and susceptibility are interpreted based on the possible geology and then the interpreted geology from apparent density and susceptibility are combined to interpret the physical map geology.

The apparent physical mapping is based on the ground variation of densities and depth estimate to the geological units and the distribution of magnetic minerals, i.e. their magnetic susceptibility. However, gravity and magnetic data measure different physical properties of rocks which make it difficult to correlate and jointly use in the interpretation of the geology of an area. A study by Henkel, (1976, 1994) established a relationship between density and magnetic susceptibility of rocks in a Precambrian environment. He used ground based rock samples, about 30 000 samples, to understand the petrological processes, magmatic differentiation, serpentinisation and delineation of local and regional secondary processes. Everaerts, (1990); and Yawsangratt, (2002) used the approach of Henkel, (1976) and applied it to the airborne gravity and magnetic data in geological mapping. They used the already known geology and their physical parameters to map the unknown areas based on the colour combination of density and magnetic susceptibility.

5.4.1. Apparent Density

Apparent density mapping turns the gravity anomaly into density distribution of rocks (Ranganai et al,. 2008). The implementation steps in apparent density calculation are listed below.

1. Upward continuation of Bouguer anomaly to produce Regional anomaly.
2. Subtraction of regional anomaly from Bouguer anomaly to produce residual anomaly.
3. Defining the thickness layer model for the density calculation (36 km layer model, average crustal thickness of Botswana after Tugume et al., (2013) was used).
4. Defining the average density of the thickness layer model (2.67 g/cm^3 average crustal density background).
5. Density values are then calculated based on the gravity values of thickness layer model and average density. The calculated density values are subtracted or added to the average density based on the gravity signal.

5.4.2. Results and interpretation of apparent density calculation

The density distribution calculated from apparent density calculation (Figure 5-3) ranged from 2.46 g/cm^3 to 2.90 g/cm^3 with the density background of 2.67 g/cm^3. Based on the average earth density, 2.67g/cm^3 and the major rocks of the basement of Botswana (Chapter 2, table 2-1), 2 classes were identified and classified as high density rocks, 2.67-2.9 g/cm^3 and low density rocks, 2.67-2.52 g/cm^3 with their possible association of rocks (Table 5-2).

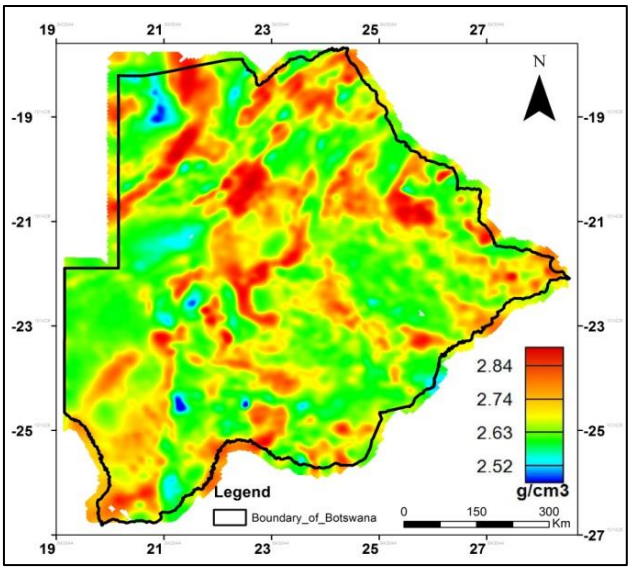

Figure 5-3: apparent density map

Density classification	density range (g/cm^3)	Rock types	Av. density (g/cm^3)
low density	2.46-2.67	Syenite	2.5
		Acidic igneous rocks	2.61
		granite	2.64
		Sedimentary rocks	2.3 - 2.7
		Granitic gneiss	2.67
		Gneissetic granitoid	2.67
high density	2.67-2.9	Dolerite	2.89
		Amphibolite	2.96
		Migmitite	2.8
		Gabbro/mafic to ultramafic	3.03

Table 5-2: interpretation of apparent density in relation to the major rock units of basement of Botswana

5.4.3. Apparent Susceptibility

Apparent Susceptibility calculation turns the magnetic anomaly into magnetic susceptibility values. The process is done as described by Ranganai & Ebinger, (2008) below:

1. Reducing the magnetic anomaly to the pole. The reduction to pole moves the magnetic anomaly from a dipole values to lie directly above the magnetic source body as if they are measured from the pole, thus making them correlates to geology (Jachens & Blakely, 1986).

2. Downward continuing the data, the downward continuation enables the data to be mapped closer to the magnetic source depth of interest. However, the magnetic signal in Botswana is from the crust and no signal was from the upper mantle based on the calculated depth estimate of the magnetic signal. As such no residual separation was needed hence upward continuation was not done on magnetic data. Furthermore, the basalts and mafic intrusion in Botswana are found at 1000m depth (Key & Ayres, 2000) hence the need to include the downward continuation filter in the apparent susceptibility calculation.
3. Dividing the magnetic values by the total magnetic intensity to produce the magnetic susceptibility values in emu (electromagnetic units).

The parameters for apparent susceptibility are same as those for reduce to pole (Tables 5-1). However, addition parameters are required which are 1) depth to the basement or where the susceptibility values are found and 2) magnetic field strength on the area. The magnetic field strength was calculated using IGRF functionality in Oasis Montaj based on the given latitudes and longitudes from the data points in the magnetic database. The final apparent susceptibility values are due to the rocks within the crust which makes them correlates with apparent density values which are also from the rocks in the earth crust.

5.4.4. Results and interpretation of apparent susceptibility calculation

The magnetic susceptibility value from apparent susceptibility calculation (Figure 5-4) produced the results in electromagnetic units (emu). The emu values were converted into SI units using a factor of 12.57. The SI values were calculated based on the conversion factor between SI units of magnetic susceptibility and electromagnetic values of $4\prod$ or $(4\prod)^2 \times 10^{-7}$ (Clark & Emerson, 1991). The symbol $\prod$ stands for pi which has a value of 3.14.

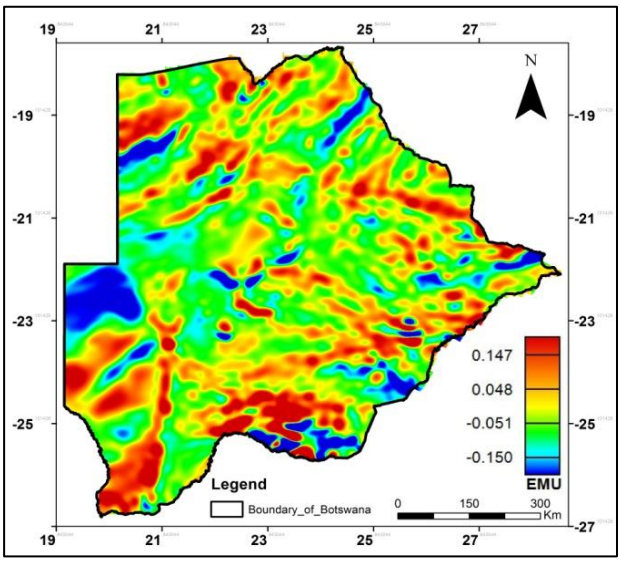

Figure 5-4: apparent susceptibility map

The magnetic susceptibility of a rock can either be zero, negative or positive. The negative susceptibility materials are diamagnetic rocks. In the apparent susceptibility calculated in this research, negative magnetic susceptibility ranges from -0.074 to 0 SI. The positive magnetic susceptibility has been divided into two, the low magnetic susceptibility 0-0.025 SI and the high magnetic susceptibility above 0.025 SI. The class were divided based on the presence of magnetite rocks in the study area. The magnetic threshold for magnetic susceptibility was the metamorphic rocks with an average magnetic susceptibility of 0.025 SI (Table 5-3).

Susceptibility class	Mag sus range (SI)	Rock types	Av. Sus (SI)
High magnetic susceptibility	0.025 and above	Gabbro	0.09
		Ultra-mafic rocks	0.2
		Basic rocks	0.12
		Gneissetic granitoid/migmatite/Granite gneiss	0.025
		Granite	0.05
		Dolerite	0.062
Low magnetic susceptibility	0 – 0.025	Sedimentary rocks	0.018
		Amphibolites	0.0075

Table 5-3 : interpretation of apparent susceptibility in relation to the rocks of basement of Botswana

5.4.5. Apparent Physical map integration

The integration of apparent density and susceptibility used a colour scheme. The apparent susceptibility map was assigned to a continuous colour, from white to magenta, representing the non-magnetic rocks and the high magnetic rocks respectively (Figure 5-5 (A)). Likewise, the apparent density was assigned to a continuous colour scheme, cyan to yellow, representing low density rocks and high density rocks respectively (Figure 5-5 (B)).

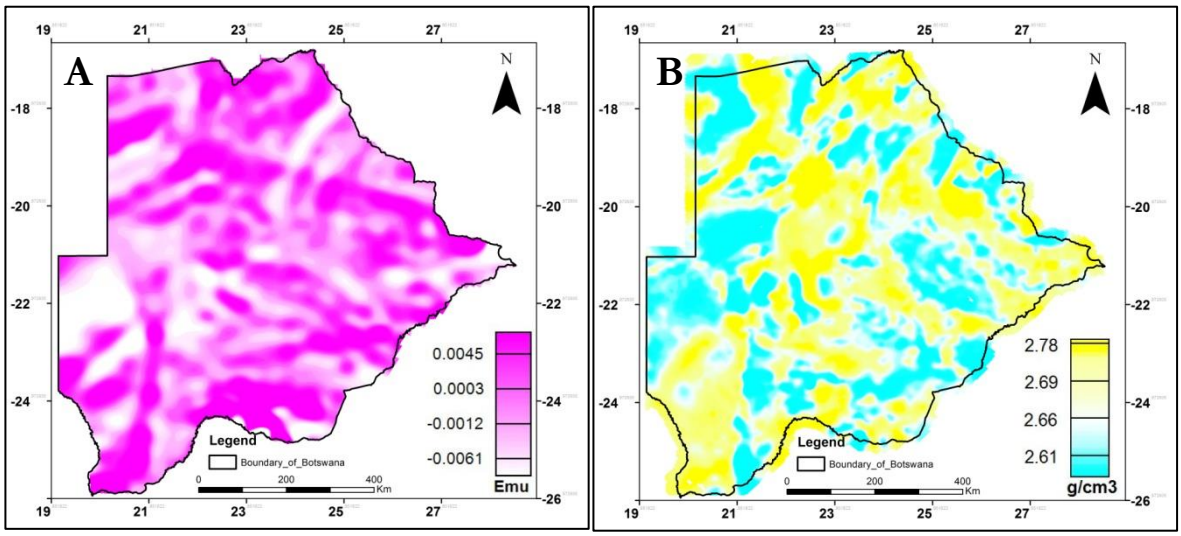

Figure 5-5: (A) Apparent susceptibility colour scheme and (B) Apparent density colour scheme

5.4.6. Physical Map Fusion

The physical apparent map was produced by fusing the colour scheme of apparent density and susceptibility (Figure 5-5 (A) and (B)) as indicated in figure 5-6 (A)-(D) below.

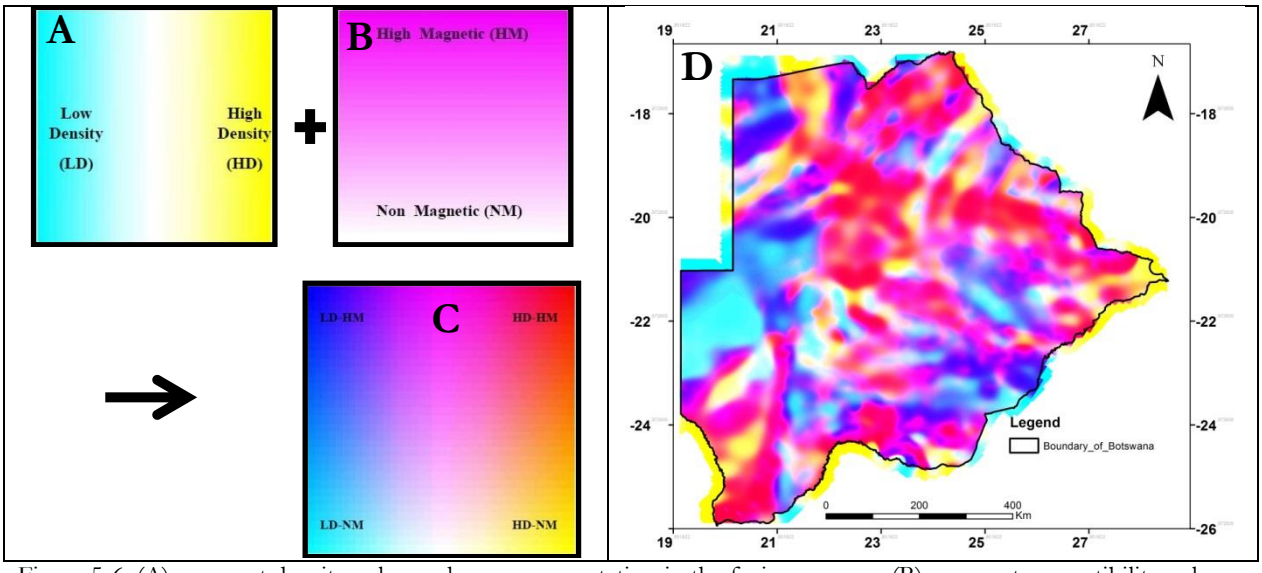

Figure 5-6: (A) apparent density colour scheme representation in the fusion process, (B) apparent susceptibility colour scheme representation in the fusion process, (C) the physical colour scheme fused representation and (D) the apparent physical map of Botswana.

5.4.7. Relationship of physical map to the rocks of basement of Botswana

The physical map from the color scheme was interpreted based on the color, the estimated physical meaning of each color, the density and magnetic susceptibility ranges of each values and finally the possible geology based on the basement geology of botswana and their densities and susceptibility. The color values

and its corresponding lithology was estimate from the avalable data (Chapter 2, table 2-1) and the calculated values of the physical map (Figure 5-6 (D)). The results are shown in (Table 5-4)

Color scheme	Physical meaning	Density value (g/cm^3)	Magnetic value (SI)	Rocks
Blue	Low density – high magnetic	2.52-2.67	Above 0.025	Syenite, Granites, granite gneiss, gnessetic granitoid
Red	High density – high magnetic	2.68-2.90	Above 0.025	Dolerite, Ultramafic rocks, Basic rocks, Migmatite, Gabbro
Cyan	Low density – Nonmagnetic (low magnetic)	2.52-2.67	0 – 0.024	Sedimentary rocks
Yellow	High density – Nonmagnetic (low magnetic)	2.68-2.90	0 -0.024	Granite gneiss, Amphibolites,

Table 5-4: the estimated values of color scheme and its estimated geology on the physical map based on basement geology of Botswana.

5.5. Improving Tectonic models using physical map

The delineated tectonic terranes include different regions with different lithologies and tectonic setting, for instance mafic complexes, mobile belts etc. These regions might have different magnetic and density properties hence different combination on the physical map which signifies different processes that happened during the formation of these regions.

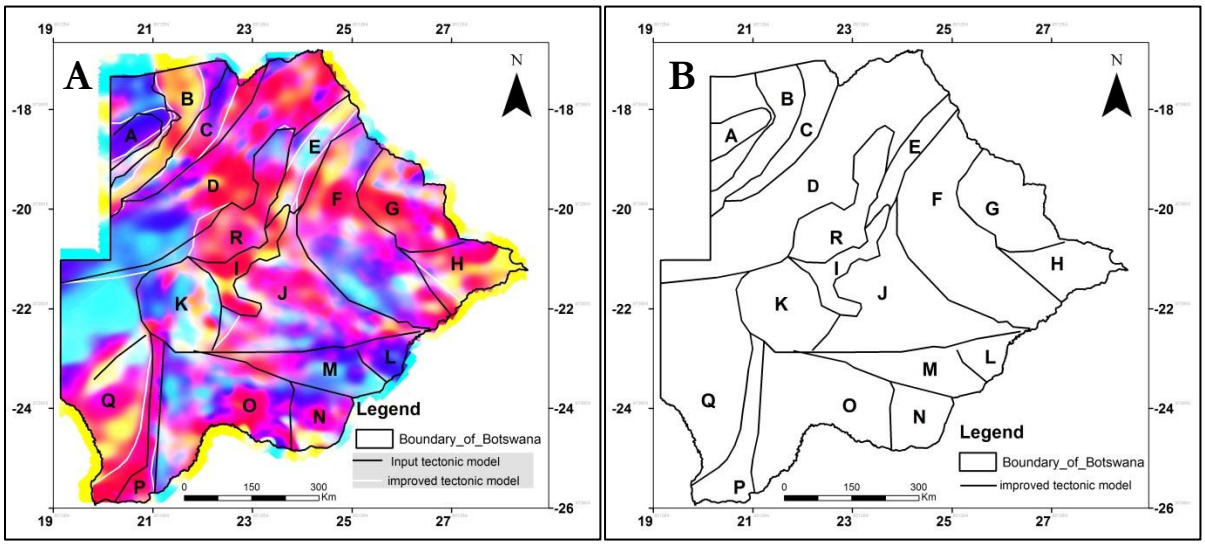

Figure 5-7: (A) overlay of tectonic models on a physical map (the black line represent the improved model and the red line represents the old model) and (B) the improved tectonic model.

The delineated boundaries were improved based on the magnetic susceptibility and density distribution. Area A (Figure 5-7 (A)), was bigger than previously delineated with a blue physical characteristic of low density and high magnetic values signifying areas with possible Syenite, granites and granite gneiss (Table 5-4). Next to it a long elongated feature, area B, had its eastern upper boundary passing through a different physical characteristic area, blue representing low density and high magnetic. Its new boundary takes the border of the same response as the elongated feature, which is yellow in colour signifying the possible presence of granite gneiss and amphibolites (Table 5-4). The same applies to the southern part of the feature. The region C, had its southern boundary shifted in the northwest direction to be in line with the difference physical properties, red and blue, between these two regions. The other regions that had their boundary improved based on their physical characteristics include the region R in the centre of the study

area, region E, region K, region P and region F. The boundary of region R falls between the red and blue colour signifying the different lithological units. Region P is characterised by high magnetic and high density values representing the presence of dolerite, ultramafic rocks, Gabbro and migmatite and basic rocks (Table 5-5). Region E is characterised by a narrow belt with low magnetic with different densities. The region E is clearly different from the surrounding geology (Figure 5-7 (A)). However, the boundary between K and J, and boundary between F and H still remains unclear even on the physical map despite been shifted in relation to the other boundaries that were shifted.

5.6. Mafic complex mapping

The major mafic complexes of Botswana include gabbro, basic and ultra-basic rocks. However, basic and ultra-basic rocks have higher magnetic susceptibility than gabbro. As such, Gabbro is chosen as a threshold for all mafic and ultra-mafic rock in the delineation. The main delineation method was contouring method of the input reduced to pole magnetic data.

Despite that magnetic response differing from place to place based on the inducing strength of the Earth's magnetic field, Galindo-Zaldívar et al., (2013) estimated the gabbro magnetic response to be between 50-150 nT with an average of 80nT Despite the difference in the earth magnetic field inducing strength, approximately 48000 nT in Antarctica and 28000 nT in Botswana (British Geological Survey, 2014), the inducing strength in Botswana is relatively half that of Antarctica. However, the threshold of 80 nT for the gabbro and mafic rock was adopted in the contouring process (Figure 5-8).

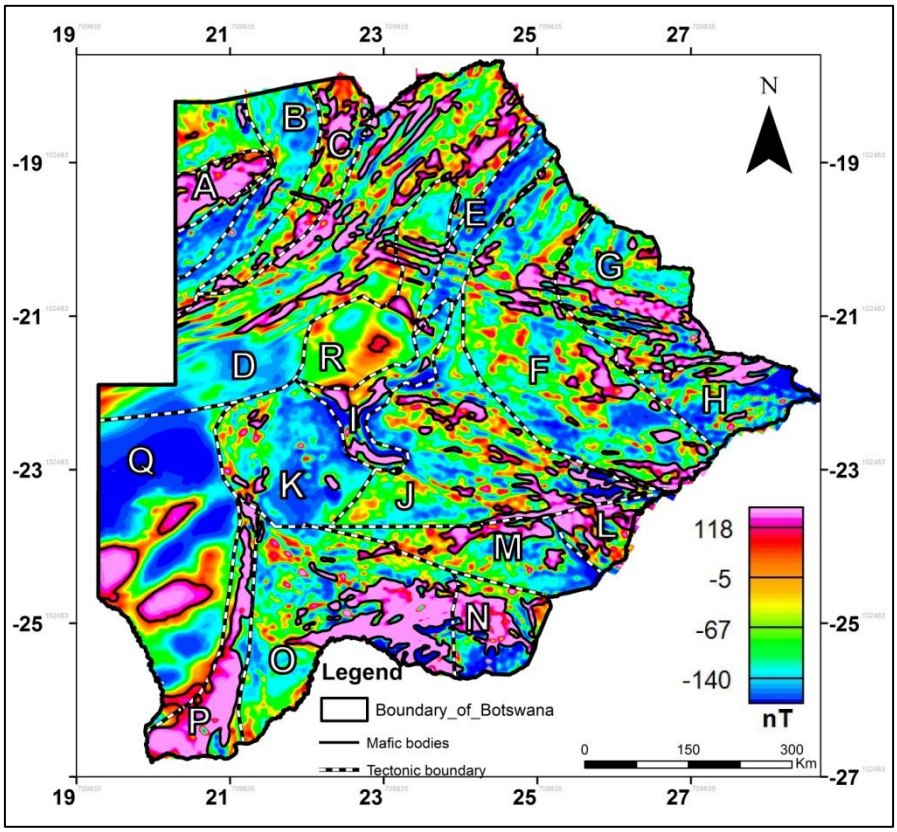

Figure 5-8: mafic complexes mapping of reduced to pole magnetic data. The black line represent a contour line with a threshold of 80nT and a tectonic model overlaid on the map

5.6.1. Combining mafic complex with tectonic terranes for basement mapping

The basement geology as defined above includes the mafic complexes and the tectonic terranes. As such, the mafic complex (Figure 5-8) was combined with the improved delineated tectonic model (Figure 5-7 (B)) to produce the delineated basement geology of Botswana.

The mafic complexes used in the study did not include all the mafic delineated using contouring method from figure 5-8. Emphasis was given on the selected few which include mafic bodies in region A, D, J, M N, K, P, O and Q (Figure 5-8). The mafic complex in region Q was included as it has not been delineated

by any previous studies. The mafic in region A, K, and P coincidently forms the tectonic provinces as delineated above (Figure 5-8). However, the mafic intrusion in region K is just the extension of mafic intrusion in region P. Not the whole of K is a mafic intrusion. As such, the mafic complexes were used to delineate the actual boundary of these regions. Key & Ayres, (2000) and Singletary et al., (2003) called them Quangwadum complex, Tshane complex and Kheis belt respectively.

The northeast-southwest trending structures in the region D is part of the Kgwebe formation (Key & Ayres, 2000; Singletary et al., 2003) which is the name given to all volcanic rocks in region D, either mafic or not. The mafic complexes in region O and N was delineated by Hutchins & Reeves, (1980) as the Molopo farm. Despite that the region was missing in the subsequent Precambrian basement geology of Botswana, Key & Ayres, (2000) discussed the complex as the highly fractured intrusion of basic to ultrabasic rocks. The extend of the Molopo farm intrusion region was not determined as only part of it was covered by aeromagnetic survey at that time (Hutchins & Reeves, 1980). This explains the high lineament density which was used to determine the region as a tectonic region. As such, the regions O, N and M represent a single tectonic province with a mafic intrusion, Molopo farm intrusion, in the terrane. The intrusion in the region J, L and M may correspond to the Mahalapye complex. The complex which is delineated in the Magondi belt (Aldiss & Carney, 1992) maybe covered and extend in the Phanerozoic cover of the Kalahari sands west of the complex (Singletary et al., 2003). Furthermore, Aldiss & Carney, (1992) discussed the effect of Palala shear zone (Schaller et al., 1999) on the Mahalapye complex. Schaller et al., (1999) describe Palala shear zone as a tectonic lineament that breaks the northern part of Kaapvaal Craton. Based on the spatial location of Palala shear zone and the high magnetic intrusion, the intrusion could be the Mahalapye complex covered by the Kalahari sand.

5.6.2. Delineated basement geology of Botswana

The initial interpreted basement geology of Botswana is based on the delineated basement geology of Botswana (Section 5.6.1) and the initial interpretation of the tectonic provinces (Chapter 4, section 4.10)

The regions that are so far known include : region A = Quangwadum complex, region D = Ghazi – Chobe with Kgwebe formation, region P = Kheis belt and Tshane complex, region K = Okwa block , region N= Molopo farm and region L = Mahalapye complex

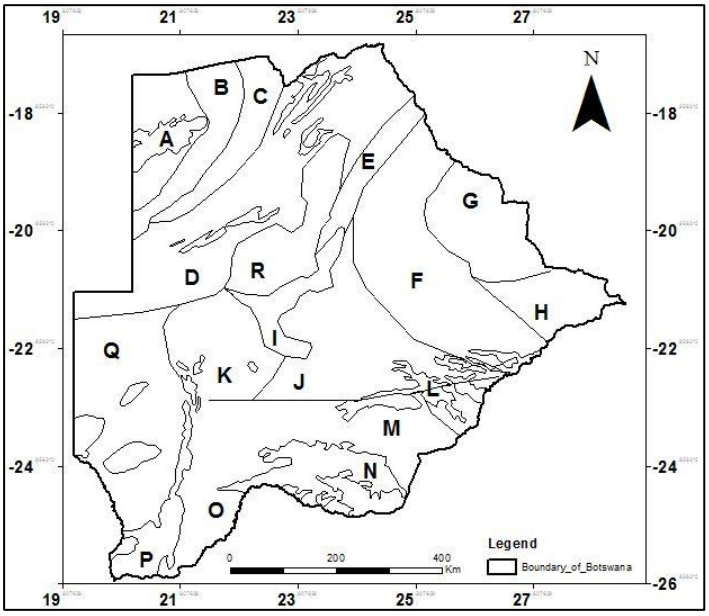

Figure 5-9: delineated basement geology of Botswana

5.7. Comparing and Combining new and existing basement geology

To produce the basement geology of Botswana, all available data have to be incorporated in the basement mapping i.e. geochronology data, geophysical data, geochemical data, geological data, drill core data etc. The delineated basement geology map (Figure 5-9) cannot reflect the true nature of the basement in Botswana on its own. As such, combining and comparing the delineated basement geology (Figure 5-9)

with the existing model (Singletary et al., 2003) produced improved basement geology for both the existing (Singletary et al., 2003) and delineated basement geology. Despite that Singletary et al., (2003) model was an improvement of the Key & Ayres, (2000) model, the former excluded some of the tectonic terranes that the latter included in their model. As such, these two models, together with the delineated tectonic model were compared and combined to produce one improved model. For the sake of comparison, the Singletary et al., (2003) model was called M2003, the Key & Ayres, (2000) model was called M2000 and the delineated model (Figure 5-9) was called the M2015. The combination criteria that were used are:

- The tectonic boundary and mafic complex boundary will come from the delineated tectonic model for all provinces that are found on the 3 models.
- The provinces and terranes that are found on one or two models but not the third was included in the final model

The letters on the map are reference from the M2015 which relates the model with M2003 and M2015.

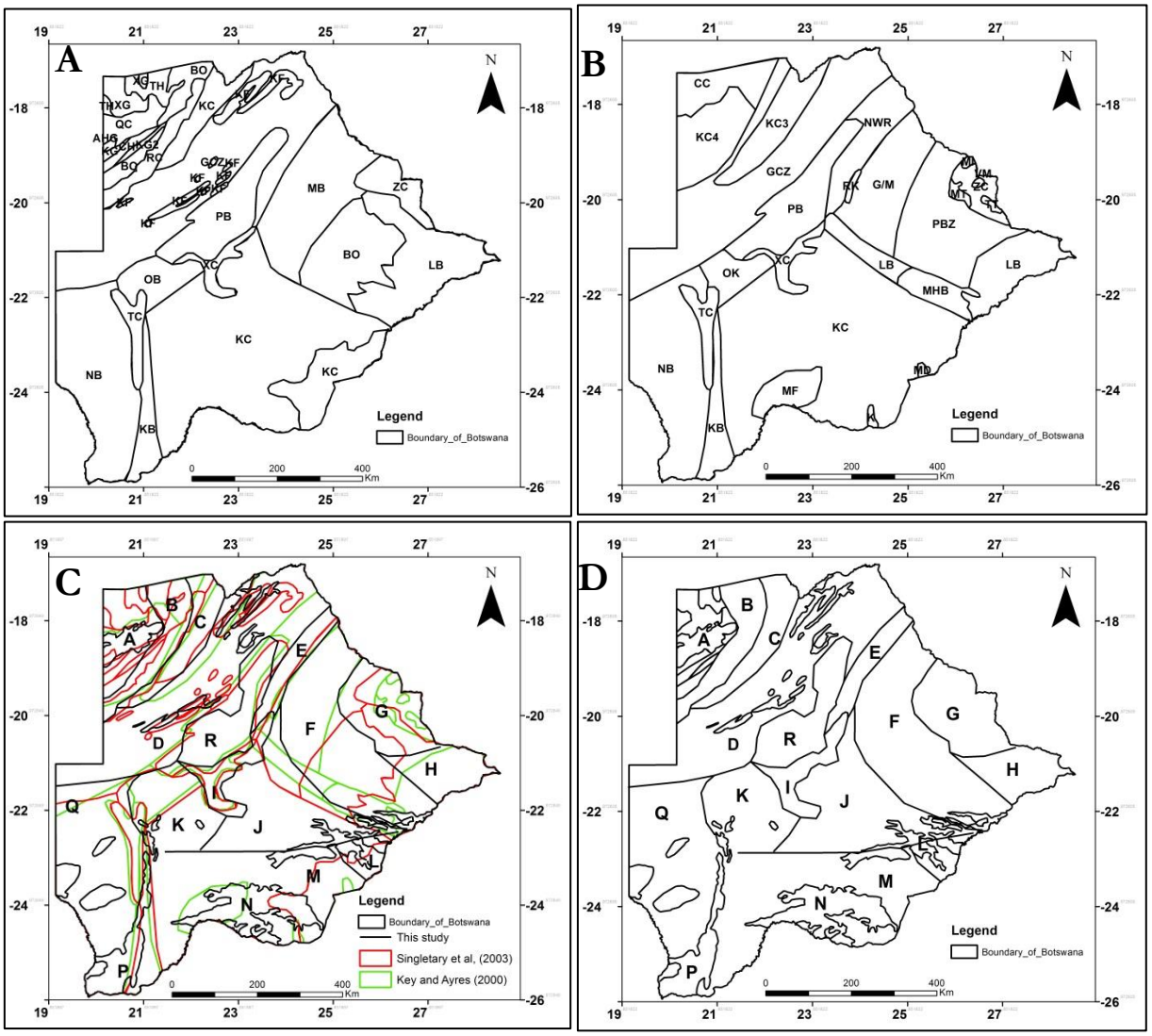

Figure 5-10: the comparison and improvement of the basement geology based on the existing basement geology models, (A) Singletary et al., (2003) basement model called M2003 in the discussion,(B) Key & Ayres, (2000) basement model called M2000 in the discussion, (C) the overlay of Key & Ayres, (2000) Singletary et al., (2003) and delineated (Figure 5-9) basement models and (D) the updated basement model, called M2015, based on the existing models and improved analysis as presented in this thesis

This paragraph gives names of the abbreviation used in figures 5-10(A) and (B). These are: MF is Molopo Farms, K is Kraaipan, MD is Modipe, MHB is Mahalapye belt, LB is Limpopo belt, TT is Tati, VM is Vumba, MI is Maitenge, ZC is Zimbabwe craton, MT is Matsitana, PBZ is plate boundary zone, RK is Rakops, G/M is Gwetabelt/Magondi belt, TC is Tshane complex, XC is Xade complex, KB is Kheis belt, KC is Kaapvaal craton, Ok is Okwa belt, NB is Nossop belt, NWR is NW Botswana rift, PB is Passarge basin, KC3 is Kwando complex, GCZ is Ghanzi-Chobe belt, CC is Congo craton, KC4 is Kihabe complex, KG is Koanaka group, AHG is Aha hills group, CH is Chihabadun complex, QC is Quangwadum complex, BO is Basement obscured by younger sediemnts, RC is Roiboc complex, KF is Kgwembe formation, MB is Magondi belt, TH is Tsodilo hills group and XG is Xaudum group.

Northeast of Botswana, all the 3 models have the region which is labelled A on M2015. However, the boundaries are not on the same spatial location (Figure 5-10(C)). The other regions from M2003 were adopted as the other two models did not have any more regions in the area. The area B on M2015, which coincided with a region on M2003 as Roibok complex, was also included in the model (Figure 5-10 (A) and (D)). However, the region consists of some part of regions from M2003. With no geophysical evidence of these boundaries, the region B from M2015 was adopted. The region C exists on both three models and its called Kwando complex from M2000 and M2003 (Figure 5-10 (A) and (B)). Four regions that are on the M2015, R, I K and D are found on the other two models. These correspond to Ghanzi – chobe zone, Passarge basin, Xadi complex, Okwa block and Nossop basin respectively (Figure 5-10 (A) and (B)). However, certain differences exist between these regions. Firstly, the Kgwebe formation which was delineated in M2015 as northeast southwest trending structure in region D and also exist in M2003 did not exist in the M2000 model. The spatial sizes of R, I, K and Q are similar in M2000 and M2003. However, a slight shift of these regions probably from digitising process. The region I and K are smaller from the M2000 and 2003 models compared with the same regions from M2015. Secondly, high magnetic bodies exist in region Q from M2015 which is missing in the other two models. The region J, L, M and O correspond to Kaapvaal craton (Figure 5-10 (A) and (B)).

In M2015 and M2000, some mafic intrusions are present in the Kaapvaal craton which are absent in M2003. However, the mafic intrusions in M2015 cover a bigger spatial region than the mafic intrusions in M2000. The intrusions correspond to Molopo farms and possible Mahalapye complex. The region P corresponds to Kheis belt and Tshane complex. The region is bigger in M2000 and M2003. According to Hutchins & Reeves, (1980); Key & Ayres, (2000) and Singletary et al., (2003) described the Tshane complex as the unexposed mafic to utrabasic bodies and attributed the lithology to gabbroic intrusion. Using aeromagnetic data to delineate the complex indicates that the region is much smaller in M2015 than previously thought. The same applies to high magnetic Kheis belt. The previous model estimated its spatial extent but the M2015 delineated its boundary from the high resolution magnetic data. No evidence of such a body on the bigger Tshane complex from M2000 and M2003 as well as the spatial location of Kheis belt. Finally, the eastern part of Botswana where the 3 regions are located, G, F and H, was the region where these 3 have so diverse boundaries (Figure 5-10 (C)). These regions correspond to Zimbabwe craton, Magondi belt and Limpopo belt (Key & Ayres, 2000; Singletary et al., 2003). The M2015 have a bigger Zimbabwe craton and relatively smaller Limpopo belt and Magondi belt than M2000 and M2003.

5.8. Improving basement geology with physical map

The improved basement geology includes some regions and terranes that were not improved with the physical map in section 5.5. Such being the case, the improved basement geology was further improved using the physical map. The improvement of basement geology using physical map concentrated on two regions, the north western part and the Tshane complex (Enclosed area on figure 5-11 (A)). Surprisingly, the other regions in the north western area show unique physical response apart from the upper left part of the region. This region was changed to be in line with the physical map characteristics (Figure 5-11 (C) and (D)). The Tshane complex is characterized by high magnetic and high density rocks, red color on the map, which is a characteristic of dolerite, ultramafic and basic rocks, migmatite and Gabbro (Table 5-4). As such, the region is not just 3 isolated mafic bodies but rather a connected region (Figure 5-11 (E) and (F)).

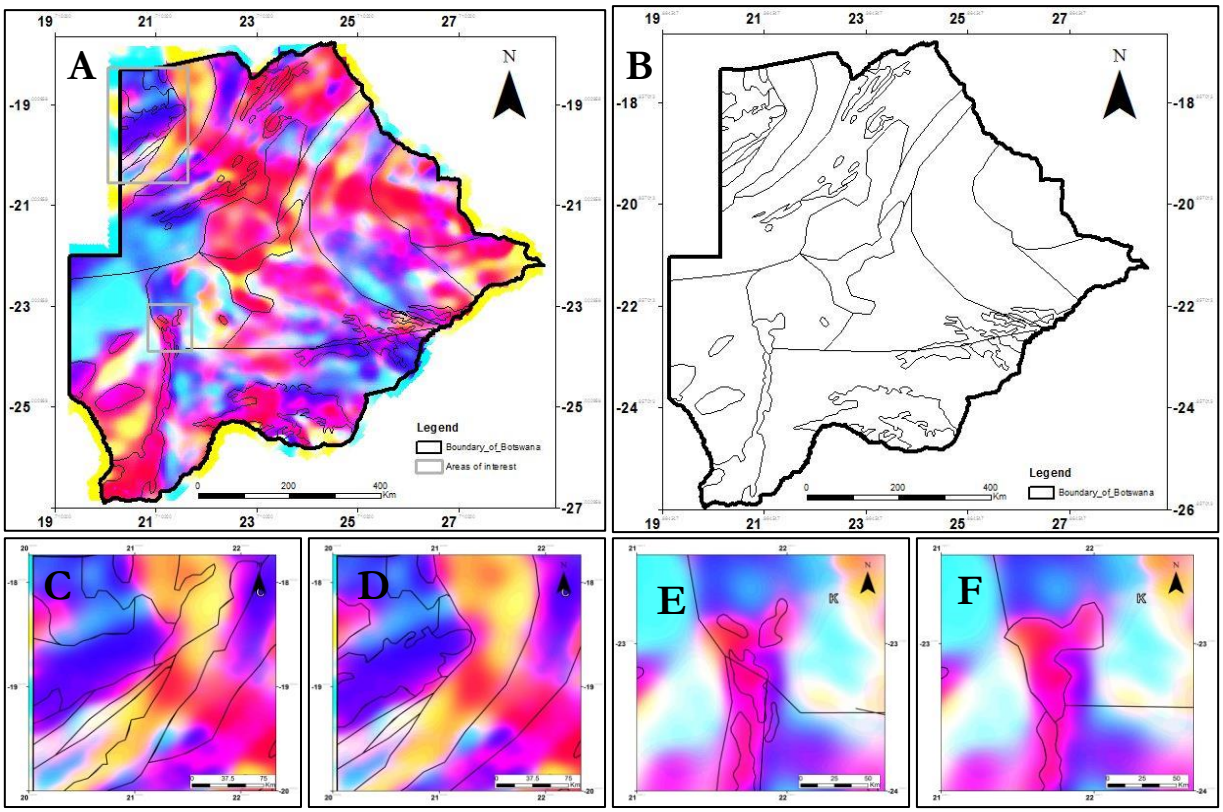

Figure 5-11: improvement of basement geology using physical map, (A) overlay of basement geology on physical map and (B) improved basement geology map,(C) North western part before improving with physical map and (D) North western part after improving with physical map. (E) Tshane complex before improvement with physical map and (F) Tshane complex after improvement with physical map.

5.9. The updated subsurface Precambrian geology of Botswana

This section shows the new basement geology of Botswana based on the tectonic boundary and basement mapping.

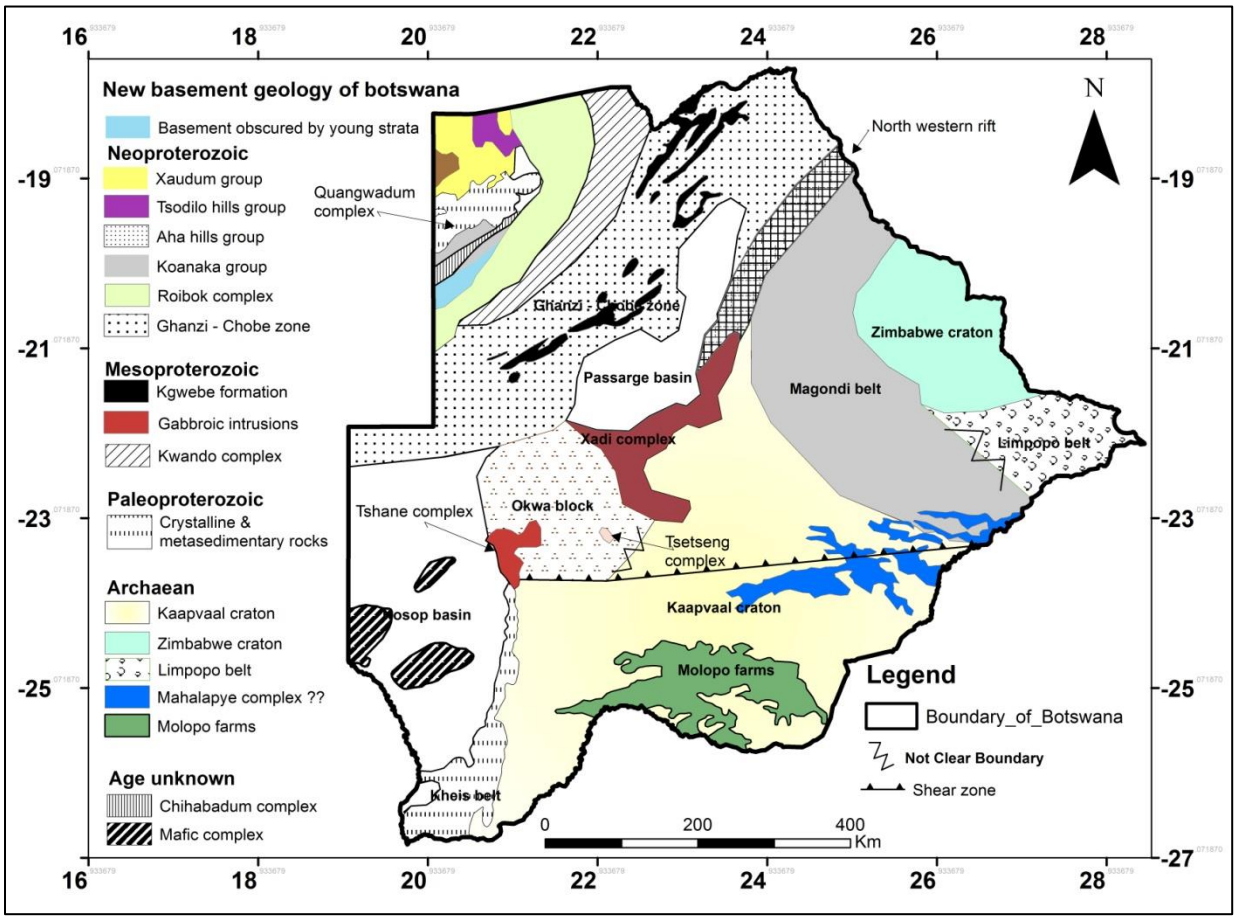

Figure 5-12: the new Precambrian basement geology of Botswana modified from Carney et al., (1994), Key & Mothibi, (1999), Key & Ayres, (2000) and Singletary et al., (2003): the chronological information for each tectonic terrane is indicated on the map.

In this section, updated basement geology of Botswana based on the gravity and magnetic data is presented. The basement geology is very important in the tectonic modelling and geodynamic processes of Botswana. The basement geology of Botswana shows two important things: 1) the tectonic boundaries and terranes which indicate the directional forces that acted on them and 2) mafic intrusion in Botswana which indicate movement of magma from the mantle to the surface. This may also indicate reworking of the crust as well as extension, rifting and compression. Furthermore, geochronological information from literature is added to the basement geology. The basement geology was used as input in the next chapter about crustal thickness and geodynamic modelling.

6. CRUST THICKNESS AND GEODYNAMIC MODELLING

6.1. Introduction

This chapter describes the geodynamic modelling of Botswana based on the crustal thickness information, tectonic terranes and boundaries and mafic intrusion. However, the first part of the chapter explains about the modelling of gravity data to produce the Moho depth of Botswana and subsequently the crustal thickness map of Botswana. The crustal thickness was discussed based on the variation in each terrane as well as the comparison with the satellite gravity derived crustal thickness maps of Botswana. The last part of this chapter combines the crustal thickness information with the tectonic boundaries and mafic intrusions of Botswana to understand the geodynamic activities in Botswana. The tectonic models of three selected profiles are explained based on the information from this research and literature.

6.2. Methodology

This section summarise the crustal thickness modelling and subsequently the geodynamic processes as indicated in the figure 6-1.

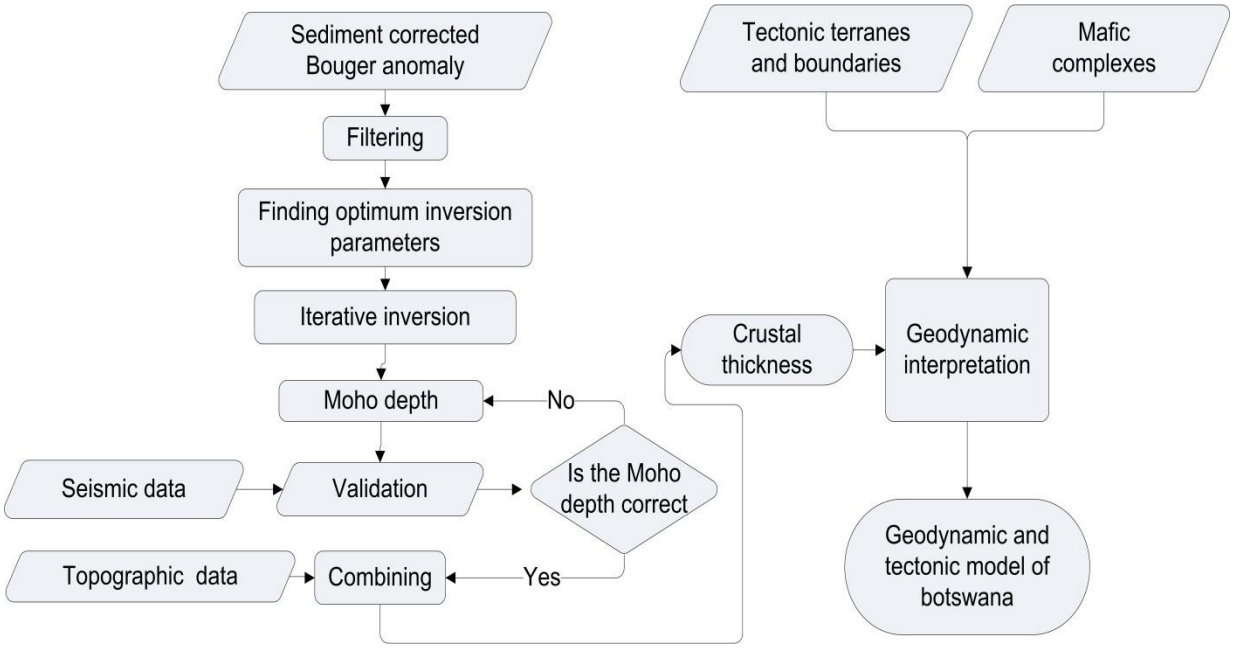

Figure 6-1: flowchart for crust thickness and geodynamic modelling

The implementation of this chapter is described in the following steps below:

1. Sediments correction for Bouguer anomaly
2. Filtering of sediment corrected Bouguer anomaly
3. Finding of optimal inversion parameters
4. Inversion of gravity data to produce Moho depth.
5. Validation of Moho depth from gravity using seismic derived Moho depth.
6. Production of crustal thickness map by combining the validated Moho depth and topography data.
7. The variation of crustal thickness based on each tectonic terrane is discussed.
8. The crustal thickness model is compared with the existing crustal thickness from satellite gravity.
9. Information from crustal thickness map is combined with tectonic terranes and mafic intrusion to interpret the geodynamics.

6.2.1. Sediments correction

This section explains how Bouguer anomaly was corrected for the effect of sediments. In the sediments correction, the lighter sediments were replaced with heavier basement material.

The sedimentary cover in Botswana is divided into 3 layers based on the sedimentary depth and velocity changes of seismic wave after Laske & Masters, (1997). The Bouguer anomaly due to the effect of sedimentary thickness and density (Figure 6-2 (A), (B) and (C)) for each of the 3 layer was calculated. The parameters used for sediments correction are shown in table 6-1 below: The Bouguer anomaly uses 2.67 g/cm^3 for correction of the mass above the geoid. However, the lighter sediments are given by the same density as the heavier basement and other rocks. As such, the effect of these sediments on the final Bouguer anomaly needs to be corrected (Figure 6-3). The sediment correction is done on each of the 3 layers based on the density contrast between that layer and the average density of the earth (Table 6-1).

Layer	depth	Sedimentary density	resolution	Earth density	Density contrast
Layer 1	0-1.5 km	2.105 g/cm^3	1 x 1 degree	2.67 g/cm^3	0.565 g/cm^3
Layer 2	1.5 km < x < 5 km	2.414 g/cm^3	1 x 1 degree	2.67 g/cm^3	0.256 g/cm^3
Layer 3	>5 km	2.536 g/cm^3	1 x 1 degree	2.67 g/cm^3	0.134 g/cm^3

Table 6-1: parameters for sediments correction

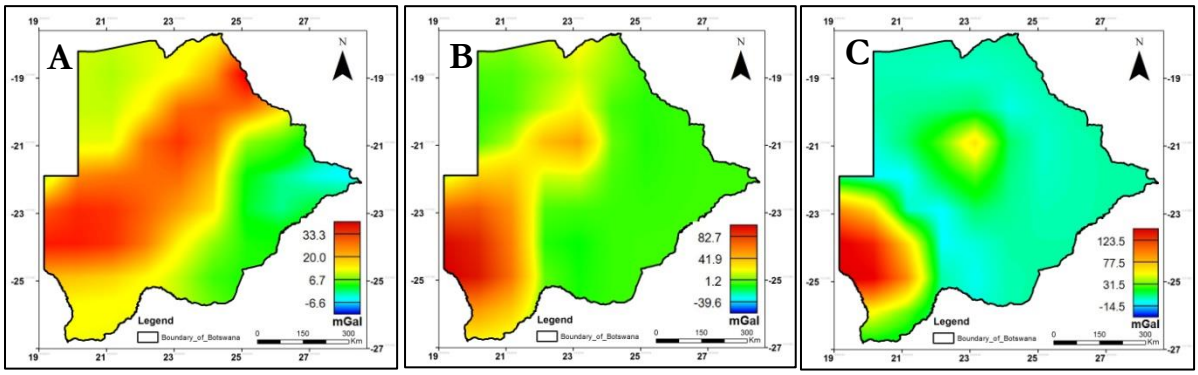

Figure 6-2: The gravity values calculated from the 3 sedimentary thickness layers(A) upper sediments layer (from the surface to 1.5 km), (B) middle sediments layer (from 1.5 km to 5 km) and (C) lower sediments layer (from 5 km to 12 km)

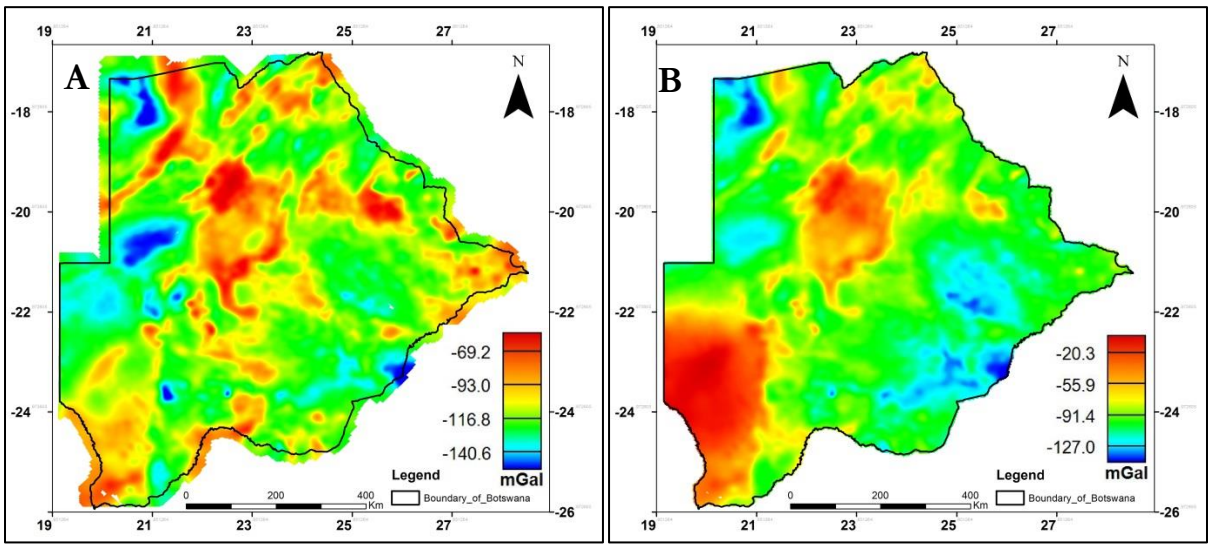

Figure 6-3: (A) Original Bouguer anomaly and (B) the sediments corrected Bouguer anomaly

6.2.2. Gravity filtering

The sediment corrected Bouguer anomaly was filtered (Table 6-2, Figure 6-4 (A)-(F)) using MAGMAP extension in Oasis Montaj. The filtering was done to remove signals due to bodies in the upper mantle as well as signal due to near surface bodies.

Filtering	Parameters	Purpose
Butterworth High pass	1000km (in ground unit)	-Applied to gravity data to remove deep sources from the mantle
Butterworth Low pass	200 km, 175km, 150 km, 125 km and 100 km (in ground units)	-This was applied to the 1000 km high pass filtered gravity data -The filtering was done to remove high frequency signals that makes iterative inversion process unstable when modeling Moho depth

Table 6-2: filtering parameters and its purpose

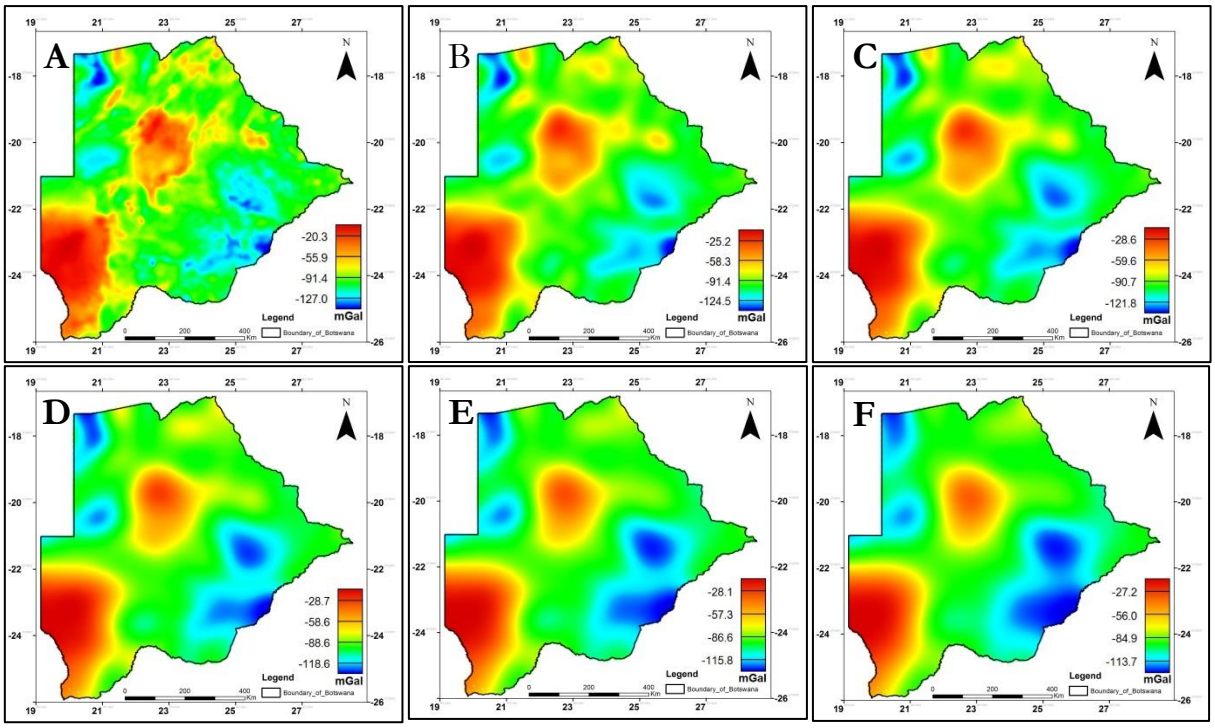

Figure 6-4: results of filtering process (A) the sediment corrected bouguer anomaly map, (B) 100 km low pass filtered map, (C) 125 km low pass filtered map, (D) 150 km low pass filtered map, (E) 175 km low pass filtered map, and (F) 200 km low pass filtered map,

6.3. Finding optimum parameters

The inversion parameters are divided into two categories: the constant parameters and the varied parameters. The constant parameters do not change during the inversion process. The varied parameters are initial Moho depth (IMD) and density contrast (DC). The constant parameters include number of rows and column of the data which is 1260, the data spacing which is 1km, the distance in the x and y direction which is 1260 km. The inversion parameters also include the upper and lower cut-off wavelengths which are 0.006 and 0.001 respectively; converging criteria of 0.02 km and truncating window of 10%.These parameter values are unique to this research. The convergence criterion was included in the inversion as the cut off root mean square error (RMS) between the input and the forwarded output gravity. The inversion run iteratively 10 times or when the root mean square between the measured and calculated signal is lower than or equal to the convergence criterion value.

6.3.1. Wavelength cut off determination

The upper cut off wavelength of 1000km was used (Block et al, 2009; Tugume et al., 2013; van der Meijde, et al., 2013). However, the lower cut off wavelength was tested based on the lowest absolute average values between the gravity derived Moho depth and the seismic derived Moho depth to determine which one gives good results. 5 lower cut off wavelength were tested, 100 km, 125 km, 150 km 175 km and 200 km. The lower cut off wavelength was included to reduce the uncertainty due to high frequency signal in the data. An initial Moho and density contrast of 39 km and 0.5g/cm^3 respectively were used in the calculation after Fadel & Meijde, (2015), of the same area which they used satellite gravity to resolve the Moho and in addition density contrast of 0.35g/cm^3 was also used bringing the number of models to test the effect of short wavelength signals to 10 to increase the number of test filter parameter and effect of changing the density contrast (Table 6-3).

The 10 models were inverted using iterative inversion method to estimate the Moho depth. Each of the 10 models was then forward modelled to produce the calculated gravity signal due to Moho topography. The root mean square error between the measured and the calculated gravity was calculated from each of the 10 models (Table 6-3). The depth estimate from each of the 10 models was compared with the depth estimates from seismic data after Youssof et al., (2013) (Appendix I, table 0-1). Then the absolute average value for each of the model was calculated based on the seismic depth estimates and gravity depth estimated of the 10 models (Table 6-3). The absolute average value is the absolute difference between a given two sets of values in relation to their mean. The absolute values of zero indicate no difference between the two data sets. Therefore, the closer the absolute value to zero the better the fit between the two data sets. The closest absolute value to zero from the 10 models is model 9 and second by model 4 (Table 6-3). These models had an initial Moho depth of 39km and density contrast of 0.35g/cm^3 and 0.5 g/cm^3 respectively. Furthermore, the filtering cut of wavelength for both models were 1000 km upper cut off and 175 km lower cut off. As such, these cut off wavelength values were used for the iterative inversion.

Models number	IMD (km)	DC (g/cm^3)	Upper cut of (km)	Lower cut off (km)	RMS	Absolute average values
1	39	0.5	1000	100	0.0074	3.777
2	39	0.5	1000	125	0.0047	3.387
3	39	0.5	1000	150	0.0031	3.066
4	39	0.5	1000	175	0.0017	2.782
5	39	0.5	1000	200	0.0017	2.948
6	39	0.35	1000	100	0.0195	3.405
7	39	0.35	1000	125	0.0123	3.194
8	39	0.35	1000	150	0.0075	2.969
9	39	0.35	1000	175	0.0050	2.696
10	39	0.35	1000	200	0.0050	2.925

Table 6-3: parameters choice for the upper and lower cut off wavelength

6.3.2. Initial Moho and density contrast values

The density contrast, the mantle density minus crust density, used was varied between 0.25 g/cm^3 and 0.5 g/cm^3 with a step increase on 0.05 g/cm^3 based on the density contrast between the mantle and crust which ranges from 0.28 and 0.48 g/cm^3 (Tenzer et al., 2011). The initial Moho depth was varied between 35-43 Km with a step increase of 2 km, based on the two crustal thickness of Botswana: 1) the crustal thickness model extracted from Tugume et al., (2013) model of Africa and 2) Youssof et al., (2013) model of southern Africa. In total 30 models were produced from the inversion with the parameters (Table 6-4).

N	MD	DC	N	MD	DC	N	MD	DC	N	MD	DC
1	35	0.25	**9**	37	0.35	**16**	39	0.4	**24**	41	0.5
2	35	0.3	**10**	37	0.4	**17**	39	0.45	**25**	43	0.25
3	35	0.35	**11**	37	0.45	**18**	39	0.5	**26**	43	0.3
4	35	0.4	**12**	37	0.5	**19**	41	0.25	**27**	43	0.35
5	35	0.45	**13**	39	0.25	**20**	41	0.3	**28**	43	0.4
6	35	0.5	**14**	39	0.3	**21**	41	0.35	**29**	43	0.45
7	37	0.25	**15**	39	0.35	**22**	41	0.4	**30**	43	0.5
8	37	0.3				**23**	41	0.45			

Table 6-4: initial Moho depth and density contrast for the 30 models.

6.3.3. Inversion method

An inversion method was used to produce a crustal thickness map. Firstly, Moho depth of the study area was calculated and then topography data added to it to produce the crustal thickness map.

Moho depth, the boundary between earth crust and the upper mantle, is calculated using Parker-Oldenburg iterative inversion method**.** It is a method used to model a two layer model, crust and mantle, with a fixed density contrast in between the layers. The Moho boundary between the crust and mantle is undulating, wave like form, which makes this method ideal for Moho topography modelling. The method do not rely on point data and assumes that all the signal is related to the topography of the Moho (van der Meijde et al., 2013). The iterative inversion method uses the inversion procedure that was developed by Parker, (1973) and an iteration procedure of the same equation rearranged by Oldenburg, (1974). Parker, (1973) developed a method on how Fourier transform can be used to calculate the magnetic or gravity anomaly caused by uneven, non-uniform layer of material for a single profile. Oldenburg, (1974) rearranged the Parker equation to make it iterative.

The iterative inversion method was implemented using a Matlab program called 3Dinver.M produced by Gómez-Ortiz & Agarwal, (2005). The 3Dinver.M program computes 3D of the horizontal density interface from gravity anomaly by using the Parker-Oldenburg iterative inversion. The algorithm uses initial Moho depth and density contrast between two layers as parameters. During inversion, the input data was extended by 10% and a cosine taper window of 10% was included to avoid side effect. Furthermore, to ensure that a convergent criterion is done a high-cut cosine filter is included in the inversion process. The algorithm is implemented as described in the steps below:

1. The average gravity value is calculated from the input gravity data.
2. The gravity data values are then demeaned based on the calculated average gravity value.
3. Average initial Moho depth and density contrast is inputted.
4. The demeaned gravity values are inverted based on the initial Moho and density contrast values
5. The calculated Moho topography is forward modeled to produce a gravity signal due to the calculated Moho topography.
6. Finally the difference between the measured gravity data and the calculated gravity data was calculated.

6.4. Gravity data inversion

The 30 models were inverted using the same iterative inversion method. The difference between the measured gravity and the forwarded gravity was calculated (Figure 6-5) and the effect of varying the parameters were noted (Figure 6-6). The inversion process produced 30 Moho depth models based on the initial Moho depth and density contrast. The inversion of one model to the next model of the 30 initial models produced variation in the modelled Moho depth depending on which parameter was varied between the models. For instance, the difference in Moho depth between two models when only step of 2 km for initial Moho depth is used is shown on figure 6-6 (B), step of 0.05 g/cm^3 for density contrast is

shown on figure 6-6 (A) and finally the combination of step of 2 km for Moho depth and 0.05 g/cm3 for density contrast is shown on figure 6-6 (C). The same also applied to calculated gravity values based on the Moho depth for instance, difference between measured and calculated gravity values for initial Moho of 39 km and density contrast of 0.5g/cm^3 is shown in figure 6-5 (A)-(C). Each of the parameter contributes to the variation in the crustal thickness both individually as well as combined

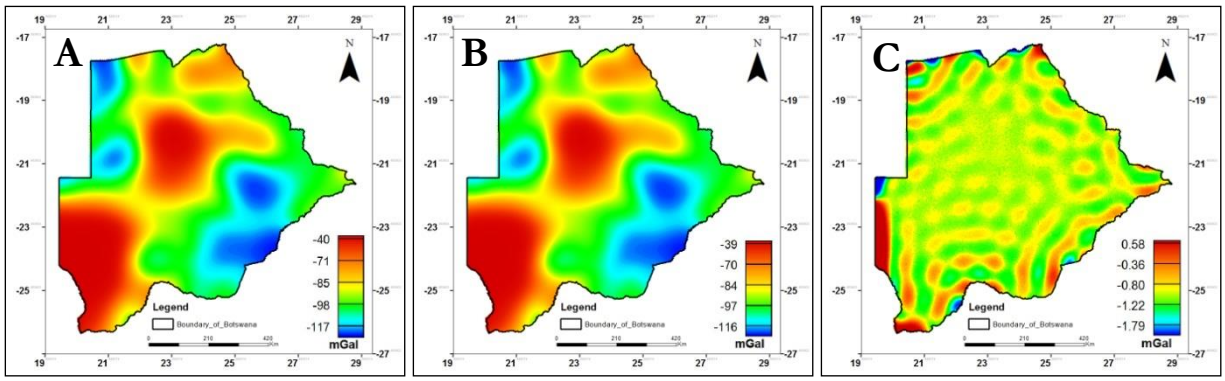

Figure 6-5: (A)input Bouguer anomaly, 175 km wavelength filtered gravity anomaly (B) calculated gravity anomaly due to the Moho topography and (C) the difference between input and measured gravity values.

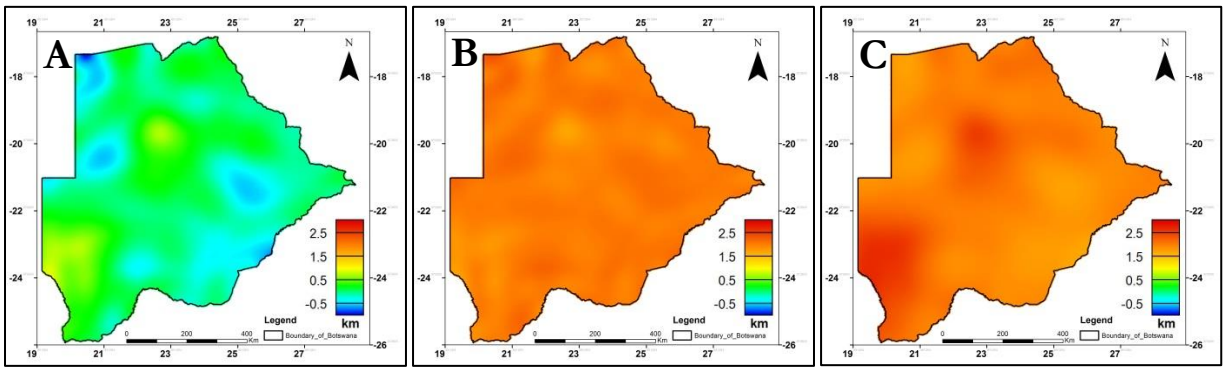

Figure 6-6: the effect of varying the initial Moho and density contrast on the crustal thickness. variation of parameters cause the variation in crustal thickness (A)variation of Moho depth for a step 0.05g/cm^3 of density contrast (B) the change in Moho depth due to variation of initial Moho depth by step of 2 km and (C) the combing effect of varying density contrast and initial Moho depth by 0.05g/cm^3 and 2 km respectively.

6.5. Model validation

The validation of Moho depth was done statistically based on the comparison of gravity derived Moho depth with the seismically derived Moho depth of the study area. The model with the best fit and the lowest absolute average value between the two Moho depths models was adopted.

The gravity derived Moho depth model was compared with the 13 points from the seismic derived depth estimates. The depth uncertainty in the area using the HK-stacking approach was within < 3 km which makes any values within it to be adopted. This research adopted the value of plus/minus 2 km to be acceptable values between the Moho depths from seismic and gravity data.

6.5.1. Validation results and discussion

The statistical approach for validation was absolute average value between two data sets. The same approach used for wavelength cut off values was used in the model validation (Section 6.3.1). Furthermore, the least root mean square approach on a one to one linear model was calculated to understand the correlation of the seismic derived Moho depth and gravity derived Moho depth. The Moho depth values from seismic data were compared with the Moho depth values from 30 models of the inverted gravity data

(Appendix I, table 0-2). The root mean square error and absolute average values for the 30 models are shown in table 6-5 below. The closest absolute average value to zero was 2.28 for model 18 with an average initial Moho depth of 39km and a density contrast of 0.5 g/cm^3. However, the density contrast between the earth crust and the upper mantle ranges from 0.28 g/cm^3 to 0.48 g/cm^3 (Tenzer et al., 2011). As such, the next best fitted model, minus the models with density contrast of 0.5 g/cm^3, has an initial Moho depth of 39 km and a density contrast of 0.45 g/cm^3 (Table 6-5).

N	MD	DC	RMS1	RMS2	AAV	N	MD	DC	RMS1	RMS2	AAV
1	35	0.25	0.0120	-3.306	5.56	**16**	39	0.4	0.0041	-7.117	2.39
2	35	0.3	0.0071	-4.381	5.9	**17**	39	0.45	0.0029	-8.834	2.33
3	35	0.35	0.0046	-5.587	6.14	**18**	39	0.5	0.0021	-10.58	2.28
4	35	0.4	0.0031	-6.948	6.32	**19**	41	0.25	0.0181	-3.481	2.71
5	35	0.45	0.0022	-8.244	6.45	**20**	41	0.3	0.0107	-4.616	2.63
6	35	0.5	0.0016	-9.854	6.57	**21**	41	0.35	0.0069	-5.793	2.62
7	37	0.25	0.0137	-3.315	3.55	**22**	41	0.4	0.0047	-7.206	2.63
8	37	0.3	0.0081	-4.386	3.89	**23**	41	0.45	0.0033	-8.752	2.68
9	37	0.35	0.0052	-5.612	4.13	**24**	41	0.5	0.0024	-10.48	2.71
10	37	0.4	0.0035	-6.612	4.31	**25**	43	0.25	0.0113	-3.43	4.1
11	37	0.45	0.0025	-8.47	4.45	**26**	43	0.3	0.0124	-4.559	3.69
12	37	0.5	0.0019	-10.15	4.57	**27**	43	0.35	0.0079	-5.829	3.4
13	39	0.25	0.0157	-3.381	2.82	**28**	43	0.4	0.0054	-7.256	3.23
14	39	0.3	0.0093	-4.476	2.58	**29**	43	0.45	0.0038	-8.546	3.09
15	39	0.35	0.006	-5.727	2.47	**30**	43	0.5	0.0028	-10.23	3.007

Table 6-5: 30 initial models and its parameters for inversion and validation: N = model number, MD = initial Moho depth, DC = density contrast, RMS1 = root mean square error between the measured and calculated gravity, RMS2 = root mean square error between the gravity derived Moho depth and the Seismic derived Moho depth and AAV = absolute average values between seismic derived Moho depth and gravity derived Moho depth for each model.

The depth values difference between the two best fit models, (0.5) and (0.45) were less than 0.3 km (Table 6-6) despite the difference density contrast of 0.05 g/cm^3. The statistical fitting of the depth values after Youssof et al.,(2013) shows 7 Points, representing about 50%, are within 1km difference. The other 3 point fall within a 3km and 3 point falls within 5 km difference with one point falling outside the 5 km difference (Figure 6-8). The big difference that falls within 3 km and 5 km may possibly be due to two reasons: 1) the uncertainty in the seismic depth estimates from these studies. both Moho depth between Kgaswane et al., (2009) and Youssof et al. ,(2013) studies shows two jumps in there inversion results at 32 km and 50.5 km and 2) the uncertainty in the depth estimate from gravity data due to the effect of sediments correction.

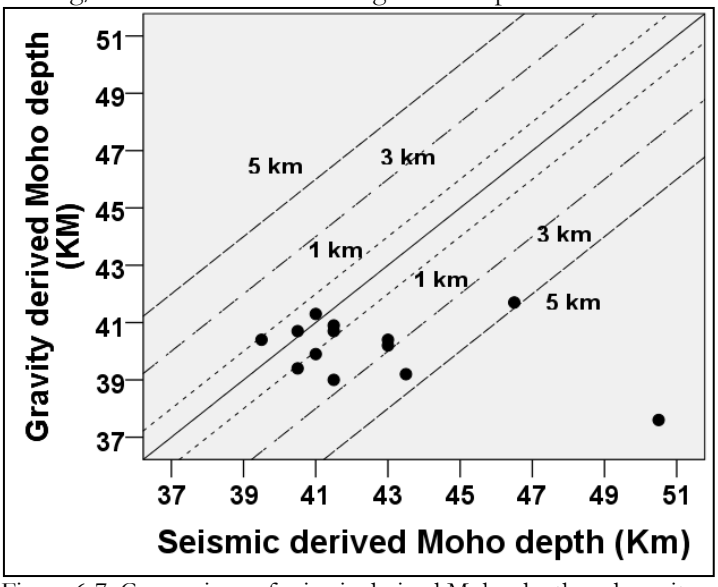

Figure 6-7: Comparison of seismic derived Moho depth and gravity derived Moho depth for 13 depth points

Point ID	Long	Lat	K	Y	(0.5)	(0.45)
Kaapvaal - SA59	24.4	-24.84	40.5	41.5	40.7	40.5
Kaapvaal - SA60	24.9	-23.85	40.5	41.5	40.9	40.7
Kheis-Okwa belt - SA61	24.0	-23.95	43.0	43.5	39.2	39.2
Kaapvaal - SA62	25.1	-24.85	40.5	40.5	40.7	40.6
Kaapvaal - SA63	26.0	-23.66		43	40.4	40.3
Kheis-Okwa belt - SA64	26.2	-22.97	40.5	41	41.3	41.0
Limpopo belt - SA65	27.2	-22.82	40.5	43	40.2	40.1
W Zimbabwe - SA66	26.3	-21.9	48	46.5	41.7	41.4
W Zimbabwe - SA67	27.2	-21.89	45.5	39.5	40.4	40.2
Limpopo belt - SA68	28.1	-21.95	45.5	41	39.9	39.8
W Zimbabwe - SA70	26.3	-21.09	50.5	50.5	37.6	37.8
W Zimbabwe - SA71	27.1	-20.93	43.0	40.5	39.4	39.3
TBTB	23.04	-26.93	43.0	41.5	39.0	39.0

Table 6-6: comparison of the validated gravity derived Moho depths and seismically derived Moho depth: In the table, (0.5) column stands for a model with initial Moho of 39 km and density contrast of 0.5 g/cm^3, (0.45) column stands for a model with initial Moho of 39 km and density contrast of 0.45 g/cm^3 K stands for results after Kgaswane et al., (2009) and Y stands for results after Youssof et al. ,(2013).

6.6. Moho Topography of Botswana

This section discussed the Moho topography of Botswana and the variation of the Moho depth in different tectonic terranes. The Moho topography of the new model derived from gravity data of Botswana is shown in figure 6-9. The crustal thickness map was produced from the addition of elevation to the Moho depth. The Moho depth is the distance between the sea level and the Moho discontinuity. The elevation is the distance between the sea level and the surface. Therefore, the crustal thickness is the distance from the surface to the Moho discontinuity. The Moho topography in Botswana is relatively very inhomogeneous. The variation of Moho depth ranges from 32 km to 44 km with a mean value of 39km and the crust thickness of Botswana ranges from 33km to 46km.

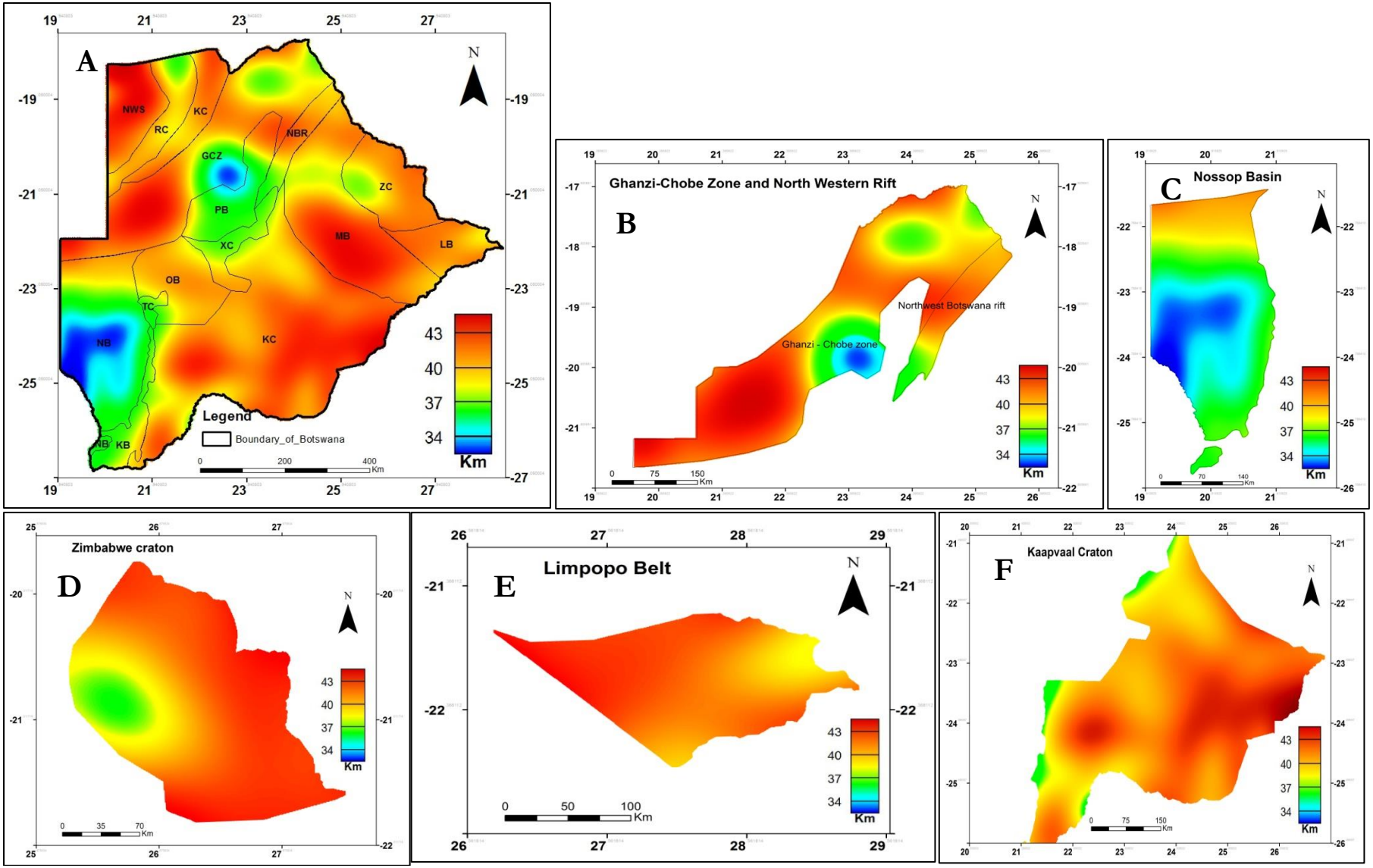
A
NWS
KC
RC
NBR
GCZ
ZC
PB
MB
LB
XC
OB
TC
NB
KC
SB
KB
Legend
Boundary_of_Botswana
43
40
37
34
Km
B
Ghanzi-Chobe Zone and North Western Rift
Northwest Botswana rift
Ghanzi - Chobe zone
C
Nossop Basin
D
Zimbabwe craton
E
Limpopo Belt
F
Kaapvaal Craton
N

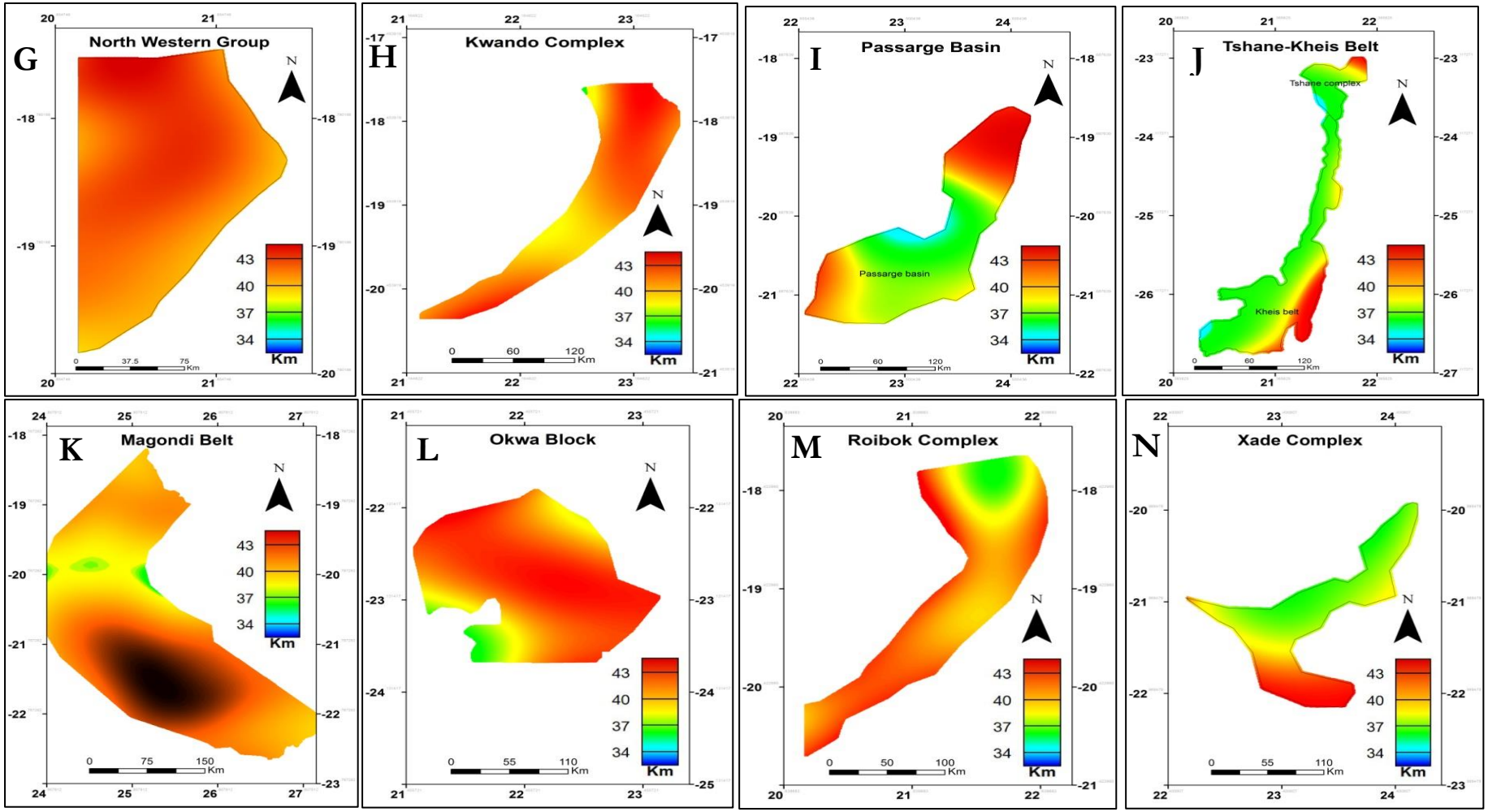

Figure 6-8: (A) The Moho topography of Botswana (in Km), the black lines indicate the major tectonic province delineated from this research and the numbers represent names of tectonic province with its Moho variation: (B) GCZ = Ghanzi-Chobe zone and NBR = North Botswana rift, (C) NB = Nossop belt, (D) ZC = Zimbabwe craton, (E) LB =Limpopo belt, (F) KB = Kaapvaal craton, (G) NWS = north western group, (H) KC = kwando complex, (I) PB = passarge basin, (J) TC = Tshane belt and KB = Kheis belt, (K) MB = Magondi belt, (L) OB = Okwa belt, (M) RC = Reboik complex, and (N) XC = Xadi complex

6.7. Discussion of crutal thickness model

In this section we discuss the crustal thickness of Botswana in relation to the previous studies. The average of Archaean provinces and Proterozoic belt in Africa is 39 km and 41 km for Palaeozoic terrane (Tedla et al., 2011) and between 33-45 km as estimated by Tugume et al., (2013) respectively. Furthermore, the major basin in Africa have a varying crustal thickness between 33 to 36 km (Tedla et al., 2011). The 2 Cratons in the study area, Zimbabwe Craton and Kaapvaal Craton shows a similar thickness with the African estimates. The average thickness in the Zimbabwe craton is 39.3 km and that of Kaapvaal craton is 40km based on the results of this research (Table 6-7). The variation of crustal thickness in Archaean terrane is larger compared with other studies. This study variation ranges from 36 km to 43 km which is greater than other studies. For instance, Zimbabwe craton ranges from 47 – 51 km (Youssof et al., 2013) and Kaapvaal craton ranges from 34 km to 39 km (Youssof et al., 2013). However, results from this research show a smaller variation of Proterozoic terranes on the crustal thickness compared to the Archaean crust. The crustal thickness variation in Proterozoic belts from this study ranges from 37 km to 41 km (Table 6-7). These variation are from Okwa block, Kwando complex, Magondi belt, North western group and Reibok complex. Previous studies on the Proterozoic belt in Botswana shows a thicker crust than this study. The variation ranges from 39 km to 48 km (Begg et al., 2009; Tugume et al., 2013; Youssof et al., 2013). However, the study of Youssof et al., (2013) showed a relatively thinner crust in Okwa block of about 34-35 km. The Nossop and Passarge basins, however, have an average thickness ranging from 35 km to 37 km based on the results from this study. These sedimentary basins fall within the Rehoboth belt. No study has estimated the thickness of these basins in Botswana. The thickness however, are in agreement with the basin thickness studies in other parts of Africa as discussed by Tedla et al., (2011). The areas with mafic intrusions show thinner crust than other areas apart from the basins. For instance, Xade complex, Tshane complex and Kheis belt have an average crustal thickness of 37 km, 2 km less than the average thickness of Botswana (Table 6-7).

Region name	Lower depth	Upper depth	Average
Botswana	32	44.45	39
Ghazi-chobe zone and North western rift	32.9	42.7	39.1
Kaapvaal craton	36	43.3	40
Kwando complex	37.7	40.9	39.7
Limpopo belt	38.3	40.7	39.7
Magondi belt	37.6	42.5	40.1
Nossop basin	32	40.9	35.4
North western group	38.6	44.3	41.3
Okwa block	36.1	39.8	38.9
Passarge basin	33.4	40.9	37
Reibok complex	36.6	40.4	38.7
Tshane complex and Kheis belt	35.2	39.4	37
Zimbabwe craton	37.2	40.6	39.3
Xade complex	36.3	39.6	37.7

Table 6-7: Moho topography variation per delineated tectonic terrane of Botswana (in KM).

6.8. Comparison with other models

The new crustal thickness model of Botswana was compared with the already existing models. The existing crust thickness models of Botswana are part of the regional studies; African crustal thickness modelling. The comparison of the existing models with the new gravity derived Moho depth which will be referred to as "This study" in this comparison includes the similarities and differences. However, since the existing models are regional with courser resolution, the new model tries to highlight the added value of high resolution crustal thickness model from the existing models. The models to be compared were taken from studies by Fadel & Meijde, (2015) and Tugume et al., (2013) (Table 6-8).

Moho depth model and difference	Lower depth	Upper depth	Average
Airborne derived	32.0 Km	44.5 Km	39 Km
Fadel & Meijde, (2015)	34.6 Km	41.2 Km	38.8 Km
Tugume et al., (2013)	33.6 Km	38.5 Km	36.8 Km
This study – Fadel & Meijde, (2015) difference	-3.0 Km	3.6 Km	0.2 Km
This study - Tugume et al., (2013) difference	-2.8 Km	6.8 Km	2.3 Km
Fadel & Meijde, (2015) - Tugume et al., (2013) difference	-0.5 Km	3.5 Km	2.0 Km

Table 6-8: the difference between the airborne derived Moho depth, Fadel & Meijde, (2015) Moho depth, Tugume et al., (2013) Moho depth

The comparison of This study Moho depth and that of the satellite derived Moho depth (Fadel & Meijde, (2015) and Tugume et al., (2013)) shown a considerable difference ranging from -0.5 km to 6.8 km with an average difference range from 0.2 km to 2.3 km. Despite that both Fadel & Meijde, (2015) and Tugume et al., (2013) models are derived from satellite gravity, EIGEN 6C and EIGEN 6C3 respectively with about 1 degrees resolution (about 110km), the latter is coarser than the former. This could be attributed to the fact that Tugume et al., (2013) model is an extract of the thickness model of Africa which was a regional study.

The statistical average thickness of Fadel & Meijde, (2015) model, 38.8 km, is 0.2 km less than the initial average of 39km used in the processing. However, this slight difference will not cause problems in the comparison. The difference between gravity derived Moho depth and Fadel & Meijde, (2015) model ranges from -3 km to 3.6 km (Table 6-8). However, the average difference of 0.2 km shows that the models do not differ much as also shown from the difference map (Figure 6-9 (D)). Most of the areas have the same depth values (Figures 6-10 (D) and (E)). Higher difference values are shown due to the high resolution of this study model (Figures 6-9 (D), (E) and (F)). Both airborne gravity derived model and Fadel & Meijde, (2015) model show considerable difference with the Tugume et al., (2013) model that ranges from -0.8 km to 6.8 km and an average difference of about 2 km (Table 6-8). The most notable differences between the airborne gravity derived model and Tugume et al., (2013) model are in the basin areas and not much deviations in other parts (Figure 6-9 (E)). On the other hand, the basin variation between the Tugume et al., (2013) model and Fadel & Meijde, (2015) model are minimal. Much of the variation is in the cratonic areas and mobile belts.

The Moho depth values from the new model are higher than the previous models of the area. The new model, due to high resolution Moho depth, the crustal variation within a tectonic terrane is higher than the previous model.

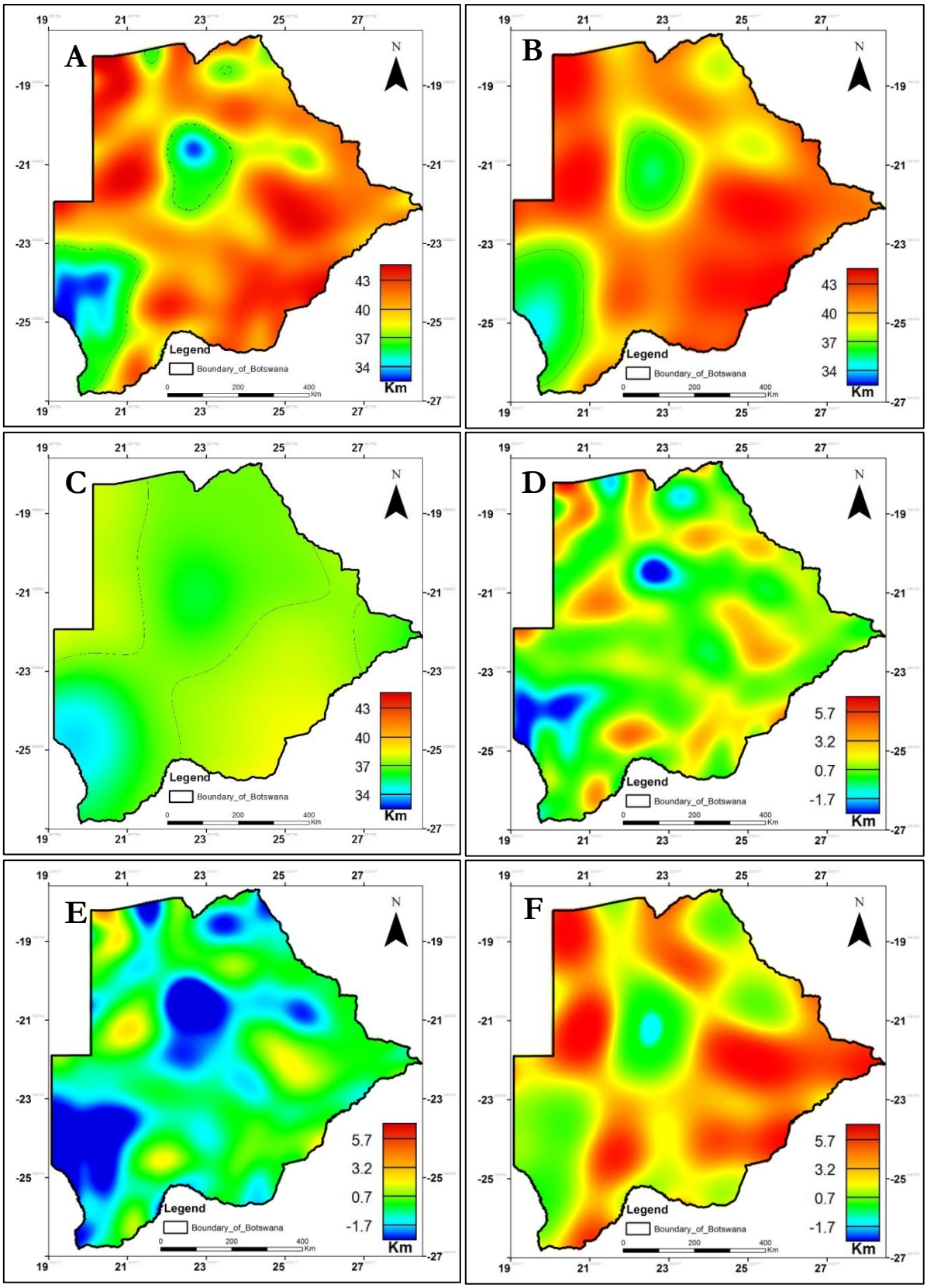

Figure 6-9: the comparison of airborne, Fadel & Meijde, (2015) Moho depth and Tugume et al., (2013) Moho depth. The black line represents a contour line for the depth of 37km. (A) airborne gravity derived Moho depth, (B) Fadel & Meijde, (2015) Moho depth, (C) Tugume et al., (2013) Moho depth, (D)difference between airborne and Fadel & Meijde, (2015)Moho depth, (E) difference between airborne derived Moho depth and Tugume et al., (2013) Moho depth and (F) difference between Fadel & Meijde, (2015) Moho depth and Tugume et al., (2013) Moho depth.

6.9. Geodynamic interpretation

The crustal thickness and crust variation can explain the geodynamics and evolution of crust. This research links the dynamics of the earth and the crust thickness variation. The Botswana tectonic setting lies between the Congo craton in the north and the Kalahari craton in the south sutured by mobile belts and basin. This study present a possible dynamic model of Botswana based on the delineated tectonic terranes, the mafic complexes and the crustal thickness model. This study also compares the spatial variation of crust thickness with the areas of magma activities and intrusion on the different tectonic provinces and its evolution. This study also includes the evidence from epicentres of seismic to help in the understanding of the geodynamic of Botswana.

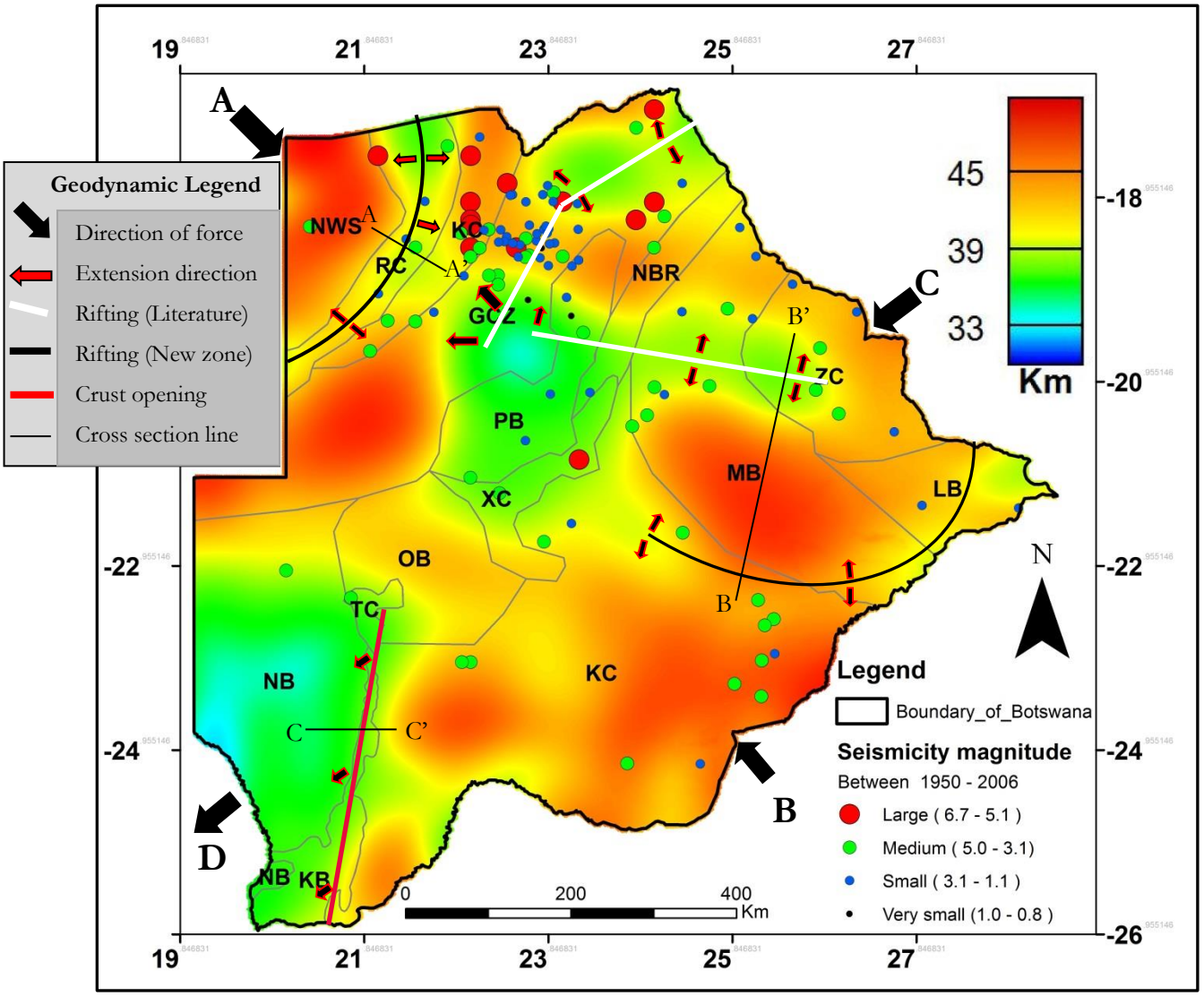

Figure 6-10 : the final crustal thickness of Botswana (in Km) and geodynamic interpretation and effect of compression and extension forces on the crustal thickness, the gray lines indicate the major tectonic province delineated from this research and the letters represent names of tectonic province: NWS = north western group, ZC = Zimbabwe craton, RC = Roibok complex, KC = kwando complex, GCZ = Ghanzi-Chobe zone, NBR = North Botswana rift, PB = passarge basin, XC = Xadi complex, MB = Magondi belt, LB =Limpopo belt, OB = Okwa belt, TC = Tshane belt, KB = Kheis belt, NB = Nossop basin and KB = Kaapvaal belt

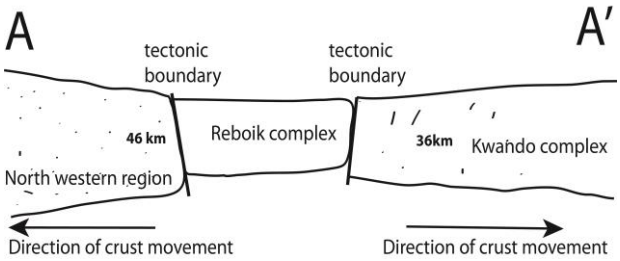

Figure 6-11: a cross section impression of crustal thickness and tectonic model across north western region (NWS), Reboik complex (RC) and the Kwando complex (KC)

- The 800 million Proterozoic magmatic in the Damara belt which forms part of the Roibok and Kwando complex
- The opposite movement (Extension) of crust is causing crust to be thin and creating a graben like structure

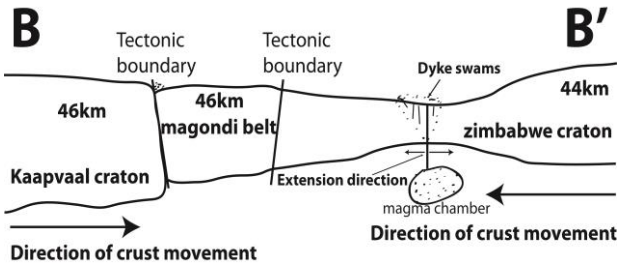

Figure 6-12: a cross section impression of crustal thickness and tectonic model across Kaapvaal craton (KC), Magondi belt (MB), Dyke swarms and the Zimbabwe craton (ZC)

- 2.7 billion years Archaean amalgamation and collision process that formed the Zimbabwe and Kaapvaal craton (compression force shown by the big arrow)
- 1.8 billion years Proterozoic pan-African metamorphism and deformation of Magondi belt (due to the compression force between Kaapvaal and Zimbabwe cratons)
- The 400 million Mesozoic reactivation of deep fault discontinuity that resulted in the formation of dyke swarms and mafic intrusion (Extension forces shown by small arrow which happen after cratonic movement stopped)

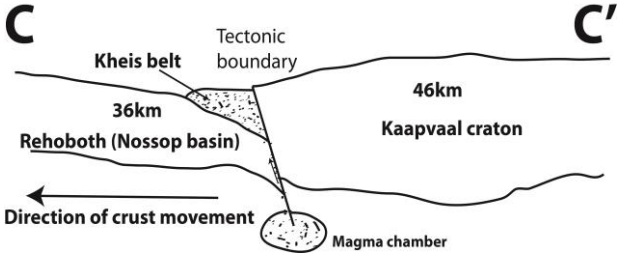

Figure 6-13: a cross section impression of crustal thickness and tectonic model across Nossop basin (NB), Kheis belt (KB) and the Kaapvaal craton (KC)

- 2 billion Archaean movement of Rehoboth belt, which Nossop basin in part of, which formed the Kheis belt overthrust with the Kaapvaal craton (The extension movement that results in magma moving to the surface and form mafic complex)
- 1.7 billion tectonic activity that resulted in the metamorphism and folded of the mafic schist (the westward continuation movement of the Nossop basin that resulted into further deformation of the Kheis belt)

The major tectonic provinces, the cratonic areas, are stable and are not affected much by the various tectonic forces in the region. The compression forces A, B, and C (Figure 6-10) that forms the African crust between 2.7 billion years and 600 million years (Begg et al., 2009) are the major drive in the tectonic evolution and geodynamic of Botswana.

The forces shown on the map above (Figure 6-10) explain both the past and present geodynamic activities in Botswana. The arrows A, B, and C are compression forces and D is the extensional force. These four

forces indicate past geodynamic activities that formed the Botswana crust. These forces explain the formation of major mafic intrusions, faulting, folding and the crust thickness in Botswana. On the other hand, the smaller arrows within Botswana are responsible for extensional directional movement of crust. Five areas of interest were selected to explain the geodynamic. These areas are shown with black, white and red lines (Figure 6-10). They were selected based on the information from major mafic intrusion, the possible thinning of crust and from unexplained theories from literature.

The north western part of Botswana is one on the thickest crust in the study area. The compression force due to the Congo craton shows the thickest part together with Kaapvaal, around 46 km. The Congo craton was discussed by Key & Ayres, (2000) which correspond to North western group (NWS) on figure 6-10. Despite the geology corresponding to Proterozoic period (Singletary et al., 2003), the crustal thickness, geophysical signature (high magnetic and low gravity (Chapter 5, figure 5-7(A)) of the North western group (NWS) indicates that the region may be the extension of Congo craton into Botswana as indicated on the studies by Begg et al., (2009); and Key & Ayres, (2000). The stability of NWS forced the Roibok complex (RC) terrane next to it to fold into an elongated shape. Reibok complex is relatively thinner than the NWS at 39 km. However, a possible opposite force due to the rifting of the incipient rifting of the Okavango region (within GCZ on figure 6-10) explain the high magnetic region due to a mafic intrusion between the Reibok complex and the Kwando complex (Chapter 5, figure 5-8). This region corresponds to the rifting zone caused by the extension forces towards NWS and the Kwando complex (Figure 6-10).

The most interesting feature in the study area is the Okavango delta within the Ghanzi-chobe zone and the Passarge basin terrane. The Okavango delta is located on the south-western part of the white line on figure 6-10 in the centre of Ghanzi-Chobe zone. The Okavango represents an incipient rifting system which south-western part of the East African Rift System within the Ghanzi-chobe zone (Bufford et al., 2012; Kinabo, 2007). The north eastern part of Ghazi-chobe zone which form part of the incipient rifting has also a thinner crust of around 35 km. furthermore, between this region and the Okavango delta a thicker crust of 42km which thins out in between the two thinner crust of incipient rifting. This thicker crust may indicate the evidence that made the Okavango incipient rifting not to fully develop into a rift zone. The rifting and the reworking of the Ghanzi-chobe crust explain the Northeast-southwest trending mafic in the Kgwebe formation (Chapter 5, figure 5-12). Furthermore, this region is associated with mafic intrusions (Chapter 5, figure 5-8). The pattern of intrusion in the region gives evidence of this rifting. The thinner crust areas in the Okavango delta and north-eastern part of Ghanzi-Chobe have more intrusion than the thicker crust in between them. These intrusions are associated with mafic to ultramafic intrusions associated with high magnetic values and high gravity values as indicated on the apparent physical map (Chapter 5, figures 5-6 (D) and 5-7(A)). Furthermore, the extension direction forces away from the Okavango delta caused it to sinking to the mantle as evidence from the thin crust. These direction forces, especially the northern movement, causes tension in the in the Kwando complex which resulted in high seismic activities in the region (Figure 6-10).

The eastern part of the study area is relatively different than what previous studies indicated especially the region corresponds to the Zimbabwe craton. Relatively, the craton crust thickness ranges from 35km to 42km with a thinner crust in the northern part of the craton. The thinner crust in the Zimbabwe Craton has previously estimated to have a thicker crust of about 50 km from previously studies from seismic data(Kgaswane et al., 2009; Youssof et al., 2013). The thinner crust in the Zimbabwe Craton extends - northward into the Magondi belt, North-western Rift into the Ghanzi-chobe zone (Figure 6-10). The spatial location of this thinner crust is most probably the evidence of the crust reworking during the mafic

intrusion and dyke swarms emplacement which exploited the major Precambrian crust discontinuity at depth which was reactivated during the placement of the dykes during the Mesozoic period (Bertrand et al., 2002) (Figure 6-10). The extension extends into the Kwando complex as evidence from the high magnetic dyke swarms (Chapter 5, figure 5-8). The geophysical signature on the physical map, red in colour (Chapter 5, figure 5-7 (A)) indicated a belt of high magnetic and high gravity values corresponding to mafic and ultramafic intrusion.

The crust movement direction, arrow C on figure 6-10, resulted in the folding of Magondi belt around the Zimbabwe craton. However, the thicker crust, around 46 km, in the Magondi belt show no evidence of folding. To its west, in the Kaapvaal craton, a narrow region that runs from the Xade complex in the central part of the study area to the Limpopo belt in the eastern part of the study area with a thickness of about 42 km may represent the suturing region and a possible extension region between the Magondi belt and the Kaapvaal craton, this narrow belt is shown as a black line on figure 6-10. This region is associated with high magnetic mafic intrusion which represent reworking and opening of the crust at depth and movement of magma from the mantle to the surface. The crust thickness of the Magondi belt in this region, the low gravity values and the low magnetic values as indicated on the physical map (Chapter 5, figure 5-7(A)), cyan and blues in colour, indicates a signature of a mobile belt.

The stability of Kaapvaal craton causes the possible major opening, extension, zone and a major fault between it and the Nossop basin to the west of it (Figure 6-10). This activity may indicate the movement of crust underneath the basin westwards away from the Kaapvaal craton and activate a deeper movement of magma from the mantle upwards (Figure 6-10). Since the craton is stable, the movement is one sided and it represent a recent activity after the formation of the crust. This formed the Kheis belt and the Tshane complex which are the mafic and gabbroic intrusion respectively (Chapter 5, figures 5-8 and 5-12) which is also evidence on the physical map as red colour (Chapter 5, figure 5-7). The crust movement in Nossop basin did not involve the crust within the whole basin. From geophysical evidence, the southern part of the basin was moving away from the Kaapvaal craton while the northern part was relatively stationery. This different directional movement caused a major fault (Chapter 4, figures 4-10 (B) and 4-11) which resulted in the extrusion of magma that forms a high mafic intrusion in the Nossop basin (Chapter 5, figures 5-8 and 5-12). Begg et al., (2009) discussed the possibility of a buried micro continent in the Nossop basin, which is part of the Rehoboth belt. However, the high gravity values and high magnetic values as shown on the physical map (Chapter 5, figure 5-7 (A)) and thinner crust (Figure 6-10) may suggest otherwise. On the other hand, the sinking of the microcontinent into the mantle may be the driving force that causes this greater movement compared to the other geodynamic activities in Botswana. The weight of the sinking microcontinent pulls the other crust deep with it causing the extension and the boundary between it and the basin.

The evidence from seismic epicentre data indicates that most of the rifting areas and the tectonic boundaries are still active (Figure 6-10). Most of the activities in the past 20 years happen within the 10 to 32 km depth (Earthquake Track, 2015). These earthquakes support the fact that the geodynamic evolution is ongoing and our model reflects the present activities.

In this chapter, we have presented a possible geodynamic processes and crust movement in Botswana that resulted in the tectonic evolution of Botswana based on geophysical evidence.

7. CONCLUSION AND RECOMMENDATION

7.1. Conclusion

This research has presented the geodynamic evolution of Botswana based on the evidence from geophysical data (gravity and magnetic data). The geodynamic evidence and tectonics movement was produced by combining the tectonic model, the mafic intrusions, geology, and the crustal thickness of Botswana. The combination of these products proved the movement that formed the Botswana crust between 2.7 billion year and 500 million years ago and the recent geodynamical movement which resulted in extension, rifting and crust thinning.

The research has produced a high resolution Moho discontinuity in Botswana and the improvement of the tectonic model and basement geology of Botswana. The boundaries of the tectonic model were not only improved but new tectonic boundaries were delineated. New information was also added to the existing basement geology especially new mafic complexes and full spatial extends of the existing mafic complexes. The combined information from these products have proved that the axis of suturing between the Kalahari and Congo craton in the Damara belt is not a straight line running through the centre of Botswana from north east to southwest as shown by Begg et al., (2009); Hutchins & Reeves, (1980); and Reeves & Canada, (1982). No evidence from the new geophysical data supports such a theory. However, the 3 directional compressional forces (Figure 6-10) and one extension force are responsible for the early geodynamic evolution of Botswana. However, this study has found that the extension within Botswana is due to the sinking microcontinent in the western part, the recent reactivation of deep fault in the eastern part and the continuing rifting movement in the north western and north eastern part of Botswana.

The research has been able to answer the question that were put forth to meet the objectives and solve the problem statement of the research as indicated below.

1. **What improvement does the new geophysical data have on the tectonic terranes and boundaries in Botswana?**
   The new geophysical data was able to delineate the tectonic boundaries and terranes in Botswana. Apart from improving the existing boundaries and terranes, the new geophysical data was also able to delineate other tectonic terranes that were not in the existing tectonic model.
2. **What relationship are the mafic intrusions of the basement complex of Botswana to the geodynamics processes?**
   The major mafic complexes in Botswana are located in the tectonic boundaries of the new delineated model. Some of them form tectonic terranes e.g. Kheis belt and Okwa complex. These mafic intrusions are located in areas of crust extension and rifting areas which gives evidence of crust movement and evolution in Botswana.
3. **What is the relationship of the tectonic terrane boundaries to the geodynamic processes in Botswana?**
   The terrane boundaries follow the geodynamic pattern and borders crustal blocks in Botswana. However, the most important is the shape and directional orientation of tectonic terrane boundaries which indicate the movement of crust as well as directional forces that resulted in the tectonic evolution of Botswana.
4. **How good can the crustal thickness map explain the geodynamic processes and tectonic evolution in Botswana?**
   The crustal thickness map show evidence of geodynamic processes in Botswana. The movement of crust and crust reworking in relation to rifting, extension and compression are explained in relation to the crust thickness variation.

5. **What is the variation of the crustal thickness in relation to the tectonic regions of Botswana?**
   This research was able to produce the crustal thickness variation in each of the tectonic terranes. The Archaean terranes show small variation in tectonic terranes which was also noticed in basin environments. However, in Proterozoic terranes, which most of them are mobile belt, showed a lot of variation and inhomogeneity of crustal thickness.

7.2. Recommendation

The research was able to understand the evolution and geodynamic processes in Botswana based on the tectonic model, Precambrian basement geology of Botswana and crustal thickness map of Botswana. However, the following recommendation can be done to improve the result from the research as well as suggestions for further research areas:

1. The automatic lineament extraction using Line module in PCI Geomatica, which uses canny edge detection algorithm, can be used to extract lineaments from the geophysical data (e.g. Gravity and magnetic). The use of this software in geological application has focused mostly from extracting lineaments from Digital elevation models (DEM) and satellite images (e.g. ASTER and LANDSAT). There is a need to further studies in the use of lineaments extraction algorithm in geophysical studies. Geophysics images the interior of the earth as such being able to extract even lineaments and geological boundaries that are not visible on the surface.
2. The sedimentary map of Botswana needs to be updated either from seismic data or drill hole data. The current sediment map of Botswana which is extracted from world sediment map (Laske & Masters, 1997) has a resolution of 1 degree, approximately 110km. The sediment correction for Bouguer anomaly used for crustal thickness modelling might not reflect the nature of the sediments in the study area.
3. Need for more depth estimates from seismic data that are well distributed in the study area. The crustal thickness map from this research was validated based on 13 depth estimates from receiver functions that are distributed only in the south and south-eastern part of Botswana.
4. Need to produce 3D earth structure and seismic tomography of the subsurface to determine the interaction and extend of the tectonic provinces into the mantle and validate the geodynamics of the crust from this research.
5. Producing rocks identification criteria from apparent physical mapping, combination of magnetic susceptibility and density distribution, in geological mapping. The research just related the physical map in the study region to the already known geology but a method should be developed where the two physical data, magnetic and gravity, can be used to identify the geology even in absent of other data.
6. Analysing the drill hole data in Botswana to determine the geology and mineralogy to validate the new tectonic provinces.
7. Determination of the age and lithology of the new mafic complex in the western part of Botswana. Could this be part of the buried micro-craton, Maltahohe craton , in the Rehoboth belt as discussed by Begg et al., (2009).

LIST OF REFERENCES

ACP Data by country. (2014). Retrieved August 20, 2014, from http://mines.acp.int/html/BW_GPH_en.html

Aldiss, D. T., & Carney, J. N. (1992). The geology and regional correlation of the Proterozoic Okwa Inlier , western Botswana ". *Precambrian Research*, *56*, 255–274.

Assumpção, M., Bianchi, M., Julià, J., Dias, F. L., Sand França, G., Nascimento, R., Lopes, A. E. V. (2013). Crustal thickness map of Brazil: Data compilation and main features. *Journal of South American Earth Sciences*, *43*, 74–85. doi:10.1016/j.jsames.2012.12.009

Bassin, C., Laske, G., & Masters, T. G. (2000). The current limits of resolution for surface wave tomography in North America. *EOS Trans American Geophysics Union (AGU)*, *81*, p. F897.

Begg, G. C., Griffin, W. L., Natapov, L. M., O'Reilly, S. Y., Grand, S. P., O'Neill, C. J., Bowden, P. (2009). The lithospheric architecture of Africa: Seismic tomography, mantle petrology, and tectonic evolution. *Geosphere*, *5*(1), 23–50. doi:10.1130/GES00179.1

Bertrand, H., Gall, B. Le, Tshoso, G., Jourdan, F., Fe, G., Tiercelin, J. J., Maia, M. (2002). Ar / 39 Ar geochronology and structural data from the giant Okavango and related ma ¢ c dyke swarms , Karoo igneous province , northern Botswana. *Earth and Planetary Science Letters*, *202*, 595–606.

Bishta, A. Z. (2009). Lithologic Discrimination Using Selective Image Processing Technique of Landsat 7 Data , Um Bogma Environs Westcentral Sinai , Egypt. *JKAU*, *20*(1), 193–213.

Block, A. E., Bell, R. E., & Studinger, M. (2009). Antarctic crustal thickness from satellite gravity: Implications for the Transantarctic and Gamburtsev Subglacial Mountains. *Earth and Planetary Science Letters*, *288*(1-2), 194–203. doi:10.1016/j.epsl.2009.09.022

Bordy, E. M., Segwabe, T., & Makuke, B. (2010). Sedimentology of the Upper Triassic–Lower Jurassic (?) Mosolotsane Formation (Karoo Supergroup), Kalahari Karoo Basin, Botswana. *Journal of African Earth Sciences*, *58*(1), 127–140. doi:10.1016/j.jafrearsci.2010.02.006

Boyce, J. I., & Morris, W. A. (2002). Basement-controlled faulting of Paleozoic strata in southern Ontario , Canada : new evidence from geophysical lineament mapping. *Tectonophysics*, *353*, 151–171.

Brandt, M. B. C., Grand, S. P., Nyblade, A. a., & Dirks, P. H. G. M. (2011). Upper Mantle Seismic Structure Beneath Southern Africa: Constraints on the Buoyancy Supporting the African Superswell. *Pure and Applied Geophysics*, *169*(4), 595–614. doi:10.1007/s00024-011-0361-8

British Geological Survey. (2014). International Geomagnetic Reference Field (IGRF) | BGS Geomagnetism. Retrieved October 22, 2014, from http://www.geomag.bgs.ac.uk/research/modelling/IGRF.html

Bufford, K. M., Atekwana, E. a., Abdelsalam, M. G., Shemang, E., Atekwana, E. a., Mickus, K., Molwalefhe, L. (2012). Geometry and faults tectonic activity of the Okavango Rift Zone, Botswana: Evidence from magnetotelluric and electrical resistivity tomography imaging. *Journal of African Earth Sciences*, *65*, 61–71. doi:10.1016/j.jafrearsci.2012.01.004

Canny, J. (1986). A Computational Approach to Edge Detection. *Pattern Analysis and Machine Intelligence, IEEE Transactions*, *PAMI-8*(6), 679 – 698. doi:10.1109/TPAMI.1986.4767851

Carney, J. N., Aldiss, D. T., & Lock, N. . (1994). The geology of Botswana. *Bulletin of Botswana*, *37*.

Catuneanu, O., Wopfner, H., Eriksson, P. G., Cairncross, B., Rubidge, B. S., Smith, R. M. H., & Hancox, P. J. (2005). The Karoo basins of south-central Africa. *Journal of African Earth Sciences*, *43*(1-3), 211–253. doi:10.1016/j.jafrearsci.2005.07.007

Clark, D. A., & Emerson, D. W. (1991). Notes on rock magnetization characteristics in applied geophysical studies. *Exploration Geophysics*, *22*(3), 547–555. doi:10.1071/EG991547

Cooper, G. R. J., & Cowan, D. R. (2005). Differential reduction to the pole. *Computers & Geosciences*, *31*(8), 989–999. doi:10.1016/j.cageo.2005.02.005

Ding, L., & Goshtasby, A. (2001). On the Canny edge detector. *Pattern Recognition*, *34*, 721–725.

Earthquake Track. (2015). Recent Earthquake Near Botswana. Retrieved February 12, 2015, from http://earthquaketrack.com/p/botswana/recent

Everaerts, M. (1990). *The compilation and interpretation of geophysical data from the Mount Isa Area, N.W.Queensland, with the support of a geographical information system*. International Institute for Aerospace Survey and Earth Sciences (ITC-Unpublished).

Fadel, I., & Van der Meijde, M.. (2015). *The crustal and upper mantle structure beneath Botswana*. Unpublished, ITC, University of Twente.

Fairhead, J. D., Henderson, N. B., & Observatory, G. (1977). Letter Section The seismicity of southern Africa and incipient rifting. *Tectonophysics*, *41*, 19–26.

Feumoe, A. N. S., & Ndougsa-mbarga, T. (2012). Delineation of tectonic lineaments using aeromagnetic data for the south-east Cameroon area. *Geofizika*, *29*.

Galindo-Zaldívar, J., Ruiz-Constán, A., Pedrera, A., Ghidella, M., Montes, M., Nozal, F., & Rodríguez-Fernandez, L. R. (2013). Magnetic anomalies in Bahia Esperanza: A window of magmatic arc intrusions and glacier erosion over the northeastern Antarctic Peninsula. *Tectonophysics*, *585*, 68–76. doi:10.1016/j.tecto.2012.09.008

Gómez-Ortiz, D., & Agarwal, B. N. P. (2005). 3DINVER.M: a MATLAB program to invert the gravity anomaly over a 3D horizontal density interface by Parker–Oldenburg's algorithm. *Computers & Geosciences*, *31*(4), 513–520.

Gwavava, O., Swain, C. J., Podmore, F., & Fairhead, J. D. (1992). Evidence of crustal thinning beneath the Limpopo Belt and Lebombo monocline of southern Africa based on regional gravity studies and implications for the reconstruction of Gondwana. *Tectonophysics*, *212*(1-2), 1–20. doi:10.1016/0040-1951(92)90136-T

Henkel, H. (1976). Studies of Density and Magnetic Properties of Rocks from Northern Sweden. *Pure and applied geophysics*, *114,* 235-249. doi: 10.1007/BF00878948

Henkel, H. (1994). Standard diagrams of magnetic properties and density—a tool for understanding magnetic petrology. *Journal of Applied Geophysics*, *32*(1), 43–53. doi:10.1016/0926-9851(94)90008-6

Hubbard, B. B. E., Mack, T. J., Thompson, A. L., & Survey, U. S. G. (2012). *Lineament Analysis of Mineral Areas of Interest in Afghanistan,* USGS Afghasistan Project Report number 233, (p. 9).

Hung, L. Q. (2001). *Remote sensing based hydrogeological analysis of Suoimuoi catchment Vietnam [MSc thesis]*. Vrije Universiteit Brussel.

Hung, L. Q., Batelaan, O., & De Smedt, F. (2005). *lineament extraction and analysis, comparison of LANDSAT ETM and ASTER imagery. Case study: Suoimuoi tropical karst catchment, Vietnam*. (M. Ehlers & U. Michel, Eds.) (Vol. 5983, p. 59830T–59830T–12). doi:10.1117/12.627699

Hunt, P., Moskowitz, B. M., & Banerjee, S. K. (1995). *Magnetic Properties of Rocks and Minerals* (pp. 189–204).

Hutchins, D. G., & Reeves, C. V. (1980). Regional Geophysical Exploration of the Kalahari in Botswana. *Tectonphysics*, *69*, 201–220.

Jachens, R. C., & Blakely, R. J. (1986). A New Isostatic Residual Gravity Map of the Conterminous United States With a Discussion on the Significance of. *Journal of Geophysical Research*, *91*(5), 8348–8372.

Johnson M.R, Key, R. M., Shoko U, Van Vuuren C.J., & Hegenberger W.F. (1996). Stratigraphy of the Karoo Supergroup in southern Africa: an overview. *Journal of African Earth Sciences*, (1), 3–15.

Key, R. M., & Ayres, N. (2000). The 1998 edition of the National Geological Map of Botswana. *Journal of African Earth Sciences*, (3).

Key, R. M., & Mothibi, D. (1999). The national geological map of the Republic of Botswana. *Botswana Geol. Surv. (1:500,000).*

Kgaswane, E. M., Nyblade, A. a., Julià, J., Dirks, P. H. G. M., Durrheim, R. J., & Pasyanos, M. E. (2009). Shear wave velocity structure of the lower crust in southern Africa: Evidence for compositional heterogeneity within Archaean and Proterozoic terrains. *Journal of Geophysical Research*, *114*(B12), B12304. doi:10.1029/2008JB006217

Khoza, D., Jones, a. G., Muller, M. R., Evans, R. L., Webb, S. J., & Miensopust, M. (2013). Tectonic model of the Limpopo belt: Constraints from magnetotelluric data. *Precambrian Research*, *226*, 143–156. doi:10.1016/j.precamres.2012.11.016

Kinabo, B. D. (2007). Early structural development of the Okavango rift zone , NW Botswana. *Journal of African Earth Sciences*, *48*, 125–136. doi:10.1016/j.jafrearsci.2007.02.005

Kiran R.S, & Ahmed, S. A. (2014). Lineament Extraction from Southern Chitradurga Schist Belt using Landsat TM , ASTERGDEM and Geomatics Techniques. *International Journal of Computer Applications*, *93*(12), 12–20.

Kocal, A., Duzgun, H. S., Karpuz, C., Technologies, G. I., Mapping, D., & Imagery, H. (2003). *Discontinuity mapping with automatic lineament extraction from high resolution satellite imagery,* International sociaty of photogrametry and remote sensing, proccedings, 35 congress (pp. 1–6).

Lam, L., Lee, S. W., & Suen, C. Y. (1992). Thinning Methodologies-A Comprehensive Survey. *IEEE Transactions on Pattern Analysis and Machine Intelligence*, *14*(9), 897.

Laske, G., & Masters, G. (1997). A Global Digital Map of Sediment Thickness. *EOS Trans. AGU*, *78*(F483).

Laske, G., Masters., G., Ma, Z., & Pasyanos, M. (2013). Update on CRUST1.0 - A 1-degree Global Model of Earth's Crust. *Geophysics*, *Abstract E*(Res. Abstracts, 15).

Mantlík, F., & Matias, M. J. S. (2010). Interpretation and modelling of regional gravity data of the Aveiro Basin (Northwest Portugal). *Comptes Rendus Geoscience*, *342*(11), 823–836. doi:10.1016/j.crte.2010.06.005

Marghany, M., & Hashim, M. (2010). Lineament mapping using multispectral remote sensing satellite data. *International Journal of the Physical Sciences*, *5*(10), 1501–1507.

Modie, B. N. (2000). Geology and mineralisation in the Meso- to Neoproterozoic Ghanzi-Chobe belt of northwest Botswana. *Journal of African Earth Sciences*, *30*(3), 467–474. doi:10.1016/S0899-5362(00)00032-4

Modisi, M. P. (2000). Fault system at the southeastern boundary of the Okavango Rift, Botswana. *Journal of African Earth Sciences*, *30*(3), 569–578. doi:10.1016/S0899-5362(00)00039-7

National Geophysical Data Center. (2014). ETOPO1 Global Relief | ngdc.noaa.gov. Retrieved September 11, 2014, from http://www.ngdc.noaa.gov/mgg/global/global.html

Oldenburg, D. W. (1974). The inversion and interpretation of gravity anomalies. *Society of Exploration Geophysicists*, *39*(4), 526–536. doi:10.1190/1.1440444

Oruç, B., Sertçelik, İ., Kafadar, Ö., & Selim, H. H. (2013). Structural interpretation of the Erzurum Basin, eastern Turkey, using curvature gravity gradient tensor and gravity inversion of basement relief. *Journal of Applied Geophysics*, *88*, 105–113. doi:10.1016/j.jappgeo.2012.10.006

Parker, R. L. (1973). The Rapid Calculation of Potential Anomalies. *Geophysical Journal of the Royal Astronomical Society*, *31*(4), 447–455. doi:10.1111/j.1365-246X.1973.tb06513.x

Prewitt, J. M. S. (1970). Object enhancement and extraction. In B. S. Lipkin & A. Rosenfeld (Eds.), *Picture Processing and Psychopictorics* (pp. 75–149). New York: Academic Press.

Ranganai, R. T., & Ebinger, C. J. (2008). Aeromagnetic and Landsat TM structural interpretation for identifying regional groundwater exploration targets, south-central Zimbabwe Craton. *Journal of Applied Geophysics*, *65*(2), 73–83. doi:10.1016/j.jappgeo.2008.05.009

Ranganai, R. T., Kampunzu, a. B., Atekwana, E. a., Paya, B. K., King, J. G., Koosimile, D. I., & Stettler, E. H. (2002). Gravity evidence for a larger Limpopo Belt in southern Africa and geodynamic implications. *Geophysical Journal International*, *149*(3), F9–F14. doi:10.1046/j.1365-246X.2002.01703.x

Ranganai, R. T., Whaler, K. a., & Ebinger, C. J. (2008). Gravity anomaly patterns in the south-central Zimbabwe Archaean craton and their geological interpretation. *Journal of African Earth Sciences*, *51*(5), 257–276. doi:10.1016/j.jafrearsci.2008.01.011

Reeves, C. (2000). The geophysical mapping of Mesozoic dyke swarms in southern Africa and their origin in the disruption of Gondwana. *Journal of African Earth Sciences*, *30*(3), 499–513. doi:10.1016/S0899-5362(00)00035-X

Reeves, C. V, & Canada, T. (1982). A progress report on the geophysical exploration of the Kalahari in Botswana. *Geoexploration*, *20*, 209–224.

Reid, A. B., Ebbing, J., & Webb, S. J. (2012). Comment on "A crustal thickness map of Africa derived from a global gravity field model using Euler deconvolution" by Getachew E. Tedla, M. van der Meijde, A. A. Nyblade and F. D. van der Meer. *Geophysical Journal International*, *189*(3), 1217–1222. doi:10.1111/j.1365-246X.2012.05353.x

Saud, M. Al. (2008). Using ASTER Images to Analyze Geologic Linear Features in Wadi Aur- nah Basin , Western Saudis Arabia. *The Open Remote Sensing Journal*, *1*, 17–25.

Schaller, M., Steiner, O., Studer, I., Holzer, L., Herwegh, M., & Kramers, J. D. (1999). Exhumation of Limpopo Central Zone granulites and dextral continent-scale transcurrent movement at 2 . 0 Ga along the Palala Shear Zone , Northern Province , South Africa. *Precambrian Research*, *96*, 263–288.

Schlüter, T. (2006). *Geological Atlas of Africa: with notes on tratigraphy, tectonics, Economic Geology, Geohazard and Geosites of Each Country*. *Geological Atlass of Africa* (pp. 46–48). Springer Berlin Heidelberg.

Scientific, E., Company, P., Coward, M. P., & Fairhead, J. D. (2000). Gravity and structural evidence for the deep structure of the limpopo belt, southern africa. *Tectonophysics*, *68*(1980), 31–43.

Singletary, S. J., Hanson, R. E., Martin, M. W., Crowley, J. L., Bowring, S. a, Key, R. M., Krol, M. a. (2003). Geochronology of basement rocks in the Kalahari Desert, Botswana, and implications for regional Proterozoic tectonics. *Precambrian Research*, *121*(1-2), 47–71. doi:10.1016/S0301-9268(02)00201-2

Sobel, I. (2014). *History and Definition of the Sobel Operator* , Presentation at Stanford A.I. Project 1968 02/2014; (pp. 2–5).

Sukumar, M., & Nelson Kennedy Babu, C. (2014). A Review of Various Lineament Detection Techniques for high resolution Satellite Images. *International Journal of Advanced Research in Computer Science and Software Engineering*, *4*(3), 72–78.

Tedla, G. E., Meijde, M. van der, Nyblade, A. A., & Meer, F. D. van der. (2011). A crustal thickness map of Africa derived from a global gravity field model using Euler deconvolution. *Geophysical Journal International*, *187*(1), 1–9. doi:10.1111/j.1365-246X.2011.05140.x

Tenzer, R., Novák, P., Gladkikh, V., & Vajda, P. (2011). Global Crust-Mantle Density Contrast Estimated from EGM2008, DTM2008, CRUST2.0, and ICE-5G. *Pure and Applied Geophysics*, *169*(9), 1663–1678. doi:10.1007/s00024-011-0410-3

Thannoun, R. G. (2013). Automatic Extraction and Geospatial Analysis of Lineaments and their Tectonic Significance in some areas of Northern Iraq using Remote Sensing Techniques and GIS. *International Journal of Enhanced Research in Schience Technology and Engineering*, *2*(2), 1–11.

Tugume, F., Nyblade, A., Julià, J., & van der Meijde, M. (2013). Precambrian crustal structure in Africa and Arabia: Evidence lacking for secular variation. *Tectonophysics*, *609*, 250–266. doi:10.1016/j.tecto.2013.04.027

Vaish, J., & Pal, S. K. (2014). Geological mapping of Jharia Coalfield, India using GRACE EGM2008 gravity data: a vertical derivative approach. *Geocarto International*, (September), 1–14. doi:10.1080/10106049.2014.905637

Van der Meijde, M., Fadel, I., Ditmar, P., & Hamayun, M. (2014). Uncertainties in crustal thickness models for data sparse environments: A review for South America and Africa. *Journal of Geodynamics*. doi:10.1016/j.jog.2014.09.013

Van der Meijde, M., Julià, J., & Assumpção, M. (2013a). Gravity derived Moho for South America. *Tectonophysics*, *609*, 456–467. doi:10.1016/j.tecto.2013.03.023

Van der Meijde, M., & Nyblade, A. A. (2014). Reply to "Comment on 'A crustal thicknes map of Africa derived from a global gravity field model using Euler deconvolution.'" *Geophysical Journal International*, *196*, 96–99.

Van der Meijde, M., Pail, R., Bingham, R., & Floberghagen, R. (2013b). GOCE data, models, and applications: A review. *International Journal of Applied Earth Observation and Geoinformation*, 1–12. doi:10.1016/j.jag.2013.10.001

Yawsangratt, S. (2002). *A gravity study of northern Botswana : a new perspective and its implications for regional geology*. MSc Thesis, Faculty of Geo-Information Science and Earth Observation (ITC), University of Twente. Retrieved from http://www.itc.nl/library/papers/msc_2002/ereg/yawsangratt.pdf

Youssof, M., Thybo, H., Artemieva, I. M., & Levander, a. (2013). Moho depth and crustal composition in Southern Africa. *Tectonophysics*, *609*, 267–287. doi:10.1016/j.tecto.2013.09.001

Zeil, P., & Volk, P. (1991). Geophysical methos for lineament studies in groundwater exploration: a case history from SE Botswana. *Geoexploration*, *27*, 165–177.

Zeng, H., Zhang, Q., Li, Y., & Liu, J. (1997). Crustal structure inferred from gravity anomalies in South China. *Tectonophysics*, *283*(l 997), 189–203.

APPENDIX I

station id	M1	M2	M3	M4	M5	M6	M7	M8	M9	M10
Kaapvaal - SA59	44.5	43.1	42.0	41.5	41.5	43.0	41.9	41.1	40.5	40.8
Kaapvaal - SA60	40.9	41.2	41.6	41.7	41.7	40.3	40.5	40.8	40.9	40.9
Kheis-Okwa belt - SA61	37.9	38.5	38.9	39.4	39.4	38.2	38.6	39.0	39.2	39.3
Kaapvaal - SA62	41.9	41.8	41.6	41.4	41.4	41.0	41.0	40.8	40.6	40.7
Kaapvaal - SA63	41.0	40.4	40.3	40.5	40.5	40.4	40.0	39.9	40.3	40.0
Kheis-Okwa belt - SA64	43.4	42.7	41.9	41.4	41.4	42.1	41.6	41.1	41.0	40.7
Limpopo belt - SA65	39.9	40.3	40.0	39.7	39.7	39.6	39.9	39.7	40.1	39.5
W Zimbabwe - SA66	41.3	41.3	41.5	41.7	41.7	40.6	40.6	40.8	41.4	40.9
W Zimbabwe - SA67	39.5	39.8	39.7	39.7	39.7	39.4	39.6	39.5	40.2	39.5
Limpopo belt - SA68	37.7	38.6	38.8	38.8	38.8	38.1	38.1	38.9	39.8	38.9
W Zimbabwe - SA70	32.1	33.7	35.3	35.3	36.3	34.3	35.4	36.4	37.8	37.1
W Zimbabwe - SA71	40.8	39.8	38.8	38.2	38.2	40.2	39.6	38.8	39.3	38.4
TBTB	37.8	38.1	38.8	39.2	39.2	38.2	38.4	38.9	39.0	39.2

Table 0-1: Moho depth estimate of 13 point from 10 gravity derived Moho depth for wavelength lower cut off determination, M stands for model number

station id	model1	model2	model3	model4	model5	model6
Kaapvaal - SA59	37.9	37.4	37.1	36.8	36.6	36.5
Kaapvaal - SA60	38.6	38.0	37.6	37.3	37.0	36.8
Kheis-Okwa belt - SA61	35.5	35.4	35.3	35.3	35.2	35.2
Kaapvaal - SA62	38.3	37.8	37.4	37.1	36.7	36.6
Kaapvaal - SA63	37.7	37.2	36.9	36.7	36.5	36.3
Kheis-Okwa belt - SA64	38.6	38.0	37.6	37.3	37.2	37.0
Limpopo belt - SA65	37.2	36.8	36.5	36.3	36.2	36.1
W Zimbabwe - SA66	39.5	38.7	38.2	37.8	37.5	37.3
W Zimbabwe - SA67	37.5	37.1	36.8	36.5	36.4	36.2
Limpopo belt - SA68	36.6	36.3	36.1	36.0	35.9	35.8
W Zimbabwe - SA70	33.0	33.3	33.6	33.7	33.9	34.0
W Zimbabwe - SA71	35.7	35.6	35.5	35.4	35.4	35.3
TBTB	35.2	35.1	35.1	35.1	35.1	35.1

station id	model7	model8	model9	model10	model11	model12
Kaapvaal - SA59	40.0	39.5	39.1	38.9	38.7	38.5
Kaapvaal - SA60	40.7	40.1	39.6	39.3	39.1	38.9
Kheis-Okwa belt - SA61	37.4	37.3	37.3	37.2	37.2	37.2
Kaapvaal - SA62	40.2	39.6	39.2	39.0	38.7	38.6
Kaapvaal - SA63	39.7	39.2	38.9	38.6	38.5	38.3
Kheis-Okwa belt - SA64	41.0	40.3	39.8	39.5	39.2	39.0
Limpopo belt - SA65	39.2	38.8	38.5	38.3	38.2	38.1
W Zimbabwe - SA66	41.6	40.9	40.3	39.9	39.6	39.4
W Zimbabwe - SA67	39.5	39.1	38.8	38.5	38.4	38.2
Limpopo belt - SA68	38.6	38.3	38.1	38.0	37.9	37.8
W Zimbabwe - SA70	34.8	35.1	35.4	35.6	35.8	35.9
W Zimbabwe - SA71	37.7	37.6	37.5	37.4	37.4	37.3

TBTB	37.1	37.1	37.1	37.1	37.1	37.0
station id	**model13**	**model14**	**model15**	**model16**	**model17**	**model18**
Kaapvaal - SA59	42.1	41.6	41.2	40.9	40.7	40.5
Kaapvaal - SA60	42.7	42.1	41.7	41.4	40.9	40.7
Kheis-Okwa belt - SA61	39.3	39.3	39.2	39.2	39.2	39.2
Kaapvaal - SA62	42.2	41.6	41.3	41.0	40.7	40.6
Kaapvaal - SA63	41.6	41.2	40.8	40.6	40.4	40.3
Kheis-Okwa belt - SA64	43.1	42.4	41.9	41.5	41.3	41.0
Limpopo belt - SA65	41.2	40.8	40.5	40.3	40.2	40.1
W Zimbabwe - SA66	43.8	43.0	42.4	42.0	41.7	41.4
W Zimbabwe - SA67	41.5	41.1	40.8	40.6	40.4	40.2
Limpopo belt - SA68	40.6	40.4	40.2	40.0	39.9	39.8
W Zimbabwe - SA70	36.6	37.0	37.3	37.5	37.6	37.8
W Zimbabwe - SA71	39.7	39.6	39.5	39.4	39.4	39.3
TBTB	39.0	39.0	39.0	39.0	39.0	39.0
station id	**model19**	**model20**	**model21**	**model22**	**model23**	**model24**
Kaapvaal - SA59	44.1	43.6	43.2	43.0	42.8	42.6
Kaapvaal - SA60	44.5	43.9	43.8	43.4	43.2	43.0
Kheis-Okwa belt - SA61	41.3	41.2	41.2	41.1	41.1	41.1
Kaapvaal - SA62	44.2	43.7	43.3	43.0	42.8	42.6
Kaapvaal - SA63	43.6	43.1	42.8	42.6	42.4	42.3
Kheis-Okwa belt - SA64	45.1	44.5	44.0	43.6	43.3	43.1
Limpopo belt - SA65	43.1	42.8	42.5	42.3	42.2	42.0
W Zimbabwe - SA66	45.9	45.1	44.5	44.1	43.8	43.5
W Zimbabwe - SA67	43.5	43.1	42.8	42.6	42.4	42.3
Limpopo belt - SA68	42.7	42.4	42.2	42.0	41.9	41.8
W Zimbabwe - SA70	38.3	38.8	39.1	39.3	39.5	39.7
W Zimbabwe - SA71	41.7	41.6	41.5	41.4	41.4	41.3
TBTB	41.0	41.0	41.0	41.0	41.0	41.0
station id	**model25**	**model26**	**model27**	**model28**	**model29**	**model30**
Kaapvaal - SA59	46.2	45.7	45.3	45.0	44.8	44.6
Kaapvaal - SA60	46.9	46.3	45.8	45.5	45.2	45.0
Kheis-Okwa belt - SA61	43.2	43.1	43.1	43.1	43.1	43.1
Kaapvaal - SA62	46.2	45.7	45.3	45.0	44.8	44.6
Kaapvaal - SA63	45.5	45.1	44.8	44.5	44.4	44.2
Kheis-Okwa belt - SA64	47.2	46.5	46.0	45.6	45.3	45.1
Limpopo belt - SA65	45.1	44.7	44.5	44.3	44.1	44.0
W Zimbabwe - SA66	48.1	47.2	46.6	46.2	45.8	45.6
W Zimbabwe - SA67	45.6	45.1	44.8	44.6	44.4	44.3
Limpopo belt - SA68	44.7	44.4	44.2	44.0	43.9	43.8
W Zimbabwe - SA70	40.1	40.6	40.9	41.2	41.4	41.5
W Zimbabwe - SA71	43.7	43.6	43.5	43.4	43.4	43.3
TBTB	42.9	42.9	42.9	42.9	42.7	42.8

Table 0-2: Moho depth estimate of 13 point from 30 gravity derived Moho depth for model validation